This is to certify that the
dissertation entitled

FRICTION ENERGY ABSORPTION IN FIBER REINFORCED COMPOSITES

presented by

THOMAS JAY BRIMHALL

has been accepted towards fulfillment
of the requirements for the

Ph.D degree in Engineering Mechanics

Major Professor's Signature

June 06/05

Date

FRICTION ENERGY ABSORPTION IN FIBER REINFORCED COMPOSITES

By

Thomas Jay Brimhall

A DISSERTATION

Submitted to
Michigan State University
In partial fulfillment of the requirements
for the degree of

DOCTOR OF PHILOSOPHY

Department of Mechanical Engineering

2005

ABSTRACT

FRICTION ENERGY ABSORPTION IN FIBER REINFORCED COMPOSITES

By

Thomas Jay Brimhall

Energy absorption of fiber reinforced composite structures is of interest to the automotive industry as their specific energy absorption (SEA), i.e. the energy absorption capability per unit mass, is higher than many metallic counterparts. However, the SEA of composite structures has been observed to decrease under dynamic crush loading when compared with quasi-static compression. This is different from metallic structures. For example, carbon fiber/vinyl ester composite crush tubes crushed at 2.0 m/sec were observed to have SEA of 23.8 J/gm, a decrease in SEA of 6.6 J/gm or 21.7% compared with quasi-statically loaded SEA of 30.4 J/gm.

Glass fiber/vinyl ester composite crush tubes were investigated with quasi-static compression and energy-absorbing modes were identified. The observed energy absorbing modes included tube corner splitting, composite delamination, matrix damage due to bending, and sliding friction of the composite with the plug type crush trigger. These same energy-absorbing modes were observed in quasi-statically compressed and dynamically crashed carbon/vinyl ester composite crush tubes. Energy absorption attributable to corner splitting at quasi-static compression was estimated using standard tensile test results. Corner splitting was estimated to absorb less that 1% of the total energy absorbed by both the glass fiber composite and the carbon fiber composite crush

tubes. Energy absorption attributable to delamination was estimated using the mode II (shear mode) strain energy release rate obtained using the end notch flexure (ENF) test. Under quasi-static compression, the glass fiber composite delamination SEA was found to be 1.31 J/gm or 6.4% of the total tube SEA. For carbon fiber composite crush tubes, the delamination SEA was found to be 0.84 J/gm or 2.8%f the total tube SEA.

Experiments seemed to suggest that sliding friction played an important role in the energy absorption of composite crush tubes. In an attempt to separate the sliding friction SEA from the SEA attributable to matrix damage due to bending, an innovative strip testing fixture was designed, fabricated, and tested and is presented in this thesis. Carbon fiber composite SEA, under quasi-static compression, attributable to matrix damage due to bending was found to be 18.9 J/gm or 62.2% of the total tube SEA. Under dynamic crush, the SEA attributable to matrix damage due to bending was found to be 18.6 J/gm or 78.1% of the total tube SEA. Carbon fiber composite SEA attributable to sliding friction under quasi-static compression was found to be 10.6 J/gm or 34.8% of the total tube SEA. Under dynamic crush, the SEA attributable to sliding friction was found to be 4.3 J/gm or 18.1% of the total SEA. The decrease in sliding friction SEA of 6.3 J/gm accounted for nearly all of the decrease in tube SEA of 6.6 J/gm between dynamic crush and quasi-static compression. Sliding friction was concluded to be responsible for the decrease in overall tube SEA from quasi-static compression to dynamic crush.

Nice

DEDICATION

I dedicate this dissertation to my wife, Carol, and to my children Elizabeth, Nicole, and Michael. They were the inspiration for my efforts and success.

ACKNOWLEDGEMENTS

I would like to acknowledge and thank the people who supported, encouraged, and helped me in the achievement described in this thesis:

To Richard Jeryan, my first supervisor at Ford Motor Company, for his suggestions, constructive criticism and coaching that motivated me to look at all possibilities.

To my current supervisor, Nripen Saha, for his support and encouragement.

To the managers and directors at Ford Motor Company, Alan Taub, Jim Boland, Priya Prasad, Paul Killgoar, Charles Wu, and Saeed Barbat for their support and encouragement to pursue a PhD by making this project a part of my employment goals.

To John Jaranson, for his encouragement and assistance in technical graphics creation.

To technical fabricators of the Ford Scientific Research Laboratory shop, Paul Ostrander and Gary Fleming, for the fabrication of and their design suggestions of the strip test fixture described in this thesis.

To Mike Starbuck and Rick Battiste of Oak Ridge National Laboratory, National Transportation Research Center, for conducting dynamic load tests.

To Dan Houston and Ron Cooper of the Ford Scientific Research Laboratory for performing quasi-static crush tests.

I would also like to acknowledge and thank the DOE program management team and the Board and staff of the Automotive Composites Consortium. This work was sponsored by the Automotive Composites Consortium and the U. S. Department of Energy, Office of Transportation Technologies, Office of Advanced Technologies,

Lightweight Materials Program under Cooperative Agreement number FC05-02OR22910.

TABLE OF CONTENTS

LIST OF FIGURES

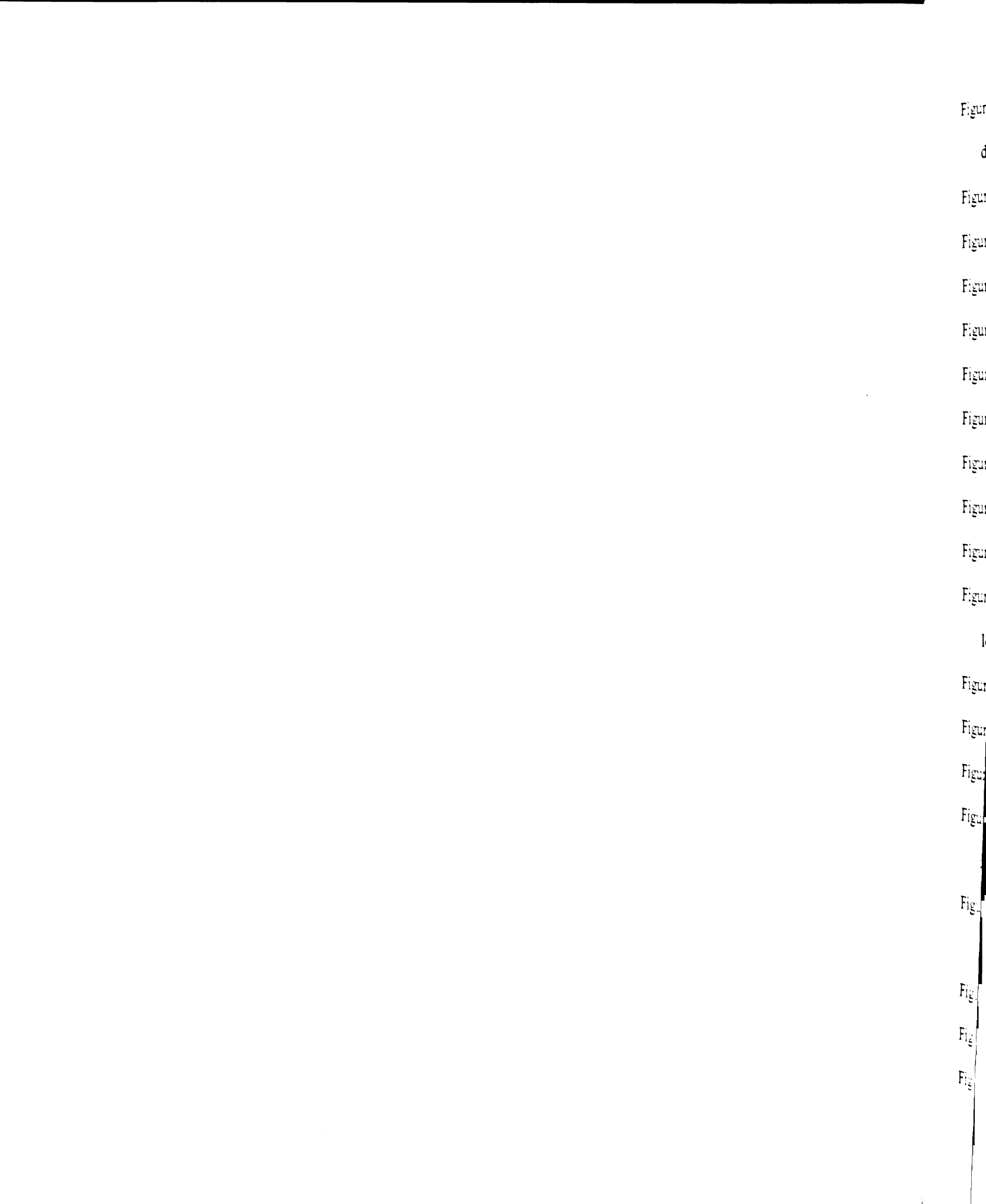

Figu

Figu

(0.0

Figu

Figu

LIST OF TABLES

CHAPTER 1. Introduction

1.1 Introduction and motivation

The body structure of the modern automobile is required to protect the occupants in the event of a crash. To this end, automobiles are designed with an occupant cell that serves as protection for the passengers in the event of a crash. Within the passenger capsule, interior components are designed to protect passengers by absorbing energy due to impact with passengers. Such items include a collapsible steering column, padding on the instrument panel, and deployable airbags. Seat belts restrain passengers in the event of a collision preventing contact with solid surfaces such as the instrument panel and windshield.

Front structures are designed to absorb crash energy by progressively collapsing during the crash event. The energy absorbing front structure consists of upper and lower rails, front crossmember, aprons, and secondary body add-on parts (Figure 1.1). The primary energy absorption structures are the upper and lower rails. The front crossmember ties the left and right lower rails providing increased torsion stiffness. The front aprons provide additional torsion stiffness by linking the upper and lower rails together. The front apron also absorbs crash energy during the crash event. Bumpers are designed to transfer load from the point of impact to the lower front rails. Bumpers provide protection to the automobile from low speed impacts and absorb small amounts of energy in high-speed frontal crashes.

Experience has shown that simple structures such as tubes can be used to help characterize the behavior of more complex structures. The primary measurement of the energy absorption capability of a structural material is specific energy absorption (SEA).

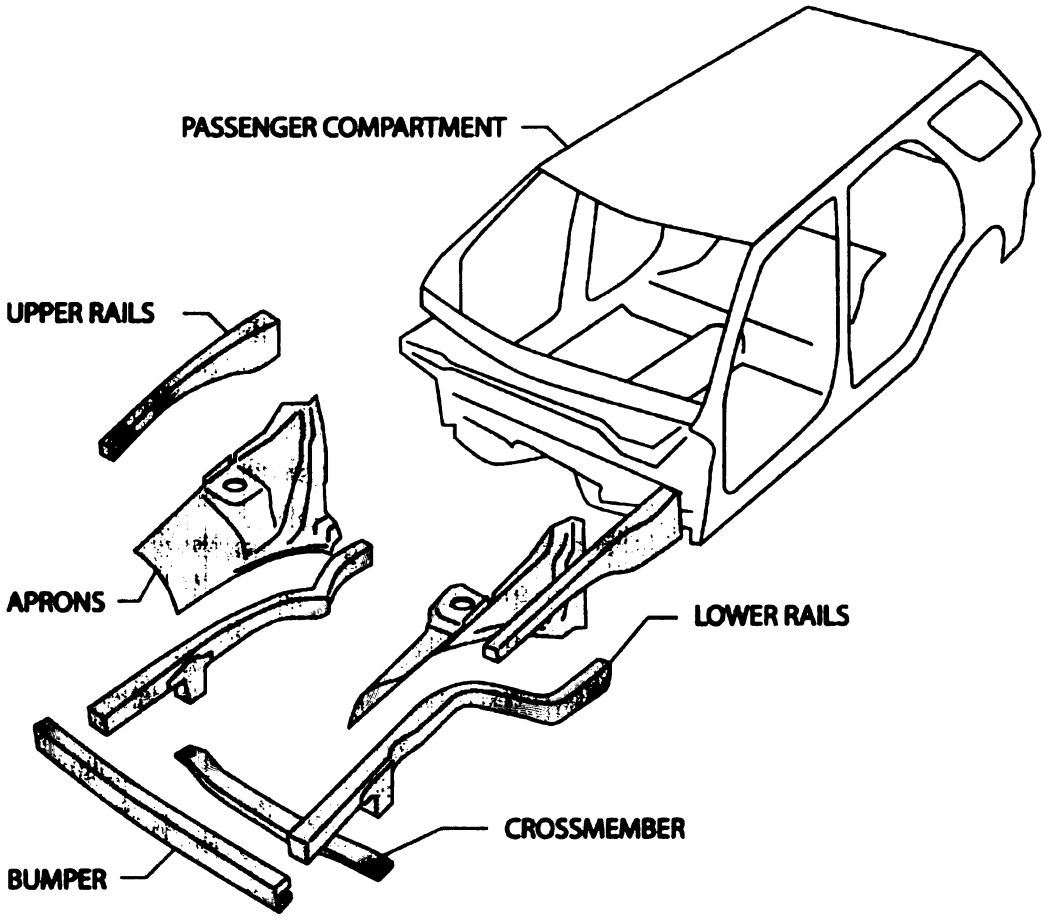

Figure 1.1 Exploded view of generic vehicle showing energy absorbing components.

The SEA is defined as the quantity of energy absorbed divided by the mass of the crash damage or deformed material. Crush tubes made from the same materials as the front rails are used for experimental measurement of energy absorption. A simple tube is used to characterize energy absorption because of its similarity in configuration with automotive energy absorbing structures such as the front rails. Typical post-test crush tubes made from steel and aluminum are presented in Figure 1.2. Metals used in automotive energy absorbing structures absorb energy primarily by plastic deformation. Note that there is extensive bending with no fracture of the metal observed. A load-displacement plot for two automotive front rail tests is presented in Figure 1.3. In addition, the dynamic behavior of steel structures is routinely predicted by computer analyses.

As an alternative to steel, composites are being considered more frequently for structural applications in automobiles because of their lower mass, high specific stiffness, tailorable mechanical properties, improved noise vibration and harshness (NVH) and simplified assembly due to a smaller number of parts due to parts consolidation. In fact, the chassis of many racecars such as Formula 1 and Indy cars are primarily fabricated from carbon fiber composite. Composites have not yet come into wide use in every day automotive structural applications because of high cost, slow fabrication cycle times, slow fastening methods (adhesives and mechanical fasteners), recyclability issues, and the inability to predict dynamic crash behavior.

Before a design for an automobile is approved, conformance to numerous requirements must be demonstrated by physical testing. The requirement of interest in this work is crash energy absorption by the front rails. A sure method to ensure

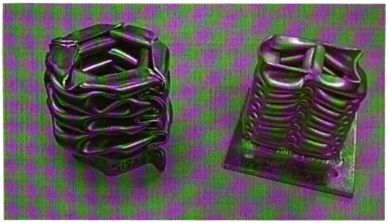

Figure 1.2 Crushed steel and aluminum crush tubes.

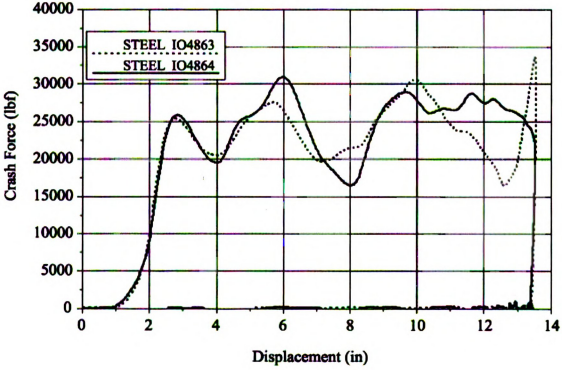

Figure 1.3 Steel rail crush load-displacement plot.

conformance to requirements is to crash test a variety of rail designs until satisfactory energy absorption is achieved. The disadvantage to this approach is the high cost and long time needed for thorough investigation. A more systematic approach for preliminary analysis is to perform computer analysis on a variety of materials and front rail architectures to identify the best candidates. Before structures can be analyzed, it is necessary that characteristics, such as SEA and crush load level, be measured. This cannot be accomplished using complex shaped structures found in the front automobile structure. It is simpler to analyze and test a simple tube of uniform cross section that is similar to that of the front rail. Such a simple tube is less costly to fabricate and allows investigation of a variety of materials while minimizing geometry effects. This approach has been used with success with metals and with mixed results using composites.

In contrast with metals, composites typically do not exhibit significant plastic deformation. Both the composite reinforcement and polymeric matrix typically exhibit elastic stress-strain behavior up to fracture. Composites, by their nature, have multiple damage modes. Any of these modes has the potential for energy absorption. Characterization of composites to be used as energy absorbing structures has been attempted using the techniques used to characterize steel structures. Specifically, simple tubes of a specific composite architecture are tested statically and dynamically using the same procedures and equipment used for steel crush tubes.

The strain-rate effect observed in most steels used in automotive structures causes the average crush load to increase with increasing crush speed. Metal structures have been well characterized and experimental data have been successfully used with computer aided engineering (CAE) software to predict energy absorption of complete

automotive structures. Also, strain-rate dependence of metallic materials has been accounted for in many non-linear CAE finite element analysis (FEA) solvers such as RADIOSS® and LSDYNA®. SEA characterization of metal structures begins with coupon testing in static and dynamic crush testing. The results of these tests are used for calibration of CAE models of the crush tube test. Larger more complex sub-component tests and analyses are performed leading to full vehicle CAE analyses and crash testing. Similar analysis success has not been demonstrated with composite materials in spite of numerous attempts to develop CAE software that can accurately model the dynamic crush behavior of composite materials.

Experiment has shown that the SEA of a composite structure when tested statically can be significantly different than observed in dynamic experiments. In most cases, the dynamic SEA is much less than the static SEA for composite materials. A plot of average crush load vs. crush speed for two fiberglass fiber composites is presented in Figure 1.4, Ref. (1). As part of the development of analysis of energy absorption of composite structures, it is necessary to identify and measure dynamic modes of energy absorption. Differences in SEA between dynamic and static testing must be explained and a method developed for each material system to predict energy absorption behavior.

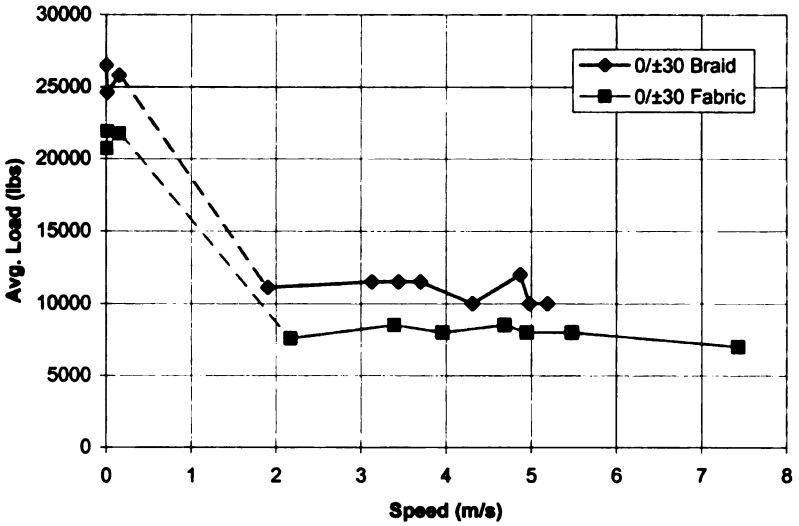

Figure 1.4 Average crush load vs. crush speed for glass fiber composite.

1.2 Literature review: Automotive crashworthiness and composite crash tubes.

1.2.1 Composite structures, weight savings, energy absorption.

Composite structures have been investigated for use in energy absorbing structures with the goal of reducing weight, simplifying assembly, and yet meeting requirements for crash energy absorption. Johnson Ref. (2) reported that polymeric composites used for large automotive structures offer advantages in weight reduction and part consolidation. Specifically, the Automotive Composite Consortium (ACC) Focal Project 1 Ford Escort front-end structure made from RTM (resin transfer molded) glass reinforced polymeric composite had a 25% weight improvement compared with the baseline Ford Escort steel structure. In addition, there was a reduction in the number of parts from 90 to 2. Botkin et al. Ref. (3) reported that ACC Focal Project 1 demonstrated that the front-end structure could absorb the necessary energy during crash. This project by the ACC demonstrated that a vehicle with a composite production feasible front structure could meet crash requirements with a reduction in weight and number of parts.

1.2.2 Design using tubes and SEA.

Efforts have been made to improve the efficiency of vehicle development by testing components and coupons rather than full vehicle structures. Browne et al. Ref. (4) stated that producing a variety of automotive front-end structures and crashing them under different conditions is time consuming. A convenient testing approach is to use simple crush tubes that are crushed using a plug initiator under static and dynamic conditions. The goal is to extrapolate the results of simpler tests to full-scale automobiles. It is reasoned that SEA, similar to elastic modulus, strength, density, etc., is a material property and crushing any well-defined structure under well-controlled

conditions will provide the SEA for a specific composite. Once the SEA is measured, the result could be applied to the design of full size structures.

1.2.3 SEA of metals and composites.

Measurement of SEA is routinely performed on metal and composite crush tubes. Composites crush tubes have been shown to have SEA that is frequently higher than steel and aluminum crush tubes. Derek Hull Ref. (5) reported that the SEA for mild steel crush tubes was approximately 28.5 J/gm and 22.5 J/gm for 50 mm cylinders with thicknesses of 1.0 to 2.0 mm. The Automotive Aluminum Crash Energy Management Manual Ref. (6) reported the SEA for a variety of aluminum tube architectures and aluminum alloys ranged from 16 J/gm to 29.5 J/gm. Hull also reported SEA for glass cloth-epoxy at 64 J/gm, 73.5 J/gm for chopped glass-polyester, 80 J/gm for oriented glass-polyester, and 130 J/gm for carbon fiber-epoxy. Hull also reported that composite crush tube geometry influences SEA in contrast with steel structures where the SEA seems to be independent of geometry. The composite specimens tested were similar to the steel and aluminum test tubes, 50 mm cylinder with wall thickness 1.0 to 2.0 mm. Hull Ref. (5) also stated that composites offer the potential for energy absorption structures with reduced weight based on the higher SEA observed for a range of composites. Frequently, damage modes, such as structural instability, which reduces energy absorption, are observed. For composites to absorb the maximum crash energy, they must crush progressively and in a controlled manner such as observed in well-designed metal structures.

1.2.4 Energy absorption modes of metals and composites.

Energy absorption by metals is primarily due to plastic deformation. The stress-strain plot for steel used for automotive structures typically has a plateau region corresponding to nearly constant loading with increasing strain. The region under this plot represents energy absorbed during progressive crush. When composites are tested as coupons, the stress-strain plot shows elastic behavior with little or no plastic deformation prior to fracture. Yet, when a plot of load-displacement for a composite tube (author generated) is examined, Figure 1.5, a plateau region of nearly constant load occurs that appears similar to that of a steel tube, Figure 1.2. Thornton Ref. (7) described composite material energy absorbing mechanisms and estimated the relative amount of energy absorption attributable to each of these mechanisms: the creation of fracture surfaces less than 1%, friction 25% to 50%, and the balance of energy absorbed due to plastic deformation of the matrix. Thornton also postulated that specific energy absorption was not affected by crush rate as long as damage modes remained the same. Farley et al. Ref. (8), in contrast to Thornton, stated that the coefficient of friction between the composite and the crushing surface is a function of crushing speed. This suggests that the effect of crush speed on SEA is dependent on the composite material properties. Farley stated that a friction related energy absorption mechanism is due to the relative motion between adjacent lamina bundles that slide against each other. Farley also stated that the magnitude of energy absorption attributable to these friction mechanisms had not been quantified. In a separate paper, Farley et al. Ref. (9) stated that the primary energy absorption mechanisms are fracturing of lamina bundles and crack growth and that friction is considered a secondary energy absorption mechanism. Mamalis et al. Ref. (10) estimated

friction energy absorption to be 50% of the energy absorbed. Mamalis found that the dynamic coefficient of friction to be higher than the static coefficient of friction. In a separate paper, Mamilis et al. Ref. (11) found energy absorption due to friction was from frictional resistance to axial sliding between adjacent laminae, frictional resistance to penetration of the annular debris wedge formed when a circular tube is crushed against a flat platen and frictional resistance to fronds sliding across the platen. Mamilis postulated that energy absorption due to friction mechanisms was the most significant of the various energy absorption mechanisms. It is apparent that a method to quantify energy absorption due to friction is needed.

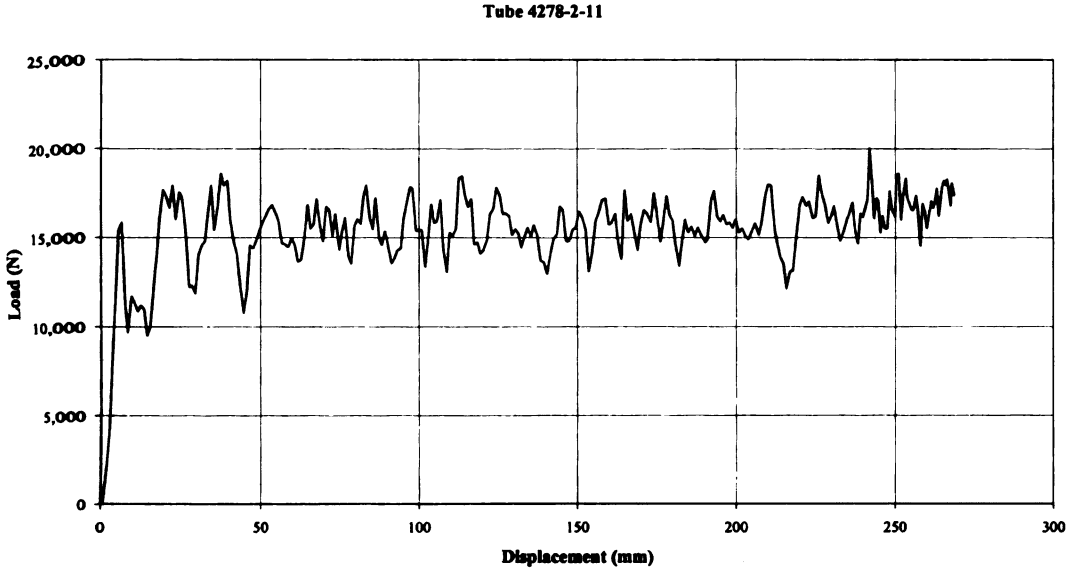

Figure 1.5 Typical load-displacement plot for carbon fiber crush tube.

1.2.5 Composite tube static vs. dynamic SEA.

Boeman and Caliskan Ref. (1) showed that the static crush load was approximately twice the dynamic load for crush speeds ranging from 2 m/sec to 7m/sec. This data is presented in Figure 1.4. Chadwick and Caliskan Ref. (12) observed that crushed vinyl-ester glass composite tubes absorbed energy by matrix cracking, fiber fracture, interfacial debonding, fiber pullout, and friction. Chadwick and Caliskan stated that analysis to determine which energy absorption mode absorbed more energy was impossible. Dynamic crushing was accomplished using a drop tower with an impact velocity of 4.99 m/s. Static testing was performed using a standard materials testing machine at 0.0508 m/min. The dynamic energy absorption was found to be significantly less than static energy absorption. The crush load was found to actually increase as the crush velocity decreases indicating energy absorption is indeed higher at lower velocities. Chadwick and Caliskan concluded that the difference in SEA between static and dynamic conditions was real and not a testing artifact. Johnson et al. Ref. (13) reported that the ratio between static and dynamic SEA varied from 0.64 to 1.70 depending on fiber architecture and tube wall thickness. However, the two fiber architectures that showed greater average dynamic SEA than average static SEA also had such a large experimental coefficient of variation that no conclusions could be drawn as to whether the static SEA was indeed less than the dynamic SEA. Crush morphology did not vary significantly between static and dynamic testing. This observation, in the light of Thornton's Ref. (7) conclusion that SEA would not vary between static and dynamic loading as long as damage modes were the same, would suggest that SEA should remain constant and not

vary as was observed by Johnson Ref. (13). Johnson's observations show that SEA is affected by crush speed and fiber architecture as well as tube thickness.

1.2.6 Strain rate dependence of steel & composite, dynamic & static composite SEA.

Bruce et al. Ref. (14) reported that a variety of automotive steels show strain rate dependence. Specifically, the tensile strength was measured to increase by 25 MPa to 50 MPa per magnitude increase in the strain rate. Weeks and Sun Ref. (15) reported that AS4/PEEK carbon fiber reinforced composite and an increase in tensile strength of 25 MPa per magnitude increase in the strain rate for [±30] laminate and no significant strain rate effect for unidirectional material tested in the fiber direction. Todo et al. Ref. (16) observed tensile strength increase of approximately 20 MPa per order of magnitude increase in the strain rate for both carbon fiber and glass fiber woven composites. These observations differ with the observed decrease in SEA between dynamic and static SEA reported by Boeman and Caliskan Ref. (1). A number of sources, as documented above, show that reduced dynamic SEA compared to static SEA is contrary to the observed unchanged or increase in strength with increase in strain rate.

1.2.7 Composite tube energy absorbing modes.

Johnson et al. Ref. (17, 18) identified energy dissipation modes as fiber tearing, resin fracture, inter-ply delamination and friction against the initiator for structural reaction injected molded (SRIM) glass tubes crushed under static and dynamic loading. Browne et al. Ref. (19) reported that energy dissipation in resin transfer molded (RTM) crush tubes loaded statically and dynamically was due to resin fracture, fiber fracture and pullout at the four tube corners, resin and resin-fiber interface fracture and inter-ply delamination and friction against the initiator. Browne also observed that among crush

tubes of different glass fiber architectures, the SEA was not proportional to volume fraction of glass in the composite. This suggests that fiber reinforcement fracture is not the primary energy absorbing mechanism. This also suggests that SEA may not be only a material property. Clearly, other researchers have observed multiple modes of energy absorption of crush tubes tested statically and dynamically without measuring the relative amount of energy absorption attributable to each energy-absorbing mode. A deeper understanding of energy absorption modes is necessary before the performance of designs of energy absorbing automotive structure designs are reliably predicted. "What are the energy absorbing modes and how much energy is absorbed by each mode?" is a question that must be answered for each material system and energy absorbing structure. To date, no one has reported a method to measure the SEA attributable to each energy-absorbing mode.

1.2.8 SEA of composites and energy absorbing modes, computer simulation.

Agaram et al. Ref. (20) reported using a continuum damage scheme to mimic the effect of damage as a localized stiffness reduction. This approach did not result in satisfactory prediction of energy absorption and requires the user to guess the constitutive behavior of the damage material. Agaram recommended that predictive computer codes be developed in conjunction with fundamental studies. The conclusion can be drawn that computer simulation and prediction of energy absorption due to composite crush cannot be accomplished until the fundamental energy absorption modes are identified, described, and quantified.

1.3 Statement of problem and objectives.

Prediction of dynamic and static energy absorption by composite automotive structures requires that all energy absorption modes be identified and quantified. The most expedient method of characterizing energy absorbing materials is to use relatively simple test coupons that are similar to actual structures so that a transfer function can be established to correlate testing of test structures with automotive structure designs.

The first part of this problem is addressed by the careful observation of tubes subjected to crush loading. Energy absorbing modes can be identified using observation. The second part of the problem, quantification, is more difficult because of the interaction between energy absorbing modes.

After energy absorption modes are identified, a test must be designed that will isolate the modes or groups of modes. It is hypothesized that the energy absorption due to friction mechanisms is one of the primary modes of energy absorption for composite materials. Further, the difference in friction energy absorption under static loading vs. dynamic loading is the primary reason that the SEA of a composite varies depending on loading speed.

The goal of the research presented is to identify and then measure the energy absorption of each identifiable, significant mode for both static and dynamic loading. The measurement of energy absorption is performed by conducting tests on simple test specimens. These simple tests are designed to isolate single or a limited number of energy absorption modes. The tests are performed under both static and dynamic loading. The energy absorption from each mode can be summed and compared with the total energy absorption observed in crush tests of a component structure with the same

composite materials, fiber architecture, and crush speed. The relative amount of energy absorbed due to friction can be compared between dynamic and static tests to demonstrate if and to what degree friction plays a part in energy absorption of a composite automotive structure.

1.4 Organization of Dissertation

The research presented within this thesis is divided into six chapters. The first chapter provides background information, literature search, and organization. The second chapter will describe damage of experimental crush tubes of two different composite systems. Within chapter 2 there will be experimental results of the full crush tube testing and of the individual simple tests that isolate energy absorption modes. Chapter 3 will characterize individual energy absorbing modes. Chapter 4 will show an analytical solution to the tapered trigger test. Chapter 5 will describe the role of friction in the crush tube damage and energy absorbing process. Chapter 6 will present conclusions and recommendations for future study and research.

CHAPTER 2. Damage of crush tube: Macroscopic and Microscopic

2.1 Materials

The two composite materials used in this study were fiberglass/vinyl ester resin and carbon fiber/vinyl ester. The glass fiber reinforcement was in the form of stitched mat. A schematic of the stitched mat is presented in Figure 2.1. Each ply of stitched unidirectional fiber tow glass mat has three layers of unidirectional glass fiber tows held together with stitching. The stitching holds the dry fiber tows together allowing handling prior to molding. The fiber tow direction of each layer is perpendicular to the adjacent layer. In this case, there are twice as many fibers oriented in the 0° direction as the 90° direction with the 0° direction parallel the longitudinal direction of the crush tubes. This configuration is designated in Table 2.1 as [0/90/0]. Six of these stitched plies were stacked together by wrapping the stitched glass fiber mat around the tube mold mandrel six times providing the desired fiber reinforcement build-up. The wrapping starts and ends on one side of the mandrel, resulting in a seam line. The tube was then molded using the resin transfer molding (RTM) process for the glass fiber composite crush tube used in this study.

Details of the glass fiber and carbon fiber crush tube geometry are presented in Table 2.2. All test tubes were manufactured with the RTM process at Excel Pattern Co. (Detroit, MI). In the RTM process, dry fiber reinforcement is placed in a mold which is then closed. Liquid resin is then injected into the heated, closed mold and allowed to cure. After cure, the molded part is removed from the mold, trimmed of resin flash, and machined to final length.

The carbon fiber reinforcement is formed by a machine that braids carbon fiber tows into a ply with axial tows oriented parallel with the longitudinal axis of the crush tubes and angle plies oriented $\pm 45°$ from the longitudinal axis of the crush tubes. One feature of the braiding process is that there were no seams in the plies. A schematic of this reinforcement architecture is presented in Figure 2.2. Two such plies were used to fabricate the carbon fiber composite crush tubes used in this study. The braiding process is being considered because it is a high-speed method of fiber architecture manufacture and is easily applied to tubular structures with little scrap. Like the glass fiber composite, the carbon fiber crush composite tubes were manufactured using the RTM process at Excel Pattern (Detroit, MI).

Table 2.1 Composite tube characteristics.

Reinforcement	Matrix	Architecture	Fiber Content (wt. %)	Fiber Volume (%)	Laminate Density (gm/cm^3)
Glass Fiber Knytex/Hexcel	Ashland Q-6050 Vinyl Ester	$[0/90/0]_6$ Stitched Mat	65.9	46.4	1.800
Carbon Fiber Fortafil 503 80k Axial Grafil 12k Off-Axis	Ashland Hetron 922 Vinyl Ester	Tri-axial Braid $[0/\pm 45]_2$	54.5	43.0	1.419

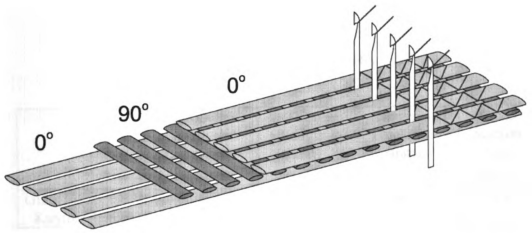

Figure 2.1 Stitched mat schematic.

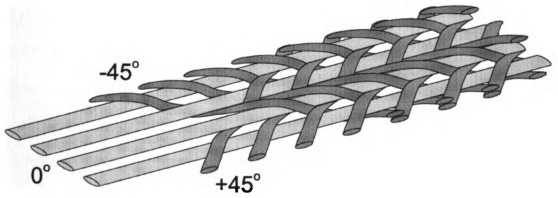

Figure 2.2 Tri-axial braid schematic.

Table 2.2 Crush tube geometry.

	Tube Outside Width and Depth (mm)	Tube Length (mm)	Nominal Thickness (mm)	Cross Section Area (cm^2)
Glass Fiber Knytex/Hexcel	55.5	229	4.7	10.1
Carbon Fiber Fortafil 503 80k Axial Grafil 12k Off-Axis	55.5	356	2.4	4.74

2.2 Test Methods and Facilities

2.2.1 Static Crush Tube Tests

All static crush tube testing was performed at the Ford Scientific Research Laboratory using an MTS 810 (servo hydraulic) material test system at ambient room conditions. The MTS load frame has a 222 KN (50,000 lb.) capacity and uses a 22.2 KN (5,000 lb.) load cell. All specimen testing and data was controlled, recorded and analyzed through the use of the SinTech software package, Test Works, on a Dell personal computer. The crosshead speed was 0.0508 m/min (2 inches/min).

Five glass fiber composite tubes were tested with the standard plug type trigger with a fillet radius of 6 mm (Figure 2.3). The trigger for each composite tube, glass fiber and carbon fiber, was machined to fit inside the tube with a tolerance of 1 mm or less. The glass fiber composite tubes were of square cross section with rounded corners (outside radius 12 mm). The upper end of the tube was contacted directly by the upper platen and was not constrained from movement transverse to the axis of the crush tube. The plug trigger was placed on the lower platen and was also unconstrained from transverse displacement. A schematic of the tube crush testing is presented in Figure 2.4. In all cases, no transverse displacement of either end of the crush tube was observed. No dynamic tests were conducted with the glass fiber composite crush tubes.

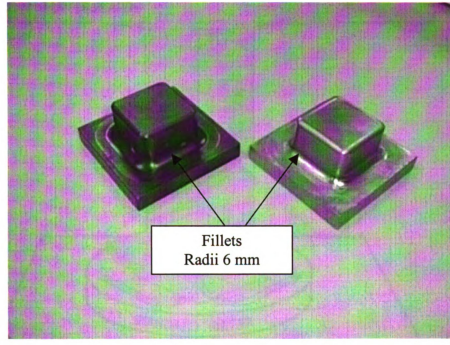

Figure 2.3 Standard crush tube triggers.

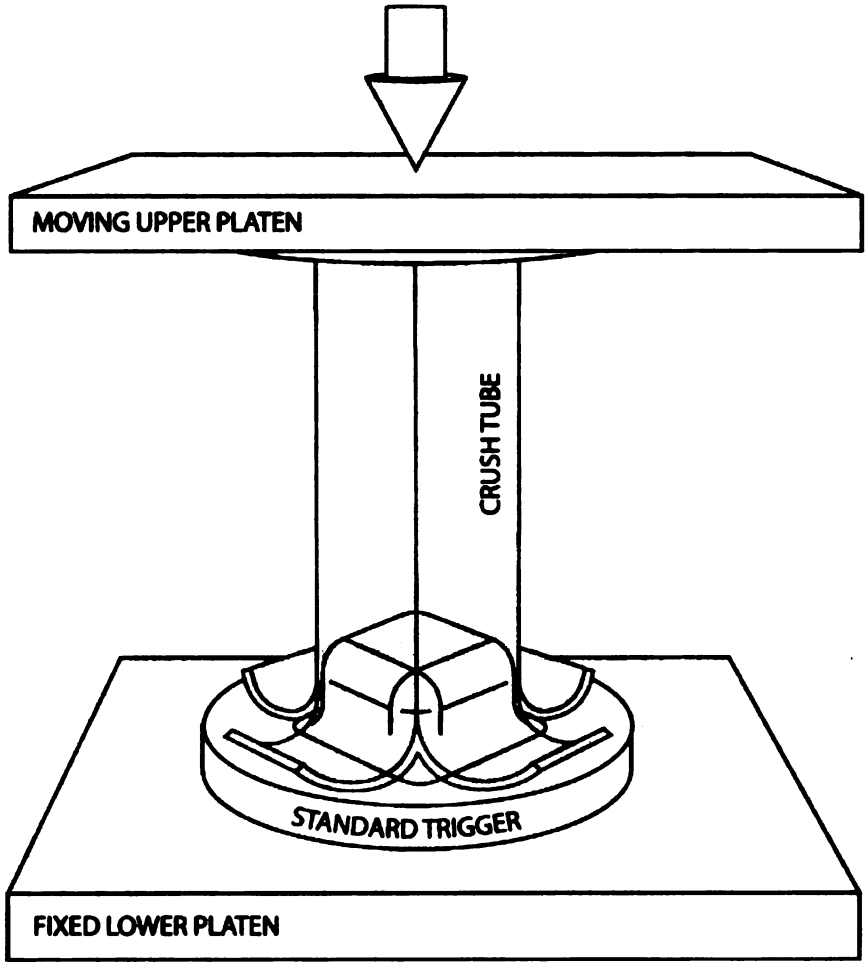

Figure 2.4 Tube crush test schematic.

2.2.2 Dynamic Carbon Fiber Composite Crush Tube Tests

Dynamic testing was performed using the Test Machine for Automotive Crashworthiness (TMAC) located at the National Transportation Research Center, Oak Ridge National Laboratory, Tennessee. The engineer responsible for its operation, Dr. J. Michael Starbuck of Oak Ridge National Laboratory, wrote the description of the TMAC presented below.

Typically standard test machines are employed for experiments at quasi-static rates whereas drop towers or impact sleds are the convention for dynamic rates. These two approaches bound a regime within which data, for experiments at constant impact velocity, are not available by conventional experimental practice. This regime is termed in this thesis the intermediate-rate regime and is defined by impact velocities ranging from 1 m/s to 5 m/s. Investigation of rate effects within this regime requires experimental equipment that can supply a large force with constant velocity within these rates. Using a drop tower or sled at intermediate rates, although technically possible, is problematic due to the prohibitively large mass required to maintain constant velocity during the crush. Consequently, the Oak Ridge National Laboratory (ORNL) and the Automotive Composites Consortium (ACC) collaborated to define specifications for a unique experimental apparatus that mitigates the shortcomings of existing equipment. MTS Systems Corporation designed and built the servo-hydraulic test machine, referred to as the TMAC. As shown in Figure 2.5, TMAC is uniquely capable of conducting controlled progressive crush tests at constant velocity in the intermediate velocity range (i.e., less than 5m/s) owing to the large energy available at those rates and to the sophisticated

simulation and control software that permits velocity uniformity to within 10%. The specifications for the machine, presented in Figure 2.6, are as follows:

- No-load velocity of 8 m/s constant to within 10% over 115 mm.
- Sustained crush force of 133 KN at 6 m/s constant to within 10% over 115 mm.
- Sustained crush force of 267 KN at 4 m/s constant to within 10% over 115 mm.

A LabView program was developed to obtain the test data from two high-speed data acquisition (DAQ) modules—a 12-bit synchronous card with four channels, and a 16-bit asynchronous card with eight channels. The program synchronizes the data and is triggered from the TMAC control software that initiates the impact. One card has higher signal resolution at the expense of temporal resolution and synchronicity, while the other card sacrifices signal resolution for fast, synchronous measurements. The merits of the two cards are being assessed.

The functionality of the data system was demonstrated and will be refined and updated as future test requirements are defined, including the capability for recording strain gage signals. The current DAQ configuration reads one LVDT for displacement, a load cell and load washer for force, and two accelerometers. The accelerometers were chosen to provide 1 g/V sensitivity and 10 g/V sensitivity. 1 g/V is equivalent to 9.81 meter/sec^2/volt. For this study, accelerometer data was not used. The location of the load cell and load washer is presented in Figure 2.7.

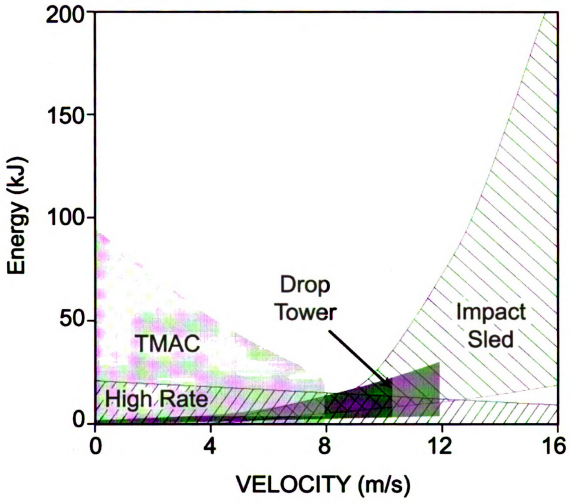

Figure 2.5 Energy plot indicating TMAC's unique capability of supplying enough energy at the intermediate rates for controlled, constant-velocity crush.

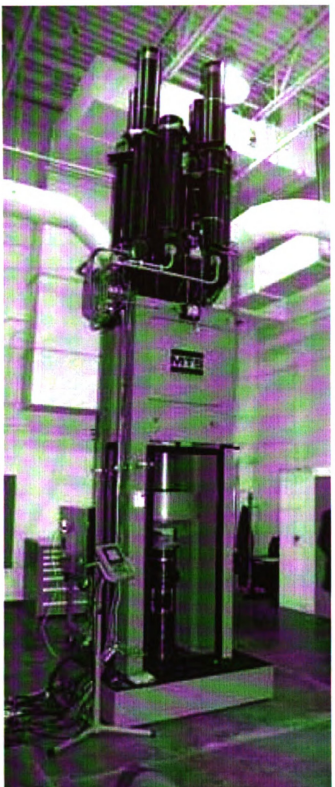

Figure 2.6 TMAC installation at NTRC.

114 m

343 m

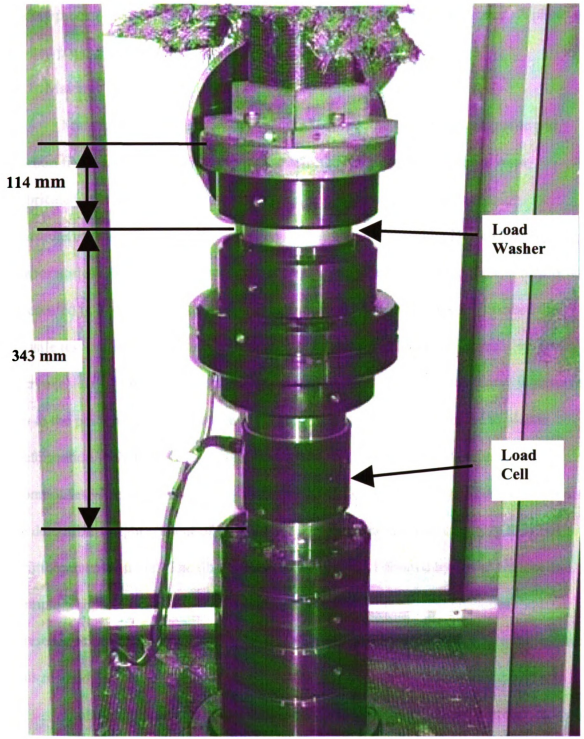

Figure 2.7 Load cell and load washer location on TMAC.

The plug trigger used in the crush testing was fixed to the TMAC platen as a safety precaution per National Transportation Research Center requirements. A photo of bolted plug initiator is presented in Figure 2.8.

2.3 Material Testing

Material property tests were conducted on both the glass fiber composite and carbon fiber composite to characterize the selected test materials. Plaques were fabricated at the same time as the crush tubes and were used for the materials characterization. Plaque characterization testing was performed by Delsen Testing Laboratories Glendale, California. Glass fiber composite characterization test results are presented in Ref. (21) and summarized in Table 2.3. A typical glass fiber composite tensile test in the 90° direction is presented in Figure 2.9. Note that the stress vs. strain curve is nearly linear over the full range of stress. An essentially linear curve is observed up to the point of material fracture indicating little energy absorption due to plastic deformation. Fiber and resin weight content for both glass fiber and carbon fiber composites were determined using method ASTM D2584, Ref. (22). This method is used to determine weight content of resin by burning away the resin leaving only the fiber reinforcement residue. The fiber residue is weighed and divided by initial composite sample weight to determine the fiber weight fraction. This method presumes the presence of only fiber and matrix. Fiber sizing and void content are not determined using this method.

Carbon fiber composite characterization test results are presented in Ref. (23) and summarized in Table 2.4. A typical carbon fiber tensile load-displacement plot in the 90° direction is presented in Figure 2.10. As with the glass fiber composite, the curve is

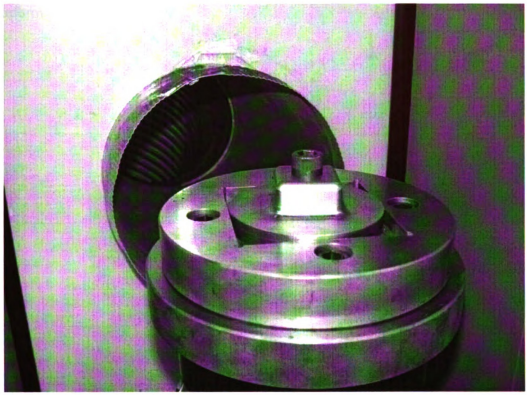

Figure 2.8 TMAC showing bolted crush trigger.

nearly

plasti

nearly linear up to material fracture indicating that there is little energy absorption due to plastic deformation.

Table 2.3 Glass fiber composite plaque mechanical properties.

Direction	Stress, Max (MPa)	Modulus (GPa)	Poisson's Ratio	Strain, Max (%)	Fracture Energy (J/cm^3)
Tensile					
0°	492	28.3	0.176	2.41	3.60
90°	189	17.1	0.107	1.34	0.791
Compressive					
0°	501	27.2		1.86	2.62
90°	203	18.0		1.15	0.669
Shear					
	64.0	4.46			
Strain Energy Release Rate	G_{Ic} (J/cm^2)	G_{IIc} (J/cm^2)			
	0.146	0.123			
Physical Properties	Density (gm/cm^3)	Fiber Weight Content (%)	Resin Weight Content (%)		
	1.8002	65.9	32.1		

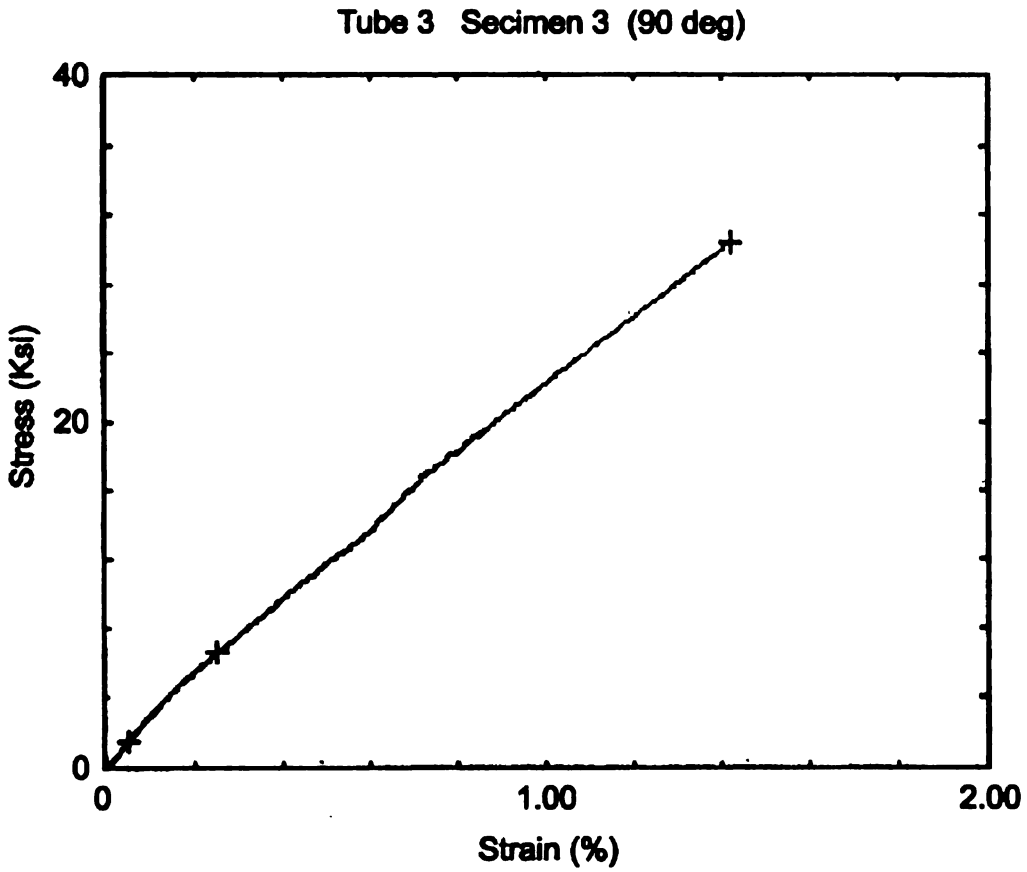

Figure 2.9 Typical glass fiber composite tensile load-displacement curve.

Table 2.4 Carbon fiber plaque composite mechanical properties.

Direction	Stress, Max (MPa)	Modulus (GPa)	Poisson's Ratio	Strain, Max (%)	Fracture Energy (J/cm^3)
Tensile					
0°	654	60.33	0.562	1.08	3.623
90°	65.2	8.756	0.109	1.20	0.475
Compressive					
0°	376	59.71	--	0.66	1.289
90°	91.7	10.06	--	0.89	0.404
Short Beam Shear					
	43.1				
Strain Energy Release Rate	G_{IIc} (J/cm^2)				
	0.159				
Physical Properties	Density (gm/cm^3)	Fiber Weight Content (%)	Resin Weight Content (%)		
Fiber	1.80				
Resin	1.14				
Composite	1.42	54.74	45.26		

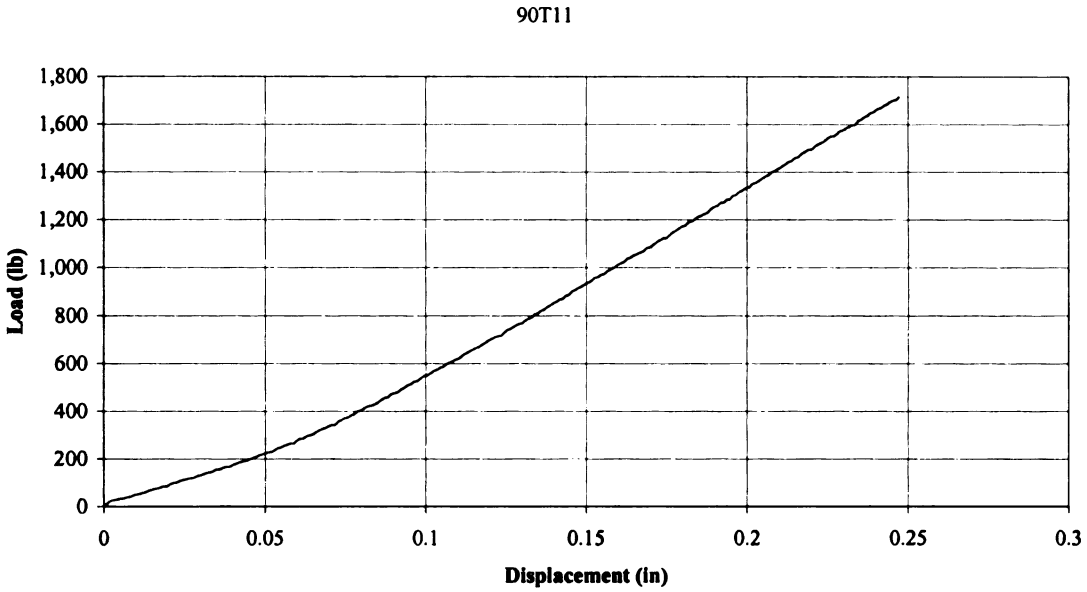

Figure 2.10 Typical carbon fiber composite 90° tensile load-displacement curve.

2.4 Quasi-Static Crush Tube Test Results

2.4.1 Introductory Remarks:

Design of composite structures requires knowledge of the physical properties of the composite material. This knowledge is obtained by experimental material characterization of small coupons to determine mechanical properties such as elastic modulus, Poisson's ratio, density, strength (tensile, compressive, shear), etc. Changing the fiber material and architecture, resin, relative fiber content, and manufacturing method can vary each of these properties. Typically, test coupons are fabricated from flat plaques because test coupon fabrication cost is low and the tests are simple to perform. Coupon testing is usually performed at quasi-static loading rates. Dynamic testing is less frequently performed on test coupons. However, dynamic testing is routinely performed on full- and sub-structures. A full structure test would be a crash test of an entire automobile or major portion of an automobile such as a frame. A sub-structure test is performed on small part of a full structure such as the front portion of an automobile frame. Small test structures, usually tubes such as those shown in Figure 2.11, are tested both statically and dynamically to determine the SEA of the material at a given crush speed. Tubes are fabricated in various cross sections such as circular, hexagonal, octangular, rectangular, or square. The primary reason for using rectangular tubes to characterize SEA is for convenience and similarity with typical automotive energy absorbing structures, which are tubular and rectangular. A simple rectangular tube is more similar to the front rail used in the crash energy absorbing front structure of an automobile than a flat coupon. The selection of square crush tubes for this study was because of their availability and the existence of previous experimental data.

Figure 2.11 Typical glass fiber composite crush tube.

2.4.2 Glass Fiber Composite Quasi-Static Crush Tube Test Results:

Test results for the glass fiber tubes are presented in Table 2.5. A typical plot of load-displacement is presented in Figure 2.12. Note the initial increase in load to a local maximum at which time the load drops to a lower level. Subsequently, the load varies about a plateau load level throughout the crush process. The plateau region of the load-displacement curve corresponds to progressive crushing of the crush tube. For the five glass fiber crush tubes tested, the average SEA was 20.62 J/gm. All testing of glass fiber crush tubes reported in this chapter were conducted with the standard crush trigger. Plots of the five glass fiber composite static crush tests are presented in Appendix A.

Table 2.5 Glass fiber composite crush tube SEA, quasi-static loading rate (0.0508 m/min).

Coupon	Ave. Cross Section Area (cm^2)	Max. Load (N)	Ave. Load (N)	Crush Distance (cm)	Total Energy Absorbed (J)	SEA (J/gm)
1A	9.95	41,350	32,140	12.7	4,082	17.96
2A	9.90	51,530	36,450	12.7	4,630	20.48
3A	9.74	46,920	38,640	12.7	4,907	22.05
3B	9.90	45,830	38,260	12.7	4,860	21.49
13B	9.91	49,940	37,680	12.7	4,785	21.14
Ave.	9.88	47,110	36,630	12.7	4,653	20.62

Note: SEA based on material density of 1.8002 gm/cm^3.

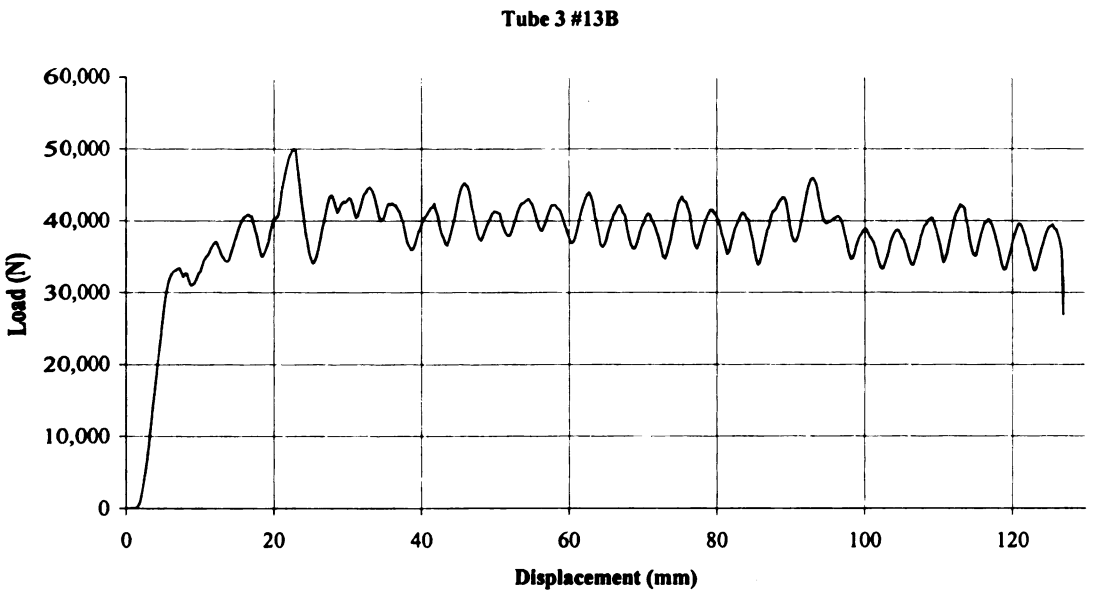

Figure 2.12 Typical glass fiber composite quasi-static crush tube.

2.4.3 Carbon Fiber Composite Crush Tube Test Results

2.4.3.1 Carbon Fiber Composite Crush Tube Quasi-Static Test Results

The carbon fiber/vinyl ester composite crush tubes were similar in geometry to the glass fiber composite tubes but with a thinner wall thickness. The carbon fiber composite tube outer section dimensions, presented in Table 2.2, were the same as the glass fiber composite tubes but with a different overall length. Quasi-static test results for the carbon fiber crush tubes are presented in Table 2.6. A typical quasi-static load-displacement plot is presented in Figure 2.13. Plots of the five carbon fiber composite quasi-static crush tests are presented in Appendix B. The appearance of the carbon fiber composite tube quasi-static load-displacement curve is similar to that observed for the quasi-static loaded glass fiber composite tubes. A plateau load follows an initial increase in load with variation above and below the average plateau load.

2.4.3.2 Carbon Fiber Composite Crush Tube Dynamic Test Results

The dynamic test results for the carbon fiber composite are presented in Table 2.7. A typical dynamic load-displacement plot is presented in Figure 2.14. Plots of the five carbon fiber composite dynamic crush tests are presented in Appendix B. Note that the average plateau load is lower for the dynamic loaded carbon fiber composite, 15,650 N, than the same material loaded quasi-statically, 21,510 N. The average SEA for dynamic loading was 23.8 J/gm vs. 30.4 J/gm for quasi-static loading. This is consistent with the observation reported in literature search of Chapter 1 that dynamic loading results in a lower SEA than static loading.

Table 2.6 Carbon fiber composite crush tube SEA, quasi-static loading rate (0.0508 m/min).

Coupon	Ave. Cross Section Area (cm^2)	Max. Load (N)	Ave. Load (N)	Crush Distance (cm)	Total Energy Absorbed (J)	SEA (J/gm)
4278-2-1	5.26	22,300	18,170	12.4	2,250	24.25
4278-2-4	4.88	28,130	21,450	12.4	2,660	30.85
4278-2-5	4.91	29,390	23,320	12.4	2,890	33.32
4278-2-9	4.93	27,590	22,260	12.4	2,760	31.66
4278-2-17	4.92	29,210	22,330	12.4	2,770	31.87
Ave.	4.98	27,320	21,510	12.4	2,670	30.39

Note: SEA based on material density of 1.42 gm/cm^3.

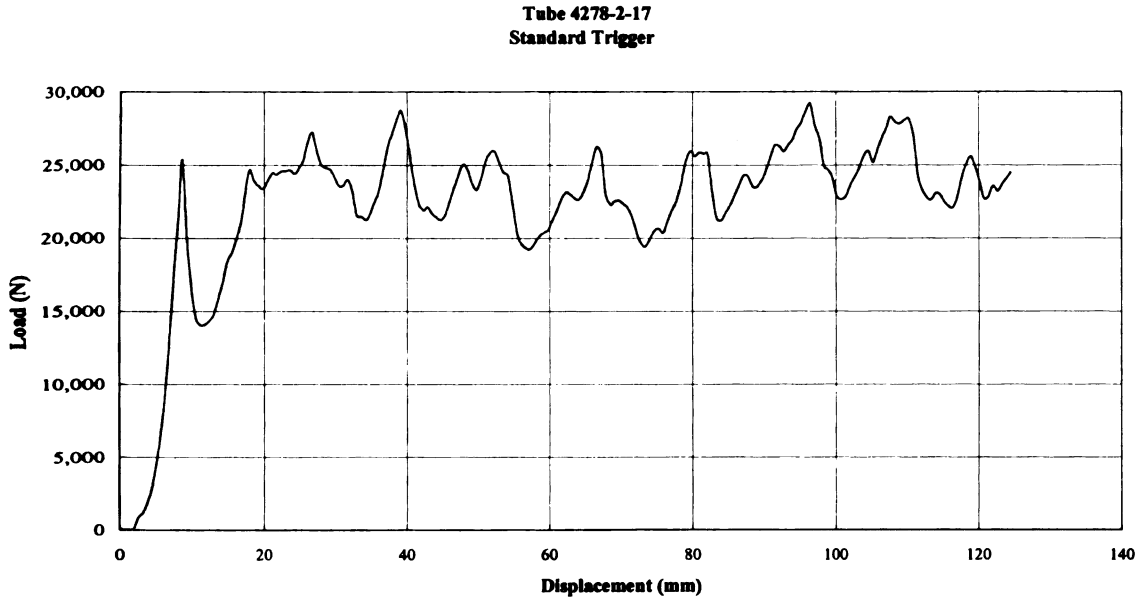

Figure 2.13 Typical carbon fiber tube quasi-static load-displacement plot.

Table 2.7 Carbon fiber composite crush tube SEA dynamic loading.

Coupon	Load Rate (m/sec)	Ave. Cross Section Area (cm^2)	Max. Load (N)	Ave. Load (N)	Crush Distance (cm)	Total Energy Absorbed (J)	SEA (J/gm)
4278-2-2	2.0	4.68	20,620	16,110	26.6	4,280	24.2
4278-2-3	2.0	4.84	22,060	16,100	26.8	4,330	23.5
4278-2-11	2.0	4.51	20,040	15,340	26.9	4,130	24.0
4278-2-12	2.0	4.53	20,890	15,030	27.3	4,100	23.4
4278-2-16	2.0	4.65	22,130	15,680	27.1	4,250	23.8
Ave.		4.64	21,150	15,650	26.9	4,220	23.8

Notes: SEA based on material density of 1.42 gm/cm^3.

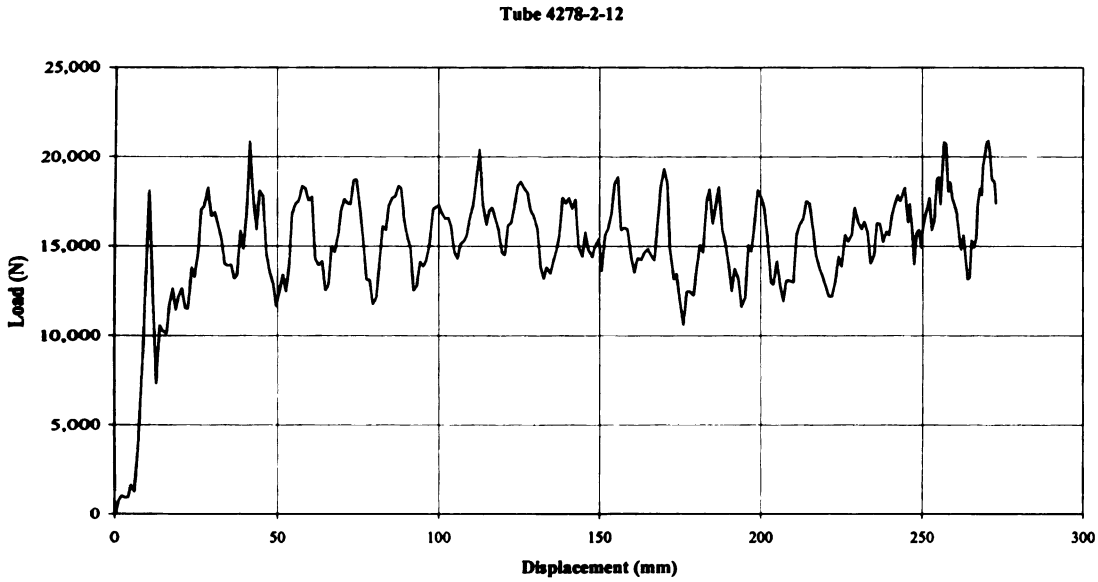

Figure 2.14 Typical carbon fiber crush tube dynamic load-displacement plot.

2.5 Macroscopic Damage Modes

As a tube is crushed, several modes of energy absorption are evident. Delamination, fiber and resin fracture, damage due to bending, and sliding friction of the composite against the plug trigger or platen were observed. Each of these energy absorption modes absorbs varying amounts of energy depending on crush speed, environmental conditions, and composite composition.

During a quasi-static or dynamically loaded tube crush test interlaminar shear loads occur when the composite is forced to bend over the fillet transition between the plug and base plane of the plug trigger that is perpendicular with the crush tube axis and crush direction. Delamination occurs when layers, or plies, of composite separate due to interlaminar shearing forces. Delamination can be seen in a multi-ply quasi-statically loaded crushed glass fiber crush tube shown in Figure 2.15. Careful examination reveals that there are six separate composite plies that have separated.

A photo of a quasi-statically compressed carbon fiber composite crush tube is presented in Figure 2.16. A photo of a dynamically compressed carbon fiber composite crush tube is presented in Figure 2.17. Careful examination shows two plies present in the damaged carbon fiber composite consistent with the fiber architecture of the carbon fiber composite. The appearance of the quasi-statically compressed and dynamically compressed carbon fiber composite crush tubes are visually similar and suggest similar energy absorption modes. These are: fiber fracture at the tube corners, delamination, and matrix damage.

During crush, the damage process zone advances intermittently as fibers are broken and fiber bundles fracture. Cracks advance to the next fiber or fiber bundle and

crack propagation is arrested until the building forces due to crush loading become greater than the strength of the fibers. Tensile forces pull the composite material apart at the corners as the tube is forced over the trigger. The increasing perimeter of the trigger that the composite tube is forced over loads the composite in tension similar to the tensile loading imposed during a tensile test of a flat coupon. In the case of the composite tube, this tensile loading is perpendicular, or 90°, to the axis of the tube. The tensile strength in the 90° material direction as reported in Table 2.1 for the glass fiber composite and Table 2.2 for the carbon fiber composite is in the same material direction perpendicular to the crush tube axis for both composites.

Damage to the composite due to bending was due to general matrix fracture of the composite as it was forced over the fillets of the crush trigger. Fracture of the composite occurs when the in-plane tension loads exceed the tensile strength of the composite. The tensile strength of the composite is usually determined by the fiber strength, which is significantly higher than the resin matrix. As the composite tube sides are forced over the trigger fillets, bending causes tensile force in the 0° direction on the inside of the tube adjacent to the trigger and compressive loading on the outside of the tube. Because the fiber is significantly stronger in tension than the matrix, the matrix cracks and delamination occurs. The damage to the matrix prevents the transfer of load between fibers and the fibers are unloaded. This was observed for both glass fiber composite and carbon fiber composite. As a result, there was fiber fracture at the tube corners where high tensile loads were imposed. The bending loads were sufficient to cause widespread matrix fracture between fibers with little fiber damage observed in the tube sides resulting in the loss of structural integrity of composite material.

Energy absorption due to friction was inferred by the physics of the crush tube test. It is readily observed that the composite is forced to slide over the trigger fillets, sides and base. Measurement of this energy absorption mode is the focus of this research.

2.6 Microscopic Damage Modes

Matrix damage is mostly the result of bending of the composite as the composite crush tube is forced against a flat platen or over a plug trigger. As the composite is crushed, bending forces cause the polymer matrix to fracture. The cracks found in the matrix are closely spaced, typically the spacing between fiber tows. This is demonstrated by the peaks of the load in the load-displacement plots presented in Appendix B. The fiber tow spacing for both the glass fiber and carbon fiber composites was measured to be 4-5 mm. Examination of the load-displacement plots shows major load peaks that are approximately 4 mm to 5 mm apart. Minor load peaks are closer together and are probably due to individual fiber tow fracture at the tube corners. Major peak loads are probably due to crack arrest at all four tube corners followed by near simultaneous fiber tow fracture with an abrupt load drop at all four corners allowing the crack to propagate to the next set of corner fiber tows where it arrests until the load builds to the ultimate strength of all four fiber tows with the process repeating progressively as tube crush continues.

Additional microscopic damage modes such as fiber/matrix debonding and fiber/matrix pullout are probably present. These damage modes are not examined in this research, as each microscopic damage mode may be present with or are a part of more than one macroscopic energy absorption mode confounding efforts to isolate and measure

energy absorption by each microscopic damage mode. Such investigation is left to future research.

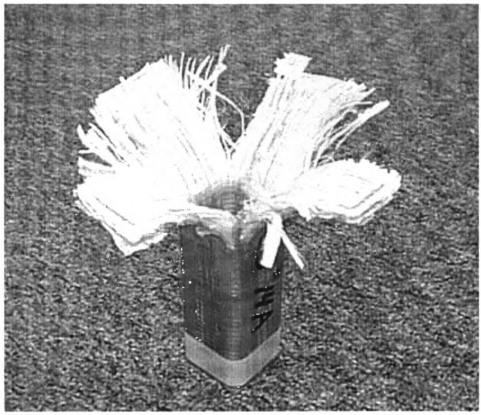

Figure 2.15 Quasi-statically compressed glass fiber tube showing delamination, corner splitting, and matrix damage due to bending.

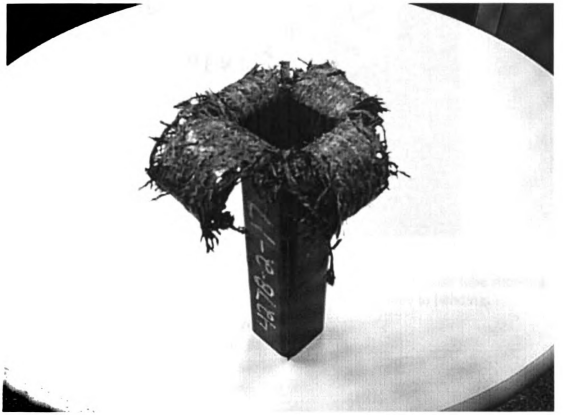

Figure 2.16 Quasi-statically compressed carbon fiber tube showing delamination, corner splitting and matrix damage due to bending.

Figure 2.17 Dynamically compressed carbon fiber composite crush tube showing delamination, corner splitting and matrix damage due to bending.

CHAPTER 3. Characterization of Individual Damage Modes

3.1 Introductory remarks

It is necessary to identify the energy absorption modes and quantify their magnitudes for a given crush rate before the energy absorption of a particular composite material is understood. The first part of this problem was addressed in Chapter 2 with the careful observation of tubes subjected to crush loading. Energy absorbing modes were identified using observation. The second part of the problem, quantification of energy absorption by mode, is more difficult because of the coupling among energy absorbing modes.

During crush, the peak load is determined by the force required to fracture the glass or carbon tows in the corner regions of the crush tube. At load levels below the strength of the glass or carbon corner tows, other damage occurs in the composite tube such as delamination and matrix damage due to bending. Energy absorption due to sliding friction is dependent on the load normal to the sliding surface.

The local load maximums that occur during tube crush, such as shown in Figure 2.13, suggest that not all energy absorption modes are occurring simultaneously. If this is so, it should be possible to isolate and measure energy absorption modes. Also, the composite systems studied show linear or near-linear behavior.

It is the purpose of this research to determine if the relative energy absorption of each mode can be separated and measured for both quasi-static and dynamic load rates. As discussed in Chapter 1, there is a strain rate effect that causes an increase in elastic modulus and tensile strength of many composites. The effect described in Chapter 1 is that for composite crush tubes the dynamic crush load and energy absorption are

significantly reduced relative to static loading and remains relatively constant over a range of dynamic load rates.

After energy absorption modes are identified, a test must be designed that will isolate and measure each mode or groups of energy absorption modes. It is hypothesized that the energy absorption due to friction mechanisms is one of the primary modes of energy absorption for composite materials. It is further hypothesized that the difference in friction energy absorption under quasi-static loading vs. dynamic loading is the primary reason that the SEA of a composite varies depending on loading speed. Friction will be addressed in detail in Chapter 5.

3.2 Crush Tube Testing

3.2.1 General SEA Calculation

Testing of crush tubes is accomplished by crushing the tube between the platens of a test machine in a controlled manner. Displacement and load data obtained in this type of test is used to calculate specific energy absorption (SEA). SEA is calculated by integrating the load-displacement curve to determine total energy absorbed and then dividing the total energy absorbed by the mass of the crushed portion of the tube. The mass of the tube that is crushed is determined by calculating the volume of the tube that is crushed and then multiplying the crush volume by the composite density. The crush volume was determined by multiplying the cross section area by the measured displacement obtained during testing. The cross section area of the tube is calculated using measurements of the cross section geometry.

3.2.2 Crush Triggers

Experience has shown that it is advantageous to use a crush trigger to start the crush process of the composite. If no trigger is used, high loads can occur before crushing begins resulting in little energy absorption due to structural instability or overload. The maximum load for the glass fiber tube base on material compressive strength was calculated to be 50.6 ken and 17.8 ken for the carbon fiber composite tube. See Tables 2.2, 2.3, and 2.4 for tube characteristics and compressive strength for glass and carbon fiber composite material. One type of simple crush trigger is a bevel at the leading edge of the crush tube as shown in Figure 3.1. For this study, a 45° bevel was machined in one end of each crush tube shown in Figure 3.2. The crush process begins at the point of the bevel at a relatively low load because of the small cross section. Once the crush process zone is established the tube crushes progressively through the duration of the test at a relatively constant load.

Figure 3.1 Glass fiber composite tube showing bevel trigger.

A plug type trigger is frequently used with the beveled tube that results in the crush process zone being established at a load plateau level below the tube buckle load. A crush tube with a plug trigger in place is shown in Figure 3.3. The crush trigger consists of a short steel plug that closely fits inside the tube and a base perpendicular to the axis of the tube with a fillet at the intersection of the plug and crush trigger base. The clearance between the composite crush tubes, both glass fiber and carbon fiber, was 1 mm. A drawing of the standard plug trigger is presented in Figure 3.4.

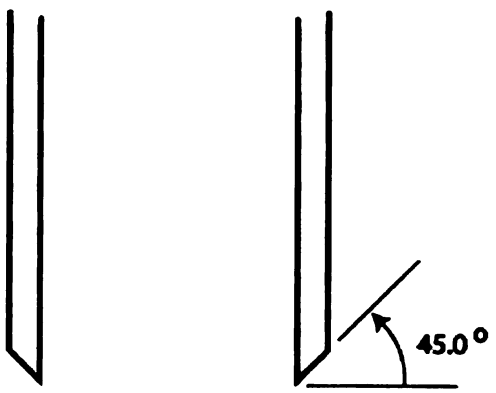

Figure 3.2 Crush tube bevel detail.

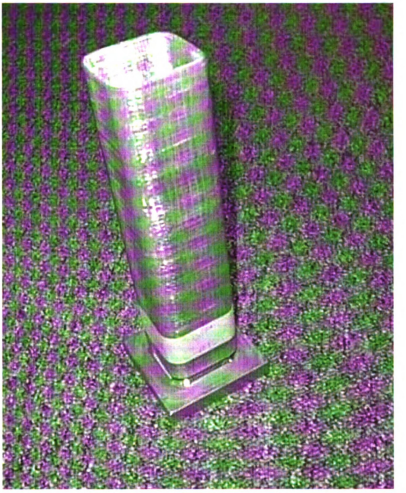

Figure 3.3 Glass fiber composite tube with bevel and plug trigger.

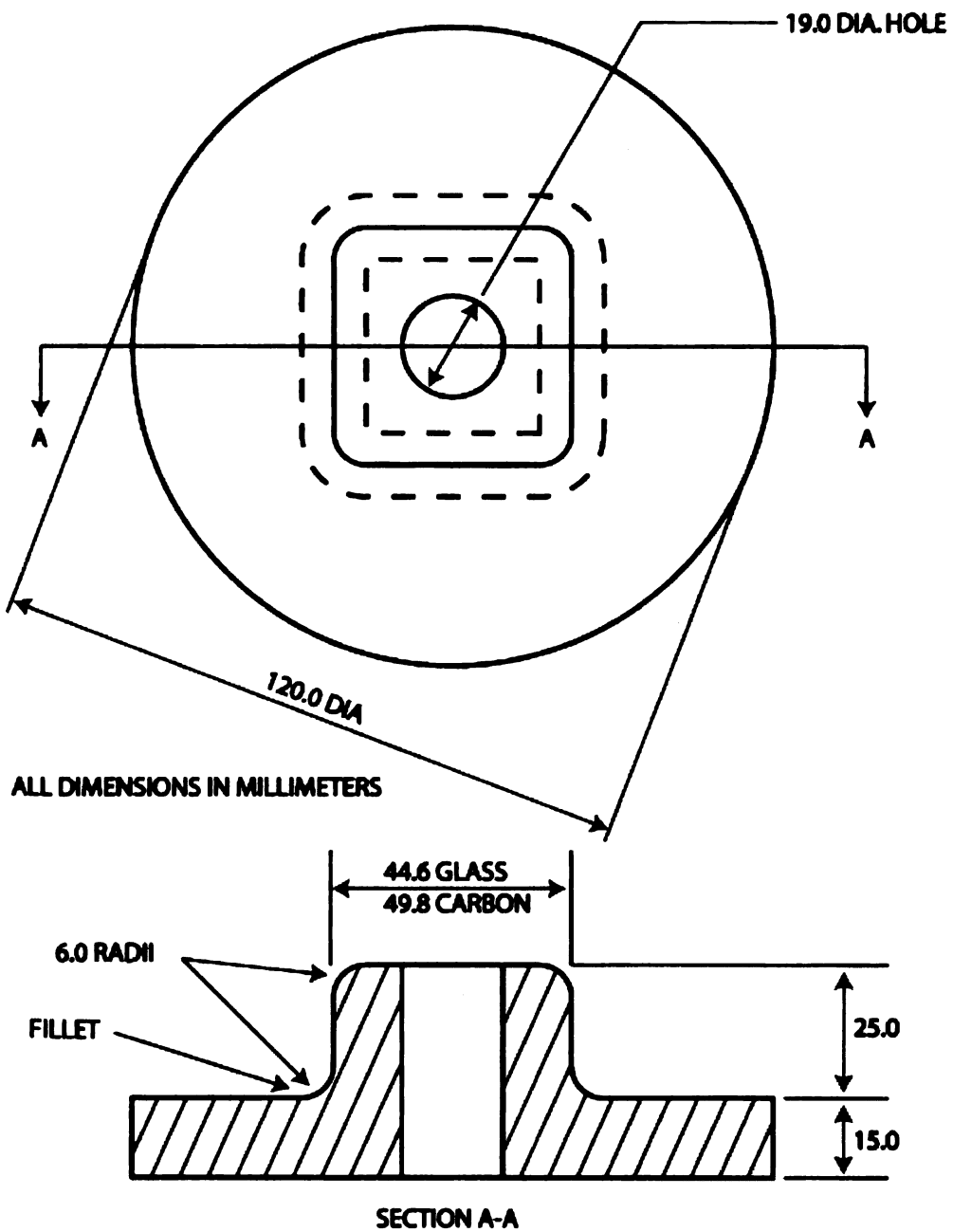

Figure 3.4 Drawing of standard plug trigger.

3.2.3 Crush Tube Energy Absorbing Modes

A typical glass fiber composite tube crush test specimen is presented in Figure 3.5. A carbon fiber composite crush tube specimen is presented in Figure 3.6. Note that there is fracture of the composite at the corners and damage of the resin matrix. The flat portions of the tube between the corners have extensively damaged resin matrix resulting in a loss of bending stiffness of the composite. Also visible is delamination of the six plies of the glass fiber composite tube in Figure 3.5 and two plies of the carbon fiber composite tube visible in Figure 3.6.

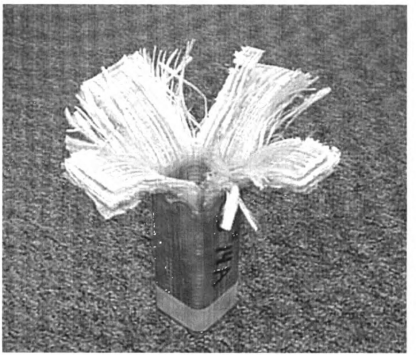

Figure 3.5 Typical quasi-statically compressed glass fiber composite tube.

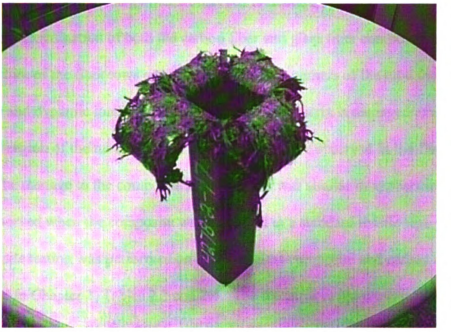

Figure 3.6 Typical quasi-statically compressed carbon fiber composite tube.

3.2.3.1 Corner splitting

The most apparent energy mode observed is fracture of the crush tube at the four tube corners. Examination of both the carbon fiber and glass fiber composite tubes reveals fracture of the fiber tows occurs only at the four corners of the tube for both quasi-static and dynamic loading. While the composite matrix is damaged extensively in the crushed region of the tube, no fractured fiber tows were observed in the flat sides of the tube. The damage to the composite at the corners was similar in appearance to the damage observed when the composite was subjected to a standard tensile test.

Tensile testing was performed on both the glass composite and carbon composite and reported in Chapter 2, Tables 2.3 and 2.4. The fractures in the crush tube corners are similar to those observed in the 90° tensile tests. The energy density at fracture measured at 0.791 J/cm^3 for the glass fiber composite (Table 2.3) and 0.475 J/cm^3 for the carbon fiber composite (Table 2.4). Strain energy density is determined by mathematically integrating strain over the affected material volume. Experimentally, the strain energy density is determined by mathematically integrating strain energy over the affected material volume.

The total corner splitting energy absorption of the crush tube is calculated by multiplying the tube corner volume by the tensile strain energy density at fracture. The SEA attributable to corner splitting energy is calculated by dividing total corner splitting energy by the total volume of the crushed tube. The corner splitting SEA is presented in Table 3.1 for glass fiber and Table 3.2 carbon fiber composite.

Table 3.1 Glass fiber composite corner splitting SEA.

Tube #	Corner Area (cm^2)	Crush Length (cm)	Fracture Energy (J/cm^3)	Tube Crush Mass (gm)	SEA (J/gm)
1A	2.54	12.7	0.791	227	0.112
2A	2.50	12.7	0.791	226	0.111
3A	2.49	12.7	0.791	223	0.112
3B	2.50	12.7	0.791	226	0.111
13B	2.50	12.7	0.791	227	0.111
Average	2.51	12.7	0.791	226	0.111

Table 3.2 Carbon fiber composite corner splitting SEA.

Tube #	Corner Area (cm^2)	Crush Length (cm)	Fracture Energy (J/cm^3)	Tube Crush Mass (gm)	SEA (J/gm)
4278-2-1	1.01	12.4	0.475	92.0	0.065
4278-2-4	0.90	12.4	0.475	85.4	0.062
4278-2-5	0.86	12.4	0.475	86.0	0.059
4278-2-9	0.91	12.4	0.475	86.3	0.062
4278-2-17	0.97	12.4	0.475	86.1	0.066
Average	0.93	12.4	0.475	87.2	0.063

3.2.3.2 Matrix Fracture Due to Bending

Matrix damage due to resin fracture is the second energy absorption mode that was observed. Figures 3.5 and 3.6 show that the flat sides of the crush tube that have been forced to follow the radius of the plug trigger and were deformed into a curved petal shape. The stiffness of the petals has been reduced to the point that the crushed petals can be deformed easily whereas the undamaged sides of the crush tube remain rigid. As the fibers in the petals are not fractured, the only composite component observed to be damaged is the resin. Close examination of the damaged composite shows that the resin has fractured into very small granules that remain attached to the fiber tow bundles. At the edges of the composite petals, individual fiber tow bundles are observed to be free from the petals. The fiber tows can be easily separated from the damaged composite showing extensive damage of the resin matrix and loss of continuity between the fiber tows. This characteristic of the damaged composite was consistent between the quasi-static and dynamic tested specimens for both the carbon fiber and glass fiber composites. A description and results of a new test method that quantifies the specific energy absorption attributable to matrix fracture and friction is presented in Chapter 5.

3.2.3.3 Delamination

Delamination was evident when the glass fiber composite and carbon composite tubes were crushed. Six separate layers were easily identified for the glass fiber composite tubes as shown in Figure 3.2. The carbon fiber composite tubes delaminated into two layers. The number of surfaces created can be determined using the relation:

$$S = 2(N - 1)$$

Where: S is the number of surfaces

2 represents the two surfaces created after delamination

N is the number of plies or layers

For the glass fiber composite, 10 surfaces were created. Two surfaces were created in the carbon fiber composite by delamination.

Calculation of the energy absorbed by this damage mechanism was determined using the Mode 2 critical strain energy release rate, G_{IIc}. The test procedure: End Notch Flexure Testing of Fiber Reinforced Composites, General Electric Specification No 4013367-059, Issue 2, was used to measure the static value of G_{IIc}. No testing was conducted to determine the dynamic value of G_{IIc}. The values of G_{IIc} of the glass fiber composite are presented in Table 2.3 and in Table 2.4 for the carbon fiber composite. Multiplying G_{IIc} by the surface area that is created during tube crush and dividing by the mass of the crush tube that is crushed results in a value for the SEA for this mode.

For example, the glass fiber composite tube #1A:

1. G_{IIc} of glass fiber composite is 0.123 J/cm^2 (see Table 2.3)
2. Crush distance is 12.7 cm (see Table 2.5)
3. Tube section perimeter is 19 cm
4. Delaminated surface area is 2,409 cm^2
5. Cross section area is 9.95 cm^2 (see Table 2.5)
6. Calculated crush volume equals 126 cm^3

7. The density of glass fiber composite is 1.8002 gm/cm^3
8. The calculated crush mass is 227.5 gm
9. The resulting delamination SEA is 1.31 J/gm

The results of these calculations are summarized and presented in Table 3.3 for the glass fiber composite and Table 3.4 for the carbon fiber composite. Only static testing for end notch flexure (ENF) was performed for both glass fiber composite and carbon fiber composite.

Table 3.3 Glass fiber composite SEA due to delamination.

Coupon	G_{IIc} (J/cm^2)	Delaminated Surface Area (cm^2)	Crushed Tube Mass (gm)	SEA (J/gm)
1A	0.123	2,409	227	1.30
2A	0.123	2,406	226	1.31
3A	0.123	2,406	223	1.33
3B	0.123	2,406	226	1.31
13B	0.123	2,406	227	1.30
			Average:	1.31

Note: SEA based on material density of 1.8002 gm/cm^3.

Table 3.6 Carbon fiber composite SEA due to delamination.

Coupon	G_{IIc} (J/cm^2)	Delaminated Surface Area (cm^2)	Crushed Tube Mass (gm)	SEA (J/gm)
4278-2-1	0.164	451	92.5	0.798
4278-2-4	0.164	450	85.9	0.857
4278-2-5	0.164	449	86.5	0.850
4278-2-9	0.164	450	86.8	0.848
4278-2-17	0.164	451	86.6	0.852
			Average:	0.841

Note: SEA based on material density of 1.42 gm/cm^3.

3.3 Tapered Trigger

3.3.1 Introductory Comments

The main difficulty in and quantifying energy absorption modes is developing a simple test to separate energy absorbing modes. One of these approaches, the tapered trigger, is discussed in this chapter. A new strip test is introduced and discussed in Chapter 5 that was used to quantify energy absorption attributable to sliding friction and energy absorption attributable to matrix damage due to bending.

When a tube is compressed quasi-statically or dynamically using the standard plug trigger, the tube corners split, the flat sides of the tube are forced follow the radius of the trigger resulting in fracture of the resin matrix and delamination between layers of the composite. The order that these damage modes occur was not determined. However, once the crush process is started, all damage modes occur throughout the crush event. In addition, there is energy absorption due to the friction of the composite sliding over the trigger. The first effort to isolate energy absorption modes was the development of the tapered trigger. It was reasoned that if the composite tube is compressed using a small angle trigger, delamination and matrix damage due to bending would be eliminated leaving only corner splitting and sliding friction.

3.3.2 Tapered Trigger Design

The design features of the tapered trigger are presented in Figure 3.7. Note that the tapered portion of the trigger is inclined 5 degrees relative to the axis of the trigger. All tapered trigger tests were conducted using quasi-static load rate. During the crush test, the composite crush tube is forced over the increasing perimeter of the tapered sides resulting is tensile loads that cause the tube to fracture in the corners, similar to the

standard plug trigger. However, because the sides of the tube are not forced to bend following the small radius between the standard plug trigger and its base, the composite sides do not delaminate and the matrix resin does not fracture. This test effectively has only two energy absorption modes, corner splitting and sliding friction. A tapered trigger is presented in Figure 3.7 and a glass composite tube that has been tested using the tapered trigger is shown in Figure 3.8. Note that the only visible damage is the fracturing of the corners.

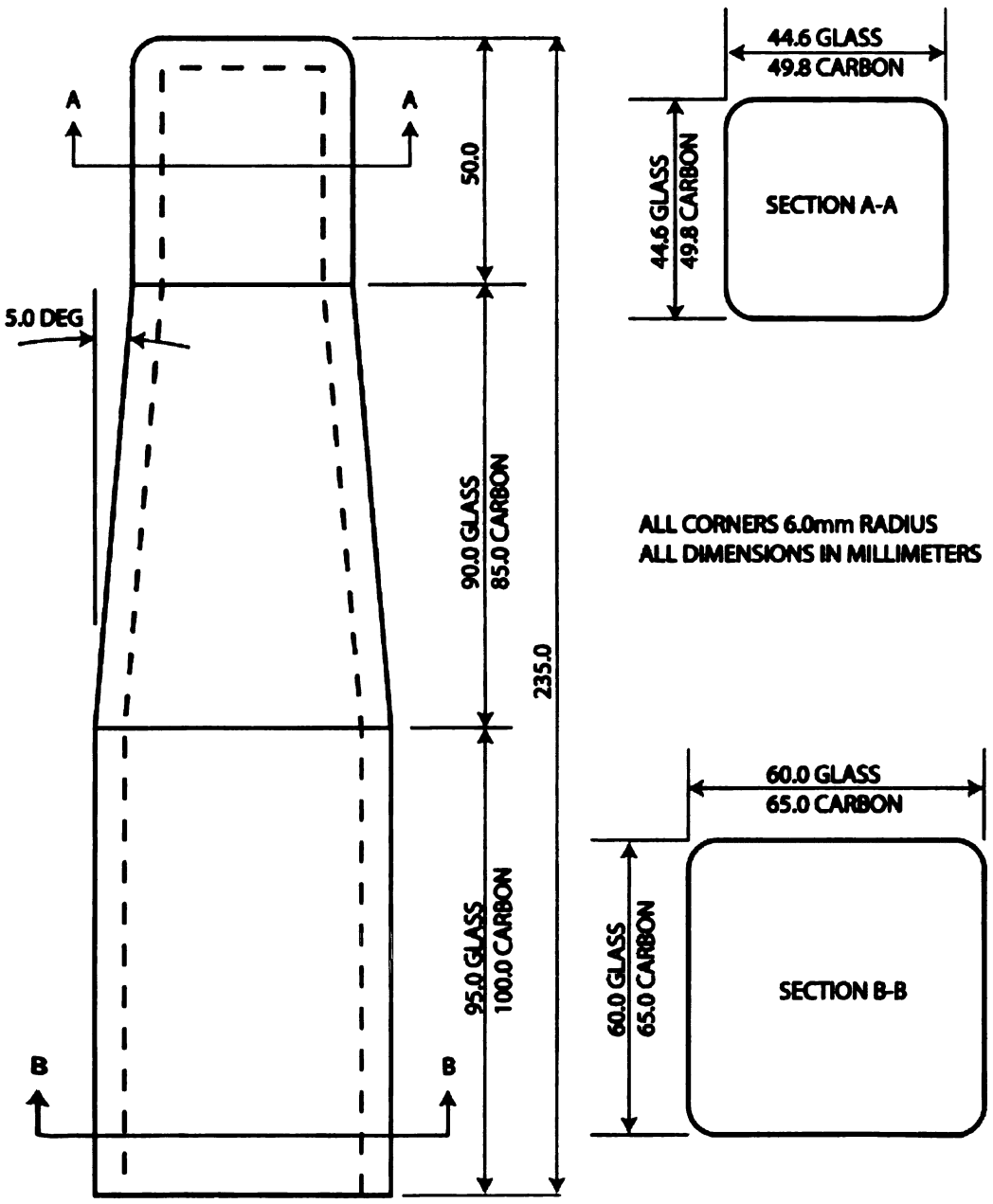

Figure 3.7 Tapered trigger drawing.

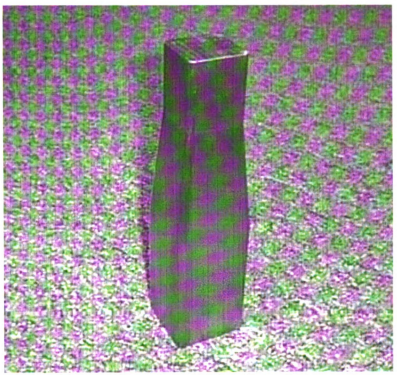

Figure 3.7 Tapered trigger.

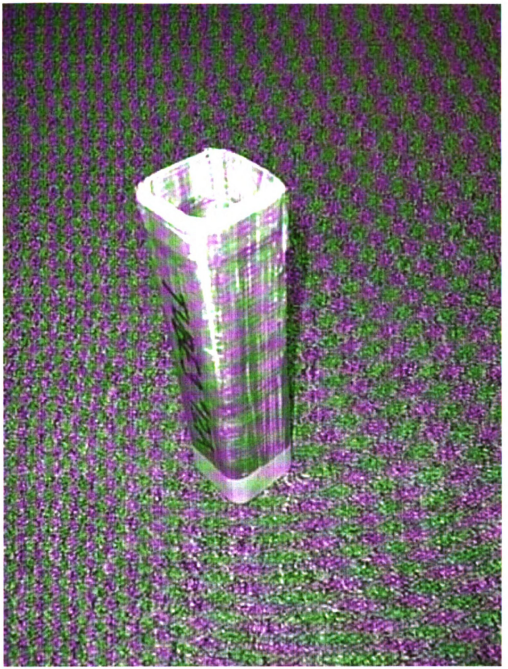

Figure 3.8 Compressed glass fiber composite tube using tapered trigger.

3.3.3 Tapered Trigger Crush Tube Results

3.3.3.1 Glass Fiber Tapered Trigger Crush Tubes

The results of tapered trigger crush tests on glass fiber composite tubes are presented in Table 3.7. A load-displacement plot of both of the tapered trigger specimens is presented in Figure 3.9. Tube corner splitting begins at approximately 8 mm of test machine crosshead travel after initial test free play is taken up. Note that tube TT-3 reached the first load peak after 20 mm of crosshead displacement while tube TT-4 reached its first load peak after only 10 mm of crosshead displacement. However, there is a low load level observed for tube TT-3 until 12 mm of crosshead displacement while only 2-3 mm of crosshead displacement corresponding to low level loading occurs in TT-4 before loading increases. Recall that there is a 45° bevel at the leading edge of each tube. The load level required to cause damage to the sharp leading edge of the bevel is low compared with the load required to cause damage to the full thickness in remainder of the crush tube. This reduced load level at the beginning of the crush test is also due to the smaller number of 90° fibers of the glass fiber composite and $\pm$45° fibers of the carbon fiber composite that are continuous in the corner regions of the beveled end of the tube. The 90° fibers of the glass fiber composite and $\pm$45° fibers of the carbon fiber composite are the primary load-bearing component and in the beveled region of the tube, these fibers are mostly severed due to machining.

Individual plots of each test are presented in Appendix C. Examination of the tested tubes showed that damage was confined to the corners with no delamination or damage of the resin in the flat sides of the tubes. Average SEA using the tapered trigger was 4.91 J/gm compared with 20.62 J/gm for a tube crushed using the standard plug

trigger. The large difference is because energy absorption attributable to matrix damage due to bending is not present. When only two of the energy absorbing modes are present, reduced load levels and energy absorption were observed.

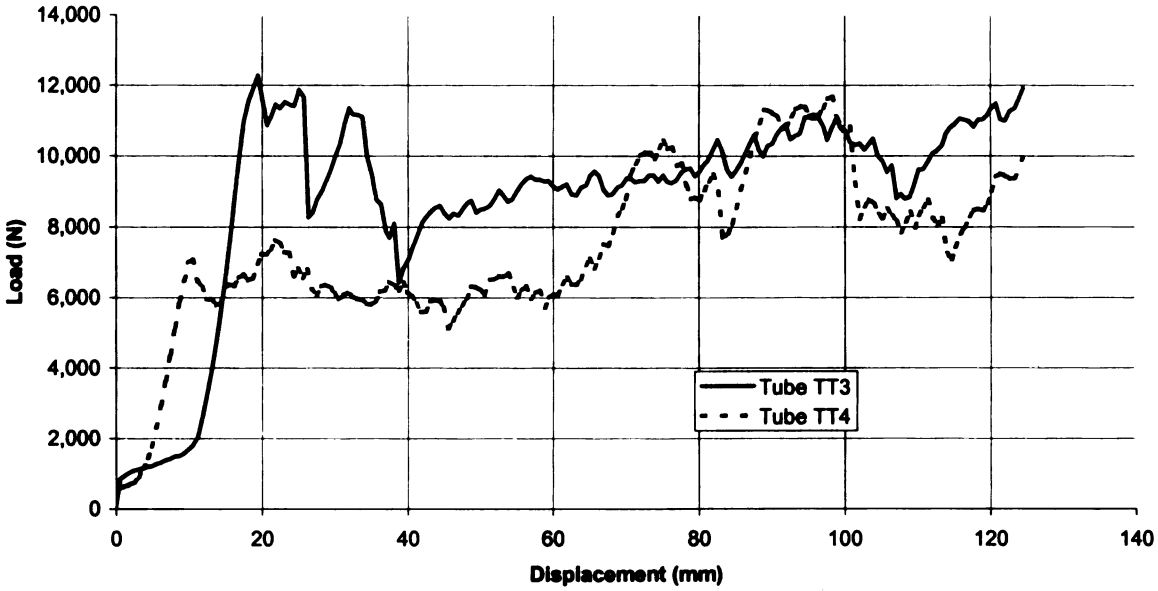

Figure 3.9 Glass fiber composite tubes, load-displacement plot for quasi-statically loaded with tapered trigger.

Table 3.7 Glass fiber composite crush tube SEA using tapered trigger quasi-static load rate (0.0508 m/min).

Coupon	Ave. Cross Section Area (cm^2)	Max. Load (N)	Ave. Load (N)	Crush Distance (cm)	Total Energy Absorbed (J)	SEA (J/gm)
TT2	10.1	14,780	10,690	12.5	1,330	5.87
TT4	10.1	11,670	7,190	12.4	895	3.95
Ave.	10.1	13,225	8,940	12.5	1,113	4.91

Note: SEA based on material density of 1.8002 gm/cm^3.

3.3.4.1 Carbon Fiber Tapered Trigger Crush Tubes

Results for the tapered trigger carbon fiber composite tube crush are presented in Table 3.8. Two of the carbon fiber composite tubes that were crushed using the tapered trigger are presented in Figure 3.10. Individual plots for each test are presented in Appendix C. Examination of the tested tubes showed that damage was confined to the corners with no delamination or damage of the resin in the flat sides of the tubes. Average SEA using the tapered trigger was 7.442 J/gm compared with 30.39 J/gm for a tube crushed using the standard plug trigger. As with the glass fiber composite tubes, when only friction and corner splitting, reduced load levels and energy absorption are observed.

Table 3.8 Carbon fiber composite crush tube SEA using tapered trigger quasi-static loading rate (0.0508 m/min).

Coupon	Ave. Cross Section Area (cm^2)	Max. Load (N)	Ave. Load (N)	Crush Distance (cm)	Total Energy Absorbed (J)	SEA (J/gm)
4278-2-13	4.863	9,564	5,729	12.4	713	8.296
4278-2-14	4.621	7,015	3,989	12.4	497	6.079
4278-2-15	4.866	8,878	5,345	12.4	665	7.735
4278-2-20	4.618	9,053	5,022	12.4	625	7.658
Ave.	4.742	8,628	5,021	12.4	625	7.442

Note: SEA based on material density of 1.42 gm/cm^3.

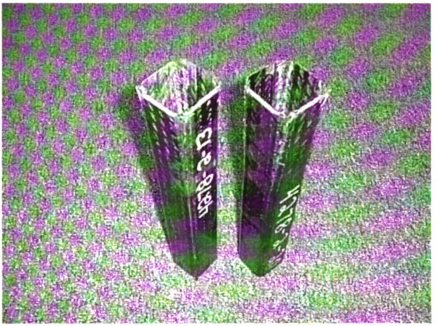

Figure 3.10 Crushed carbon fiber composite tube using tapered trigger.

3.4 Tapered Trigger Summary

The use of a tapered trigger to isolate corner splitting energy absorption provided insight into the relative amounts of SEA attributable to the energy absorption modes identified for square tube crush at quasi-static load rate. An energy balance for both the glass fiber composite and carbon fiber composite crush tubes is presented in Table 3.9. Table 3.9 shows that if energy superposition holds, splitting the corners of the tube accounts for less than 1% of the total energy absorbed for both the glass and carbon fiber composites.

This table also shows that delamination accounts for 6.4% of the energy absorbed by the glass fiber composite and less than 1% of the energy absorbed by the carbon fiber composite. This difference can be partially explained by the difference in the fiber architectures. The glass fiber consists of six layers whereas the carbon fiber composite contains only two layers. It was expected that the relative energy absorption due to delamination of the carbon fiber composite would be less than that of the glass fiber composite due to fewer layers present.

When the standard trigger is used, the balance of the SEA for the glass fiber composite, 92%, and for the carbon fiber composite, 97%, is attributable to energy absorption due to sliding friction and matrix damage due to bending. These figures were arrived at based on the analysis given earlier and not by direct measurement. A unique method of measuring energy absorption attributable to matrix damage from bending and sliding friction is presented in Chapter 5. In addition, dynamic measurement of sliding friction and matrix damage due to bending was also directly measured and is presented in Chapter 5.

Table 3.9 Energy absorption summary for quasi-static loading.

	Glass Fiber Composite		Carbon Fiber Composite	
Energy Absorption Mode	SEA (J/gm)	SEA (%)	SEA (J/gm)	SEA (%)
Corner splitting	0.111	0.54	0.063	0.21
Delamination	1.31	6.36	0.841	2.8
Friction	4.80	23.3	7.38	24.3
Remainder (Matrix Damage)	14.38	69.8	22.11	72.7
Tube Crush (Total)	20.6	100	30.4	100

CHAPTER 4. Analytical Solution to the Tapered Trigger Crush Test

4.1 Introduction

The tapered trigger test described in Chapter 3 was developed to isolate energy absorption modes for a crush tube. It was demonstrated that corner splitting and sliding friction were the most significant energy absorption modes present.

The purpose in developing an analytical solution for the tapered trigger crush test is to evaluate the reasonableness of the experimental results. It is also valuable to develop insight into the physics of the crush process by modeling the crush tube and analytically predicting its mechanical behavior using simple mechanics of materials concepts.

4.2 Free body diagram

A simple free body diagram of the tapered trigger tube crush test is presented in Figure 4.1. A cross section of the composite tube at the beginning of the tapered plug is presented with the applied load, Q, the normal force, N, and the tangential or friction force, T. In addition, there is transverse shear force present because the composite is put into bending as it is forced over the tapered trigger.

Note that the normal force is the resolved force from the distributed normal force, n, over the length of composite from the point where the crush tube is forced to begin bending by the tapered trigger to the point at which the composite fractures as it is forced by Q over the increasing cross section of the tapered trigger. The distributed normal force is shown as having a triangular shape. This is consistent with the constant slope of the tapered trigger. A distributed force can be represented as a point load passing through the centroid of the distributed load. As the distributed load is a triangular shape, the

centroid of the distributed force is located 1/3 the distance from the base of the triangular load distribution to the beginning of the distributed load.

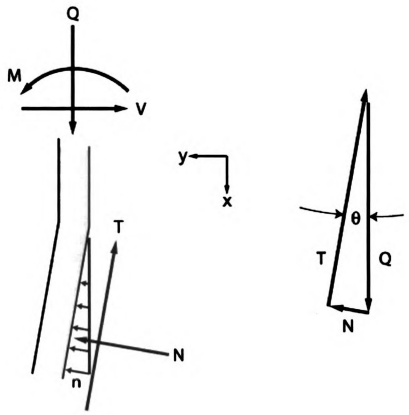

Figure 4.1 Tapered trigger tube crush free body diagram.

The forces in the x-direction, parallel with the direction of the applied load, are summed as follows to obtain an expression for the tangential force, T, and the normal force, N.

$$\Sigma Fx = 0$$

or,

$$0 = Q - T \cos\theta - N \sin\theta ,$$

thus:

$$T = Q/\cos\theta - N \sin\theta/ \cos\theta ,$$

leading to :

$$T = Q \sec\theta - N \tan\theta \qquad \text{eqn. (4.1)}$$

The tangential force, T, is related to the normal force, N, by the relation:

$$T = \mu N$$

μ is the dynamic coefficient of friction between the fiberglass composite and the steel trigger. This value for μ was measured to be 0.24 using modified ASTM method D1894-01 "Standard Test Method for Static and Kinetic Coefficients of Friction of Plastic Film and Sheeting" Ref. (24), thus:

$$\mu N = Q \sec\theta - N \tan\theta$$

and:

$$N = Q \sec\theta/(\mu + \tan\theta) \qquad \text{eqn. (4.2)}$$

The forces in the y- direction are developed as:

$$\Sigma Fy = 0$$

or,

$$0 = -V + N\cos\theta - T\sin\theta$$

writing as:

$$V = N\cos\theta - T\sin\theta \qquad \text{eqn. (4.3)}$$

The moment, Mz , is determined at the point where the composite begins to deflect due to the angle of the tapered trigger. The displacement distance, a, is the distance from the point that the composite begins to deform to the point the maximum value of the distributed force, n. The moment arm, 2a/3, is the distance from the point that the composite begins to deflect to the centroid of the distributed force, n. Finally, the moment is accounted for:

$$\Sigma Mz = 0$$

$$0 = Mz - V\,(2a/3)$$

or,

$$Mz = V\,(2a/3) \qquad \text{eqn. 4.4}$$

As the composite is forced over the increasing perimeter of the tapered trigger, hoop forces are created perpendicular to the direction of the applied force and in the plane of the composite. The maximum hoop force that is developed is limited by the tensile strength of the composite in the hoop stress direction. This value for glass composite used in this study presented in Table 2.3 as 189 MPa with corresponding ultimate strain of 1.34%. At that point, the circumference of the composite tube has increased to 101.34 % of its unstressed circumference. Referring to Figure 4.2, the width of one side of the composite tube is L. The increase in length of one side of the tube at the point of composite fracture is 2δ, the change in length of one side of the composite

tube. The distance that the tube is pushed down the tapered trigger is a. The radius of the corners, R, of the trigger is constant. For one side, the change in length is:

$$L + 2\delta$$

and,

$$L + 2\,\delta = L + 2\,a \tan\theta$$

or,

$$\delta = a \tan\theta$$

The total change in length is:

$$8\delta = 8\,a \tan\theta$$

The total initial perimeter, P, is:

$$P = 4L + 2\,\pi\,R$$

R is the radius of the tapered trigger corners. Engineering strain is calculated by dividing the change in perimeter length by the initial perimeter length:

$$\varepsilon = 8\,\delta/P$$

$$\varepsilon = 8\,a \tan\theta/(4L + 2\,\pi\,R) \qquad \text{eqn. (4.5)}$$

The crush distance, a, from the point at which the composite is first subjected to hoop forces sufficient for corner splitting can be calculated by rearranging eqn. 4.5 as:

$$a_{max} = \varepsilon_{max}(4L + 2\,\pi\,R)/8 \tan\theta \qquad \text{eqn. (4.6)}$$

The measured, calculated and given values for the variables described above are presented in Table 4.1.

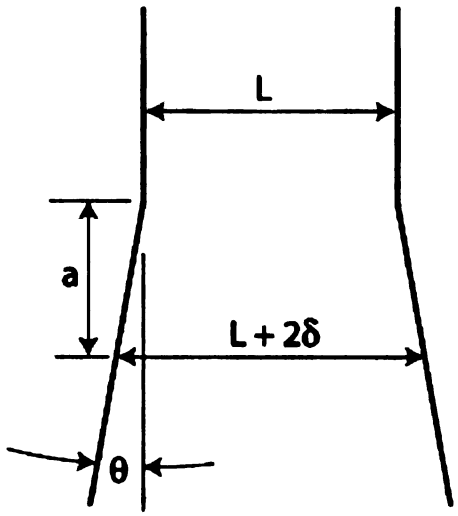

Figure 4.2 Section details for tapered trigger.

Table 4.1 Variable values.

Variable Name	Variable	Variable Value Source	Value
Plateau Load	Q	Measured	8,940 N
Plug Taper Angle	θ	Measured	5°
Dynamic Coefficient of Friction	μ	Measured	0.24
Maximum Tangential or Friction Force	T_{max}	Calculated	6,576 N
Maximum Normal Force	N_{max}	Calculated	27,403 N
Maximum Transverse Shear	V_{max}	Calculated	27,872 N
Maximum Bending Moment	M_{zmax}	Calculated	59.8 N m
Undeformed Tube Side Length	L	Measured	32.6 mm
Maximum Change in L/2	δ_{max}	Calculated	0.282 mm
Tube Displacement at Corner splitting	a_{max}	Calculated	3.218 mm
Tapered Trigger Corner Radius	R	Measured	6 mm
Maximum Crush Tube Hoop Strain	ε_{max}	Measured	1.34%

The SEA attributable to friction can be calculated by dividing the product of the tangential force, T_{max}, (6576 N) and displacement with the mass of the tube crushed. The cross section area of the glass fiber composite tubes is 10.11 cm^2 and the crush distance was 12.4 cm resulting in a total compressed volume of 125.4 cm^3. The density is 1.8002 gm/cm3 and the total crush mass was calculated to be 225.7 gm. The friction SEA is calculated to be 3.65 J/gm.

In Chapter 3, the SEA attributable to sliding friction for the tapered trigger was estimated to be 4.80 J/gm or 98% of the total SEA. The analytical solution provides a reasonable estimate of SEA due to sliding friction.

The SEA due to sliding friction with the standard plug was estimated in Chapter 3 to be 23% of the total SEA. Additional energy absorbing modes such as delamination and matrix damage due to bending are observed during tube crush using the standard trigger. An improved method of measuring sliding friction SEA for both static and dynamic load rates is described in Chapter 5.

CHAPTER 5. Friction and Damage Process

5.1 Lubricated Crush Tubes, Quasi-Static and Dynamic Loading

Based on the studies in the previous chapters, friction is believed to be a significant energy absorption mode for composite tube crush. A simple experiment was performed to see if a change in the coefficient of friction would result in a change in energy absorption. The first test was to apply a low friction coating in the interior surface of two carbon composite crush tubes. These tubes were the same material, geometry, and fiber architecture as those tested and reported in Chapter 2. The coating selected was Sprayon™ S00312 dry powder zinc stearate mold release. The coating is supplied in a spray can and applied similarly to spray on paint. The coating dries immediately to a white, dry, slippery film. Two crush tubes were then loaded quasi-statically (0.508 m/min) in the same manner as the tubes discussed in Chapter 2. The results of these tests are presented in Table 5.1 and with load-displacement plot presented in Figure 5.1. The results show average SEA of 18.0 J/gm compared with 30.4 J/gm (Table 2.6) for carbon fiber composite tubes loaded quasi-statically without zinc stearate coating, a reduction of 12.4 J/gm, over 40%. The damage appearance of the crushed zinc stearate treated tube was similar to the untreated tube. This result suggests that energy absorption due to sliding friction is significant and can be isolated from SEA attributable to delamination and matrix damage due to bending.

Table 5.1 Carbon composite crush tube SEA with zinc stearate coating at quasi-static loading (0.0508 m/min).

Coupon	Ave. Cross Section Area (cm^2)	Max. Load (N)	Ave. Load (N)	Load Distance (cm)	Total Energy Absorbed (J)	SEA (J/gm)
4278-2-7	5.26	15,870	11,420	11.4	1,302	17.4
4278-2-10	4.48	14,910	11,770	11.4	1,340	18.5
Ave.	4.87	15,390	11,595	11.4	1,321	18.0

Note: SEA based on material density of 1.42 $gm.cm^3$

The appearance of the load-displacement curves was different between the two specimens that were tested. The curve of tube #4278-2-7 displays local peaks with a difference between the local minimum and maximum loads of approximately 4,000 N that were approximately 20 mm apart. Compare with approximately 1,000 N between the local maximum and minimum loads that were approximately 5mm between load peaks displayed for tube #4278-2-10. One possible explanation for this difference is the damage process between the two tubes was different in the way the ± 45 fibers were fractured. If the fractures advanced by fracture of the ± 45 fibers in the corners simultaneously and then arrested at the next set of ± 45 fibers, the load would decrease to a much lower level than in the case where the corner splitting advanced sequentially and the load-displacement diagram would show a higher frequency. Evidence for this explanation can be seen by noting that the difference between local maximum and minimum loads was 4,000 N with approximately 20 mm between load peaks for one tube and for the other tube 1,000 N between local maximum and minimum loads with approximately 5 mm between load peaks. The appearance of the damaged specimens was identical and the average loads were similar. The difference in damage behavior between the two tubes is likely normal variation in the architecture of the fiber reinforcement.

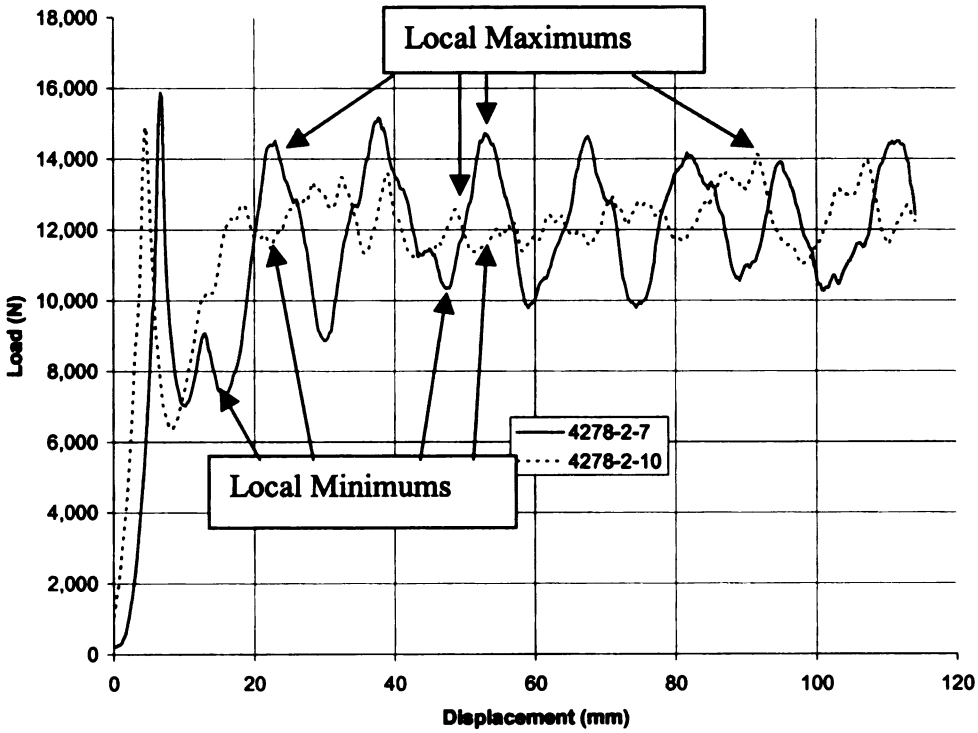

Figure 5.1 Carbon fiber composite tube crush quasi-static (0.0508 m/min) coated with zinc stearate.

Dynamic testing was conducted on carbon fiber composite crush tubes lubricated with zinc stearate coating. The results of this testing are presented in Table 5.2 and Figure 5.2. Note that the test conducted at 500 mm/sec had SEA similar in value to the two tests conducted at 2.0 m/sec with similar load-displacement curves. This shows that for these two load speeds, the SEA is insensitive to load rate. The dynamically loaded SEA for this group was slightly higher than the quasi-statically crush tubes lubricated with zinc stearate (21.8 J/gm vs. 18.0 J/gm). It is important to note that the quasi-statically loaded tubes were not coated with zinc stearate at the same time as the dynamic loaded tubes presented in Table 5.2. Zinc stearate lubricant was applied from a hand held spray can and application quality was evaluated visually. It is possible that the application of lubricant was not consistent between these two groups of specimens and the coefficient of friction was different between the two sets of tests. It is important to note that the application of zinc stearate lubricant did make a difference in energy absorption in both non-lubricated, quasi-statically and dynamically loaded carbon composite crush tubes. A summary of the zinc stearate lubricated tubes vs. the non-lubricated tubes is presented in Table 5.3.

Table 5.2 Carbon fiber composite crush tube SEA with zinc stearate low friction coating, dynamic loading.

Coupon	Load Rate (m/sec)	Ave. Cross Section Area (cm^2)	Max. Load (N)	Ave. Load (N)	Load Distance (cm)	Total Energy Absorbed (J)	SEA (J/gm)
4278-2-6	2.0	4.66	20,450	15,090	26.9	4,052	22.0
4278-2-18	2.0	4.53	18,680	13,830	26.8	3,709	21.5
4278-2-19	0.5	4.84	20,660	15,100	27.0	4,082	22.0
Ave.	--	4.68	19,930	14,673	26.9	3,948	21.8

Notes: SEA based on material density of 1.42 gm/cm^3.

Table 5.3 Carbon tube test summary non-lubricated vs. lubricated with zinc stearate.

	SEA (J/gm) Quasi-Static Loading	SEA (J/gm) Dynamic Loading
Without Zinc Stearate	30.4	23.8
With Zinc Stearate	18.0	21.8

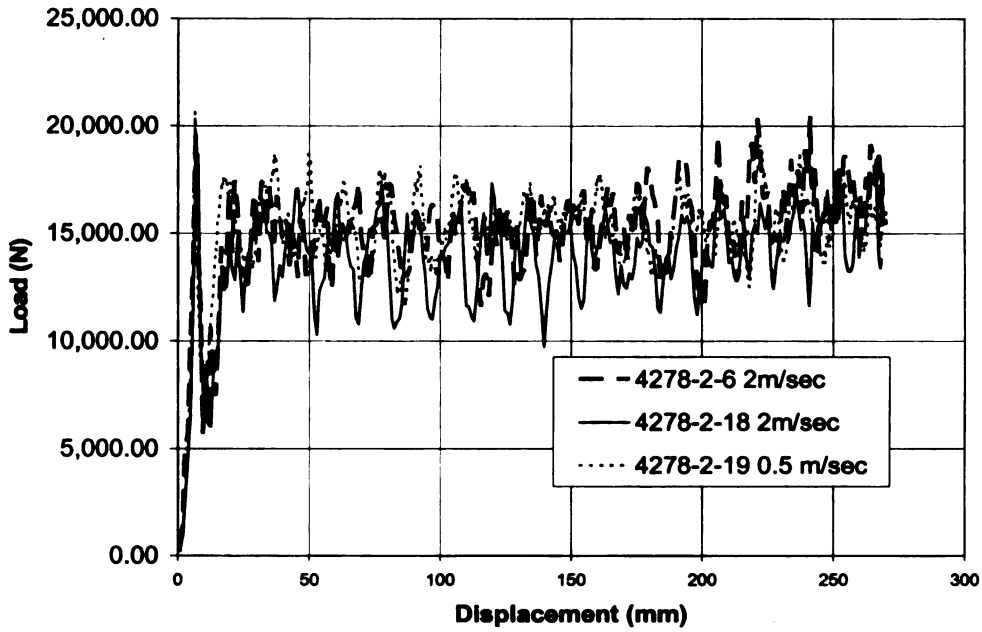

Figure 5.2 Carbon fiber composite tube crush dynamic loading coated with zinc stearate.

5.2 Strip Testing

5.2.1 Strip Test Introduction

Crush tubes lubricated with zinc stearate has demonstrated that altering the coefficient of friction significantly affects the SEA of quasi-statically loaded carbon fiber composite crush tubes. What this experiment did not do was to quantify the SEA attributable to friction. What is needed is a test that isolates friction by removing it from the crush process. To accomplish this goal, a test fixture was proposed to test strips of composite material that would remove friction energy absorption from the crush process present when carbon composite is forced to slide over the steel surface of a crush trigger for quasi-static and dynamic load rates. The test fixture was designed to simulate the damage process present in the sides of the crush tube when it is compressed using the standard plug trigger described previously.

Figure 5.3 presents a schematic of the strip test fixture. The main working parts are four rollers mounted in low friction ball bearings. Because rollers are supported by ball bearings, there is no sliding friction present when the rollers rotate as the strip specimen is forced downward. Three guide rollers that support the test strip are of the same diameter, 12.7 mm. The design and fabrication was simplified by keeping the diameters of the three top rollers the same. The diameter of the three rollers was selected because the roller radius is similar to the 6 mm radius of the standard plug trigger used in the tube crush test. Rollers A and C are aligned in the vertical direction. The diameter of the top two rollers, rollers, A and B, was minimized to keep the test fixture compact and minimize the length of the strip specimen. The roller second from the top, roller B, is adjustable horizontally to accommodate varying thicknesses of samples. The lowest

roller, roller D, is twice the diameter, 25.4 mm, of the other three rollers and is also horizontally adjustable. The larger diameter of roller D was chosen so that the range of curvature imposed on a strip test specimen could be varied over a large range by adjusting the horizontal position to simulate the curvature imposed on crush tubes when triggers with fillets of varying radii are used. Roller D is positioned to force the composite strip specimen to bend against the bottom guide roller, roller C, as the specimen is forced downward during testing.

Roller D was designed to have two test modes, locked and unlocked. When unlocked, roller D is free to rotate. When locked, roller D is prevented from rotating with a pin that fits into a hole in the roller that prevents the roller from rotating forcing the strip specimen to slide over roller D. The difference in the manner of loading from the unlocked or free mode is due only to the sliding friction present when the roller D is kept from rotating, forcing the strip to slide over the surface of the roller D. Delamination and matrix damage due to bending are present for both locked and free roller D conditions. Sliding friction is removed from the process when the roller D is free.

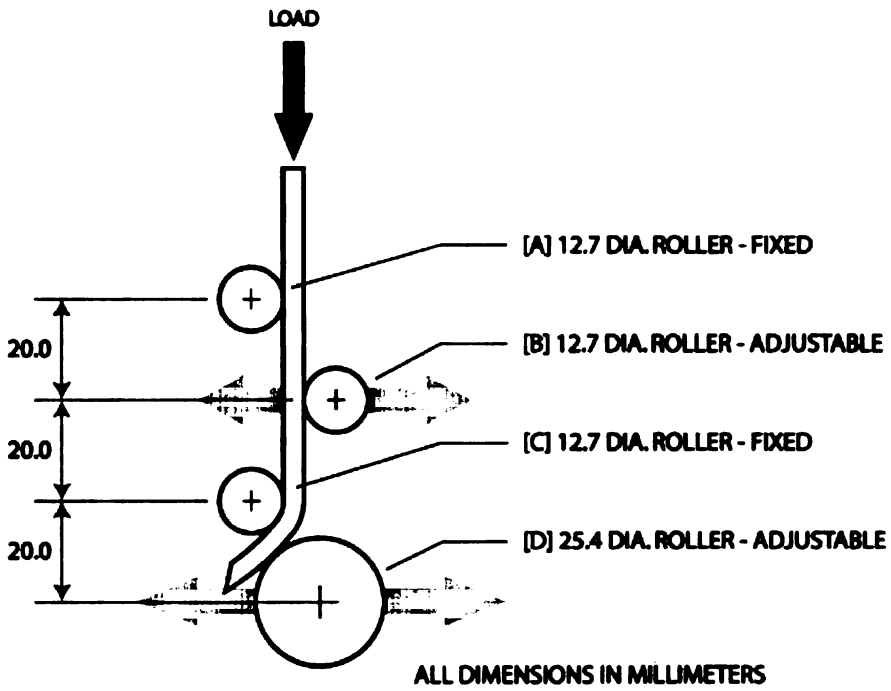

Figure 5.3 Strip test fixture schematic.

5.2.2 Strip Test Specimen and Fixture Description

Test specimens were machined from a flat plaque made from the same material as the crush tubes but with a thicker gage (4.0 mm vs. 2.0 mm) that was fabricated by doubling the number of layers of braided carbon tows. The flat plaque was fabricated for material characterization and needed greater thickness for some of the mechanical tests such as short beam shear test, end notch flexure test, and compression tests. Several strip specimens were machined from crush tubes and were tested in the strip test fixture. The thinner strip could not be tested due to structural instability. The portion of the thin strip above the rollers buckled as soon as the end of the strip contacted roller D and the load began to increase.

The strip dimensions are nominally 25.4 mm wide and 200 mm long. One end of each strip is beveled at a 45° angle similar to the bevel present in the crush tubes described previously. The purpose of the bevel is the same as the bevel in the crush tubes, to lower the initial load peak at the start of the test and improve structural stability of test. When the strip is compressed, the bevel is oriented away from the roller D, or to the left as shown in Figure 5.3. A strip test specimen is shown in Figure 5.4. The strip test fixture with a strip specimen ready to be tested is presented in Figure 5.5. A typical crushed specimen is presented in 5.6.

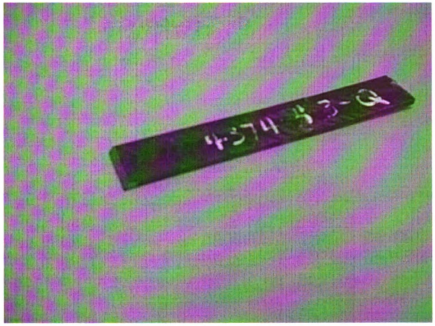

Figure 5.4 Strip test coupon.

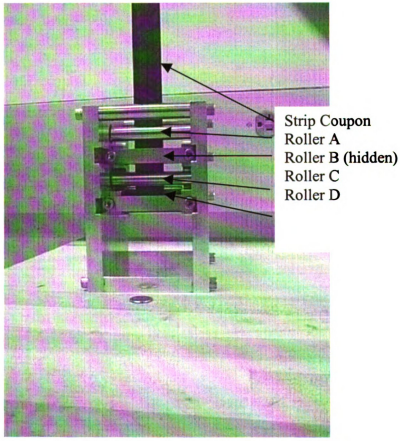

Figure 5.5 Strip test fixture with coupon.

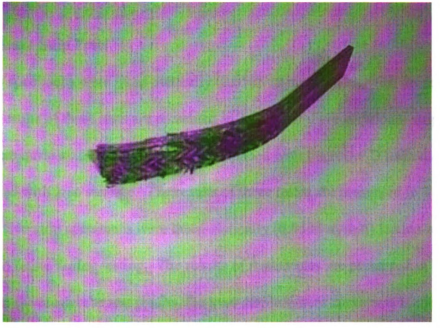

Figure 5.6 Typical tested strip coupon.

5.2.3 Quasi-Static Strip Tests

Five strip specimens were quasi-statically (0.0508 m/min) loaded with the roller D locked. The results of these tests are presented in Table 5.4. Five additional strip specimens were quasi-statically (0.0508 m/min) loaded with the roller D locked and the strips lubricated with zinc stearate. The results of these testes are presented in Table 5.5. A third set of five strip specimens were quasi-statically (0.0508 m/min) loaded with the roller D free to rotate during testing. The results of these testes are presented in Table 5.6. Similar to the crush tube test results, the load-displacement curve was numerically integrated to calculate the absorbed energy. The calculated absorbed energy was divided by the mass of the portion of the strip that was compressed to determine the SEA for each specimen tested. A typical load-displacement plot is presented in Figure 5.6. Note that there is a high peak load with load drop-off to a plateau load. No damage to the composite strip occurs until a peak load is achieved at which time the damage process begins in the strip. Once damaged, the load required to create new damage in the tube occurs at a lower level. However, in the strip test there is no need for the load to become large enough for fiber fracture as in the crush tubes. All plots for the specimens listed in Tables 5.4, 5.5, and 5.6 are presented in Appendix D. A discussion of these results is presented in section 5.2.5.

Table 5.4 Carbon fiber composite strip SEA, locked roller D quasi-static loading (0.0508 m/min).

Coupon	Cross Section Area (cm^2)	Max. Load (N)	Ave. Load (N)	Load Distance (cm)	Total Energy Absorbed (J)	SEA (J/gm)
4374-4-3-V	1.19	7,035	3,414	11.5	391	20.1
4374-4-3-W	1.18	7,201	3,295	11.4	377	19.5
4374-4-3-X	1.05	4,285	2,815	11.4	322	18.8
4374-4-3-Y	1.18	6,115	3,170	11.4	368	18.8
4374-4-3-Z	1.15	7,961	3,147	11.4	360	19.1
Ave.	1.15	6,519	3,168	11.4	364	19.3

Notes: SEA based on material density of 1.42 gm/cm^3.

Table 5.5 Carbon fiber composite strip SEA, locked and lubricated roller D, quasi-static loading (0.0508 m/min).

Coupon	Cross Section Area (cm^2)	Max. Load (N)	Ave. Load (N)	Load Distance (cm)	Total Energy Absorbed (J)	SEA (J/gm)
4374-4-3-AA	1.16	7,344	2,534	11.4	290	15.3
4374-4-3-BB	1.19	6,685	2,553	11.5	292	15.1
4374-4-3-CC	1.16	7,041	2,400	11.5	275	14.5
4374-4-3-DD	1.14	6,973	2,420	11.5	277	14.9
4374-4-3-EE	1.16	6,719	2,273	11.5	260	13.7
Ave.	1.16	6,952	2,436	11.5	279	14.7

Notes: SEA based on material density of 1.42 gm/cm^3.

Strip lubricated with zinc stearate dry film.

Table 5.6 Carbon fiber composite strip SEA, free roller D, quasi-static loading (0.0508 m/min).

Coupon	Cross Section Area (cm^2)	Max. Load (N)	Ave. Load (N)	Load Distance (cm)	Total Energy Absorbed (J)	SEA (J/gm)
4374-4-3-FF	1.16	5,782	2,133	11.5	244	12.9
4374-4-3-GG	1.16	5,996	2,417	11.5	277	14.6
4374-4-3-HH	1.16	5,887	2,171	11.5	249	13.1
4374-4-3-II	1.16	6,332	2,363	11.5	271	14.3
4374-4-3-JJ	1.13	2,556	1,881	11.5	215	11.7
Ave.	1.15	5,311	2,193	11.5	251	13.3

Notes: SEA based on material density of 1.42 gm/cm^3.

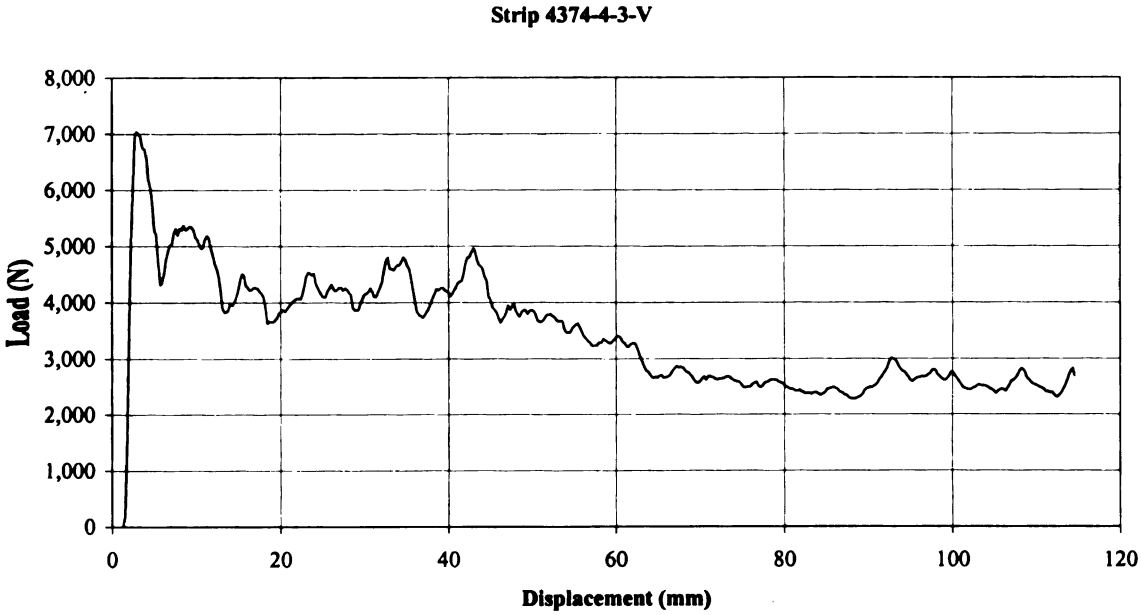

Figure 5.7 Typical load-displacement plot for quasi-static loaded (0.0508 m/min) carbon composite strip with locked roller D.

5.2.4 Dynamic Strip Tests

Five strip specimens were tested dynamically at 2.0 m/sec with roller D locked, and three additional specimens were tested at 0.5 m/sec with the roller D locked. The results of these tests are presented in Tables 5.7 and 5.8. There was no significant difference in the SEA of strips tested at 2.0 m/sec and 0.5 m/sec (15.5 J/gm vs. 15.4 J/gm). This shows that for these two load rates that the carbon composite is load rate insensitive. A plot of a typical load-displacement curve for 2.0 m/sec and 0.5 m/sec loading is presented in Figure 5.7. The curves are similar with no obvious difference in appearance. The curves for all of the specimens described in Tables 5.7 and 5.8 are presented in Appendix D.

Table 5.7 Carbon fiber composite strip SEA, locked roller D, dynamic loading (2.0 m/sec).

Coupon	Cross Section Area (cm^2)	Max. Load (N)	Ave. Load (N)	Load Distance (cm)	Total Energy Absorbed (J)	SEA (J/gm)
4374-4-3-QQ	1.07	6,607	2,253	10.9	246	16.6
4374-4-3-RR	1.12	8,194	2,429	10.8	263	15.7
4374-4-3-SS	1.11	10,307	2,322	11.0	256	14.6
4374-4-3-TT	1.13	6,882	2,243	10.9	244	13.8
4374-4-3-UU	1.04	5,035	2,513	10.9	275	16.9
Ave.	1.09	7,405	2,352	10.9	257	15.5

Notes: SEA based on material density of 1.42 gm/cm^3.

Table 5.8 Carbon fiber composite strip SEA, locked roller D, dynamic loading (0.5 m/sec).

Coupon	Cross Section Area (cm^2)	Max. Load (N)	Ave. Load (N)	Load Distance (cm)	Total Energy Absorbed (J)	SEA (J/gm)
4374-4-3-BBB	1.08	6,897	2,139	11.1	237	13.9
4374-4-3-CCC	1.12	6,958	2,503	10.9	273	15.6
4374-4-3-DDD	1.08	7,706	2,579	11.0	285	16.7
Ave.	1.09	7,187	2,407	11.0	265	15.4

Notes: SEA based on material density of 1.42 gm/cm^3.

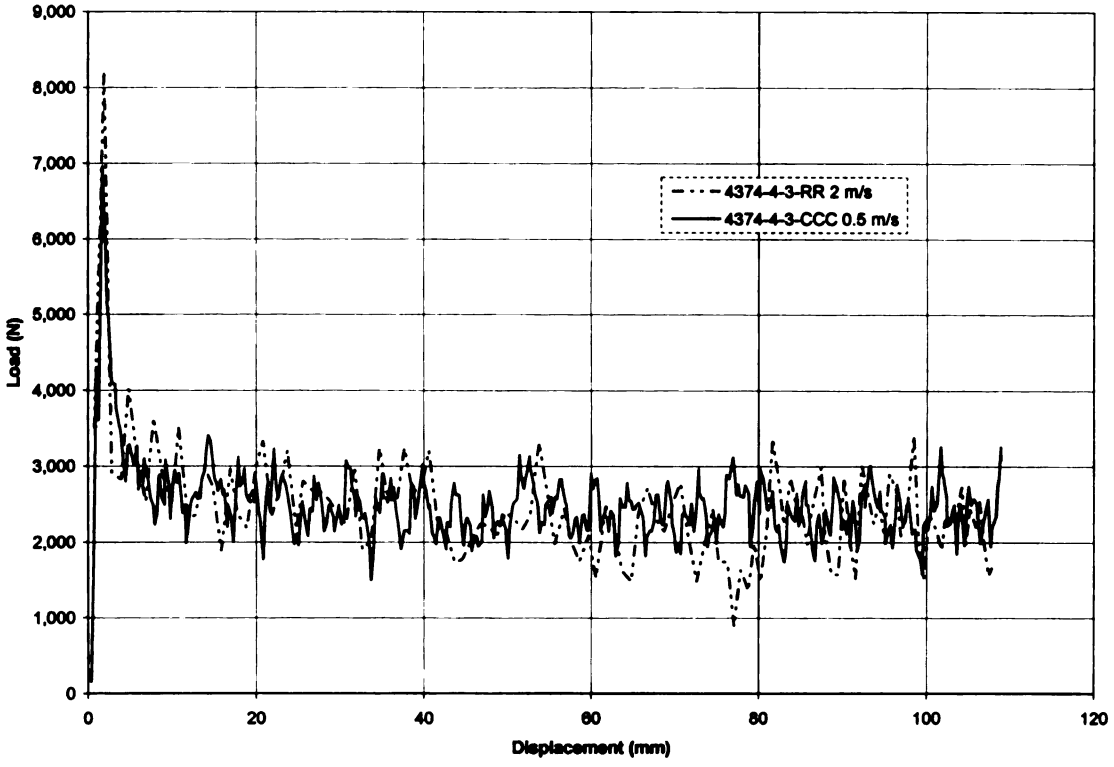

Figure 5.8 Typical carbon composite strip load-displacement dynamic loading with locked roller D.

Roller D was locked and specimens were loaded at 2.0 m/sec for the next set of five strip specimens. However, these five strips were coated with zinc stearate to reduce sliding friction. The results of these tests are presented in Table 5.9. The curves of the tests are presented in Appendix D.

Table 5.9 Carbon fiber composite strip SEA, locked and lubricated roller D, dynamic loading (2.0 m/sec).

Coupon	Cross Section Area (cm^2)	Max. Load (N)	Ave. Load (N)	Load Distance (cm)	Total Energy Absorbed (J)	SEA (J/gm)
4374-4-3-VV	1.13	6,592	2,132	10.9	233	13.2
4374-4-3-WW	1.09	8,453	2,095	10.6	222	13.4
4374-4-3-XX	1.10	8,850	2,284	11.0	249	14.6
4374-4-3-YY	1.10	10,468	2,278	11.0	251	14.5
4374-4-3-AAA	1.19	8,835	2,305	10.8	249	14.6
Ave.	1.12	8,640	2,219	10.9	241	14.1

Notes: SEA based on material density of 1.42 gm/cm^3.

Lubricated with zinc stearate dry film.

The results for dynamic loading of strips with roller D free to rotate are presented in Table 5.10 for 2.0 m/sec and in Table 5.11 for 0.5 m/sec. A typical plot with load-displacement curves for 2.0 m/sec loading and 0.5 m/sec is presented in Figure 5.8. The appearance of the curves is similar and the average SEA for 2.0 m/sec and 0.5 m/sec are close in value (13.0 J/gm vs. 13.3 J/gm). Plots of all strip specimens shown in Tables 5.10 and 5.11 are presented in Appendix D.

Table 5.10 Carbon fiber composite strip SEA, free roller D, dynamic loading (2.0 m/sec).

Coupon	Cross Section Area (cm^2)	Max. Load (N)	Ave. Load (N)	Crush Distance (cm)	Total Energy Absorbed (J)	SEA (J/gm)
4374-4-3-LL	1.13	6,546	1,934	10.9	210	11.9
4374-4-3-MM	1.13	9,659	2,073	10.9	227	12.8
4374-4-3-NN	1.05	7,706	2,081	10.9	228	13.8
4374-4-3-OO	1.09	7,385	2,170	10.9	237	13.9
4374-4-3-PP	1.10	6,119	2,018	10.9	220	12.8
Ave.	1.10	7,479	2,055	10.9	224	13.0

Notes: SEA based on material density of 1.42 gm/cm^3.

Table 5.11 Carbon fiber composite strip SEA, free roller D, dynamic loading (0.5 m/sec).

Coupon	Cross Section Area (cm^2)	Max. Load (N)	Ave. Load (N)	Crush Distance (cm)	Total Energy Absorbed (J)	SEA (J/gm)
4374-4-3-EEE	1.05	2,960	1,794	11.0	198	12.0
4374-4-3-FFF	1.09	5,402	2,317	11.1	256	14.8
4374-4-3-GGG	1.09	5,493	2,038	11.1	226	13.1
Ave.	1.08	4,618	2,050	11.1	227	13.3

Notes: SEA based on material density of 1.42 gm/cm^3.

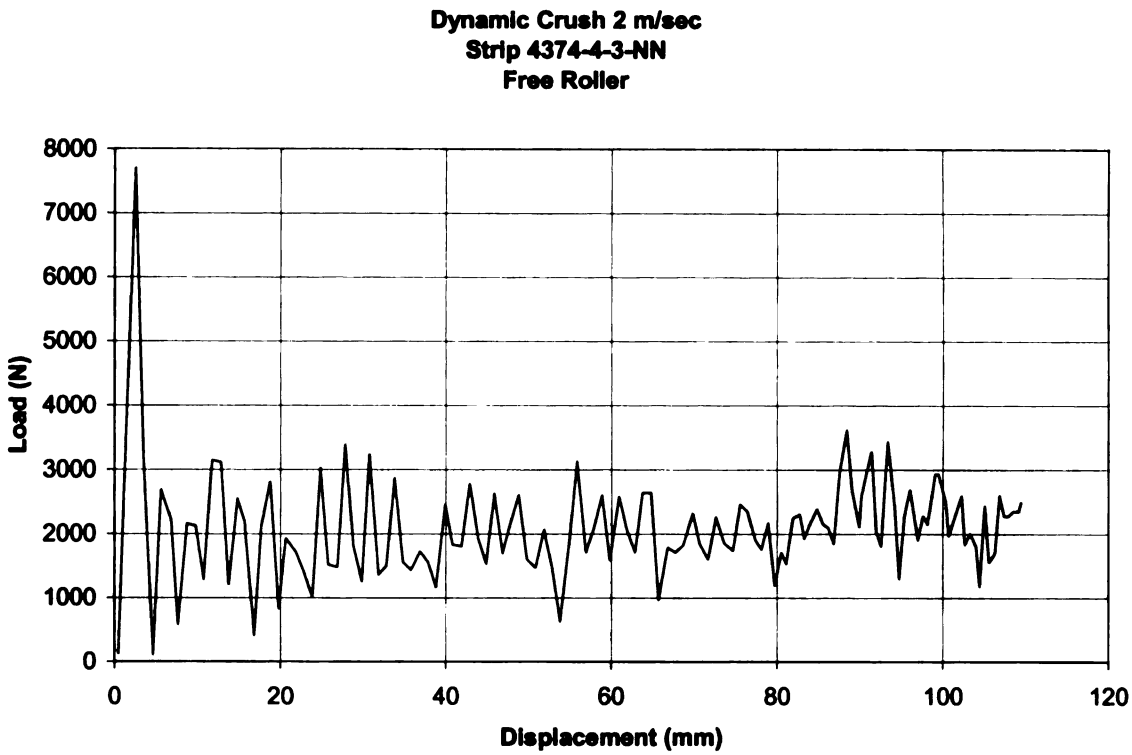

Figure 5.9 Typical strip load-displacement dynamic loading and free roller D.

5.2.5 Strip Test Results Discussion and Summary

A summary of strip testing is presented in Table 5.12. The variables presented are: load speed, roller D fixity, and the presence or absence of lubrication. The first comparison can be made for cases with varied load speed, locked roller D, and specimens lubricated or not lubricated with zinc stearate. When the loading is quasi-static (case 1), the average SEA is 19.3 J/m. When the loading is dynamic, either at 2.0 m/sec (case 4) or 0.5 m/sec (case 7), the average SEA is 15.4 J/m, a 20% reduction compared with the quasi-static result.

When the roller D is locked and the strips are lubricated with zinc stearate, the SEA for quasi-static loading (19.3 J/gm of case 1 vs. 14.7 J/gm of case 2) vs. dynamic loading at 2.0 m/sec (14.1 J/gm of case 5). The zinc stearate lubrication resulted in a reduction in SEA of 23.8% (14.7 J/gm of case 2 vs. 19.3 J/gm of case 1) compared with quasi-static loading. However, when tested dynamically at 2.0 m/sec, the reduction in SEA for the lubricated strips was only 8.4% compared with the non-lubricated test strips (14.1 J/gm of case 5 vs. 15.4 J/gm of case 4). This was the first test that shows that sliding friction absorbs smaller relative amount of energy when a composite tube is crushed dynamically. The difference may also be attributed to the relatively reduced roll that friction plays in dynamic loading cases than in the quasi-static cases. The difference in laboratory facilities may also be a factor . The static strip testing was performed at the Ford Scientific Research Laboratories whereas the dynamic testing was conducted at the National Transportation Research Center at Oak Ridge National Laboratory, Tennessee. The application of the zinc stearate dry film lubricant was with a hand-held spray can and the application may have differed between the two sets of strip specimens.

When the roller D is free to rotate there was little difference observed in the SEA between quasi-static loading (13.3 J/gm of case 3) and dynamic load rate of 0.5 m/sec (13.3 J/gm of case 8). There was only a slight difference in SEA when the dynamic load rate is 2.0 m/sec (13.0 J/gm of case 6). This result and the results described in the previous two paragraphs clearly demonstrate that:

1. Sliding friction absorbs a significant amount of energy at least in quasi-static cases.
2. Altering the coefficient of friction of the composite tube surface can vary SEA.
3. Energy absorption due to sliding friction can be separated from those due to damage formation.
4. Energy absorption due to delamination and bending was affected by loading rate for the load rates tested.

Table 5.12 Strip test results summary.

Case	Crush Speed	Roller D	Lubrication	Average SEA (J/gm)
1	Quasi-Static	Locked	None	19.3
2	Quasi-Static	Locked	Yes	14.7
3	Quasi-Static	Free	None	13.3
4	2.0 m/sec	Locked	None	15.4
5	2.0 m/sec	Locked	Yes	14.1
6	2.0 m/sec	Free	None	13.0
7	0.5 m/sec	Locked	None	15.4
8	0.5 m/sec	Free	None	13.3

5.3 Energy Balance

The energy absorption modes described in Chapter 3 were partially quantified using simple mechanical tests. Specifically, corner splitting and delamination were determined to be minor energy absorption modes. Corner splitting accounted for only 0.21% (0.063 J/gm) of the quasi-static SEA. Delamination accounted for 2.7% (0.84 J/gm). The remaining 97%, 29.5 J/gm (Table 3.9) was attributed to sliding friction and matrix damage due to bending. A tapered crush plug was used to obtain an inferred energy absorption value of 24.3 %, 7.38 J/gm (Table 3.9) for friction with the balance of 72.7%, 22.11 J/gm (Table 3.9) attributable to bending damage. There was no matrix damage or delamination observed in any of the tubes tested using the tapered trigger. The strip test results provide an improved estimate of energy absorption due to sliding friction and bending.

The energy absorbed in the strip test with quasi-static loading and locked roller D was 19.3 J/gm (Table 5.13). The SEA attributed to sliding friction and damage due to bending in a carbon composite crush tube was 29.5 J/gm (Table 3.9). The difference of 10.2 J/gm can be attributed to the reduced damage observed in the strips. The appearance of the damaged strips does not show the degree of matrix damage seen in tubes. A limitation of the strip test is the larger radius that the composite strip is forced over during the strip test compared with the tube crush tube. The strip test fixture is limited to bending the strip over a minimum radius of 6.3 mm, the radius of roller C. In addition, the test specimens were twice the thickness of the composite crush tubes (4 mm vs. 2 mm). The deformation radius of the outside of a strip is at least 10 mm when the minimum inside radius is 6 mm. When the carbon composite tube is forced over the

standard trigger, the maximum bending radius of the composite is the radius of the plug trigger, 6 mm. The minimum bending radius is smaller by the thickness of the 2 mm thick composite, or 4 mm. Thinner specimens could not be tested with the strip test fixture due to test coupon structural instability. A 2 mm carbon strip coupon was tested with poor results. The thin test specimen buckled above the test fixture. The test fixture was designed with the capability of testing various width specimens. As a result, the diameter of rollers A, B, and C could not be fabricated with the required diameter, 8 mm, correct for 2 mm thick strips and yet be stiff and strong enough to test thicker strips. A refined design of the strip test fixture that contains guides above roller A and with reduced width could yield improved test data. The important information obtained from the strip test described in this thesis is the ratio of SEA due to sliding friction compared with SEA due to bending.

There is one additional adjustment to the calculation of friction and bending SEA that must be made due to the increased thickness of the strip used in the strip test. The material used for strip testing was taken from a plaque that was twice the thickness containing twice the number of braided plies. This means that there are three delamination planes compared with the one delamination plane of the carbon composite tubes. Thus, the SEA value for delamination for the strip test is 2.52 J/gm or three times the delamination value for carbon composite tubes, 0.84 J/gm (Table 3.6). This delamination SEA value of 2.52 J/gm was subtracted from the quasi-static load rate, locked roller D strip test SEA of 19.3 J/m (Table 5.12), giving a sliding friction plus bending damage SEA of 16.8 J/gm. The sliding friction and bending SEA values were then calculated and tabulated in the second column of Table 5.13.

The friction and bending SEA for the carbon composite tubes loaded quasi-statically was determined to be 97% of the total SEA or 29.5 J/m. This value was divided by the strip friction plus bending damage SEA of 16.8 J/gm to obtain a ratio to quantitatively determine the friction and bending SEA for carbon composite tube crush. These values are presented in the third column of Table 5.13. Because friction is dependent upon the crush load which is affected by the bending strength as well as the delamination and corner splitting forces required for progressive crush, the ratio of sliding friction SEA to bending SEA is assumed to not vary between the strip test results and the tube crush results. Note that friction is determined to account for 10.6 J/gm or 34.8 % of the energy absorbed when the carbon composite tubes are crushed at the quasi-static rate.

Determination of the dynamic crush energy balance was determined in a similar manner and is presented in Table 5.14. The energy absorption due to bending was essentially unchanged (10.78 J/gm vs. 10.43 J/gm). Dynamic energy absorption due to sliding friction decreased significantly, 4.26 J/gm vs. 10.6 J/gm for quasi-static loading. Compare this reduction in SEA due to sliding friction of 6.34 J/gm with the overall reduction in carbon composite tube crush SEA from 30.4 J/gm for quasi-static load rate to 23.8 J/gm for dynamic load rate, a reduction of 6.6 J/gm. It can be concluded that for this composite system, nearly all of the measured SEA reduction when the load rate is changed from quasi-static to dynamic, 2.0 m/sec, is attributable to sliding friction. A summary is presented in Table 5.15.

Table 5.13 Carbon composite strip and crush tube energy balance quasi-static loading.

Energy Mode	Strip		Tube	
	J/gm	%	J/gm	%
Delamination + Bending	13.3	68.9	--	
Friction + Bending	16.8	87.0	29.5	97.0
Delamination	2.5	13	0.84	2.8
Bending	10.8	56	18.9	62.2
Friction	6.0	31	10.6	34.8
Corner splitting	0.0	0.0	0.06	0.2
Total	19.3	100	30.4	100

Table 5.14 Carbon composite strip and crush tube energy balance dynamic loading (2.0 m/sec).

Energy Mode	Strip		Tube	
	J/gm	%	(J/gm)	%
Delamination + Bending	13.0	84.4	--	
Friction + Bending	12.9	83.8	22.9	
Delamination	2.5	16.2	0.84	3.5
Bending	10.5	68.2	18.6	78.1
Friction	2.4	15.6	4.3	18.1
Corner splitting	0.0	0.0	0.06	0.3
Total	15.4	100	23.8	100

Table 5.15 Quasi-static vs. dynamic loaded carbon composite tube crush dynamic load rate (2.0 m/sec).

Energy Mode	Quasi-Static		Dynamic		Difference	
	J/gm	%	J/gm	%	J/gm	%
Delamination	0.84	2.8	0.84	3.5	0	0
Bending	18.9	62.2	18.6	78.1	-0.3	5
Friction	10.6	34.8	4.3	18.1	-6.34	96
Tube Corner splitting	0.063	0.2	0.06	0.3	0	
Total	30.4	100	23.8	100	-6.6	100

CHAPTER 6. Conclusions and Future Research

6.1 Introductory Remarks

The need for lightweight materials in automotive applications was introduced in Chapter 1 with discussion of benefits and challenges of using these materials. One of the most important challenges to the use of fiber-reinforced composite materials for energy absorbing structures is the understanding of how these materials absorb energy. Typically, materials to be used for energy absorptions have been characterized using simple tube structures that are loaded using standard test machines at quasi-static and dynamic load rates. Simple test tubes are used for testing because of their simple geometry and convenience. When metallic materials are tested in this way, the specific energy absorption, SEA, differs only slightly between quasi-static and dynamic load rates. Thus, the dynamic behavior of metals can be predicted reasonably well using computer-aided engineering, CAE, based on quasi-static testing. This approach has had limited success with composite materials. Testing composite materials at quasi-static load rate provides SEA values that can be nearly twice as high as dynamic test results. This observation provides the motive for the research presented in this thesis.

Metallic crush structures absorb energy by plastic deformation. This mode of energy deformation is consistent with the behavior of the metals used in automotive energy absorbing structures. Metals used in automotive energy absorbing have a load-displacement curve that shows a load plateau where the average load changes very little over a large displacement range. The integrated area under this curve represents energy absorption.

The composite materials tested were observed to absorb energy by several modes. The energy absorbing modes identified for the crush tubes considered were: tube corner splitting, delamination, matrix damage due to bending, and sliding friction. The approach used to quantify the energy absorption of each mode was to develop simple tests that would isolate energy absorbing modes.

Mechanical testing of the glass fiber and carbon fiber composites considered in this thesis showed elastic behavior. Crush tube corner splitting was measured using a standard tensile test. Delamination was measured using an end notch flexure test. Matrix damage due to bending and sliding friction were measured using a strip test fixture developed for this purpose.

Tube testing was conducted at a quasi-static load rate for a glass fiber/vinyl ester composite and for a carbon fiber/vinyl ester composite. Dynamic testing was performed at 2.0 m/sec on carbon fiber composite tubes. Quasi-static and dynamic testing of carbon composite coupons was performed at two rates, 0.5 m/sec and 2.0 m/sec, on the carbon fiber composite using the strip test fixture. The higher load rate, 2.0 m/sec, was the slowest dynamic rate that has been previously tested as shown in Figure 1.3.

6.2 Conclusions

Glass fiber/vinyl ester composite crush tubes were investigated with quasi-static compression and energy absorbing modes were identified. The observed energy absorbing modes included tube corner splitting, composite delamination, matrix damage due to bending, and sliding friction of the composite with the plug type crush trigger. These same energy-absorbing modes were observed in both quasi-statically compressed and dynamically crashed carbon composite crush tubes. Energy absorption attributable to

corner splitting at quasi-static compression was estimated using standard tensile test results. Corner splitting was estimated to absorb less that 1% of the total energy absorbed by both the glass fiber composite and the carbon fiber composite crush tubes. Energy absorption attributable to delamination was estimated using the mode II (shear mode) strain energy release rate obtained using the end notch flexure (ENF) test. Under quasi-static compression, the glass fiber composite delamination SEA was found to be 1.55 J/gm or 7.5% of the total tube SEA. For carbon fiber composite crush tubes, the delamination SEA was found to be 0.84 J/gm or 2.8%f the total tube SEA.

Experiments seemed to suggest that sliding friction played an important role in the energy absorption of composite crush tubes. In an attempt to separate the sliding friction SEA from the SEA attributable to matrix damage due to bending, an innovative strip testing fixture was designed, fabricated, and tested and is presented in this thesis. Carbon fiber composite SEA, under quasi-static compression, attributable to matrix damage due to bending was found to be 18.9 J/gm or 62.2% of the total tube SEA. Under dynamic crush, the SEA attributable to matrix damage due to bending was found to be 18.6 J/gm or 78.1% of the total tube SEA. Carbon fiber composite SEA attributable to sliding friction under quasi-static compression was found to be 10.6 J/gm or 34.8% of the total tube SEA. Under dynamic crush, the SEA attributable to sliding friction was found to be 4.3 J/gm or 18.1% of the total SEA. The decrease in sliding friction SEA of 6.3 J/gm accounted for nearly all of the decrease in tube SEA of 6.6 J/gm between dynamic crush and quasi-static compression. Sliding friction was concluded to be responsible for the decrease in overall tube SEA from quasi-static compression to dynamic crush.

6.3 Future Research

Other composite systems must be evaluated individually until reliable predictive methods are developed. In the mean time, the physics of damage for each energy absorption mode identified should be examined and quantified at both quasi-static and dynamic loading rates.

The strip test fixture used in this thesis should be refined so that the strip test specimens are damaged to a similar level of damage to that observed in tube crush testing. Possible improvements include guides that eliminate structural instability so that a thin strip specimen could be compressed. The diameter of roller C, the roller that the composite strip is forced to bend around, could be reduced to 8 mm so that outer radius of a 2 mm thick strip specimen is the same as when a 2 mm thick crush tube is forced over the standard plug trigger.

REFERENCES

(1) Boeman, R.G. and Caliskan, A.G., "Crush Response of Crash Energy Management Structures at Intermediate Rates", 2002 Future Car Congress, Arlington VA, June 2002. (SAE# 2002-01-1954).

(2) Johnson, C. F., "Resin Transfer Molding", Engineering Materials Handbook V1-Composites, ASM International 1987

(3) Botkin, M., Fiday, S., and Jeryan, R., "Crashworkthiness development of a Composite Front Structure for a Production Vehicle", Advanced Composites Conference, Detroit 1997, Engineering Society of Detroit p 11-27

(4) Browne, A. L., Waling, P. J., Houston, D. Q., Lalik, L., "Generic Tube Crush Program: Part I: RTM Tubes", 1998 ASME Mechanical Congress and Exposition, Nov 18, 1998, Anaheim, CA

(5) Hull, Derek, "Energy Absorbing Structural Composites", a report to the Automotive Composites Consortium, August, 1994

(6) Automotive Aluminum Crash Energy Management Manual, 1998, The Aluminum Association, Inc., Washington, D. C.

(7) Thornton, P.H., "Energy Absorption in Composites", Proc SEM Spring Conference on Experimental Mechanics, June 709, 1993, Dearborn, MI

(8) Farley, Gary, Jones, Robert, "Crushing Characteristics of continuous Fiber-Reinforced Composite Tubes", Journal of Composite Materials **26** (1992) 27-50

(9) Farley, Gary, Jones, Robert, "Analogy for the Effect of Material and Geometrical Variables on Energy-Absorption Capability of Composite Tubes", Journal of Composite Materials **26** (1992) 78-89

(10) Mamalis, A. G., Manolakos, D.E., Demosthenous, G. A., Ioannidis, "The static and dynamic axial collapse of fiberglass composite automotive frame rails", Composite Structures **34** (1996) 77-99

(11) Mamalis, A. G., Manolakos, D.E., Demosthenous, G. A., Ioannidis, "Analysis of Failure Mechanisms Observed in Axial Collapse of Thin-Walled Circular Fiberglass Composite Tubes", Thin-Walled Structures **24** (1996) 335-352, Elsevier Science Limited, Great Britain

(12) Chadwick, M. M. and Caliskan, A. G., "Fracture Mechanisms Observed in Crush of Vinyl Ester-Glass Composite Tubes", Private Communication, 1998

(13) Johnson N. L., Houston, D. Q., Watline, P. J., Lalic, L., "Generic Tube Crush Program: Crush Tests of Structural Reaction Injection Molded Tubes", Crashworthiness, Occupant Protection and Biomechanics in Transportation Systems-1998, ASME Publication AMD-Vol. 230 BED-Vol. 41, pp 53-74

(14) Bruce, Denise M., Matlock, David K., Speer, John G., De, Amar K., "Assessment of the Strain-Rate Dependent Tensile Properties of Automotive Sheet Steels", Innovations in Steel Sheet and Bar Products and Processing, and Modeling and Testing of Steel Structures (SP-1837)2004 SAE World Congress, Detroit, Michigan March 8-11, 2004

(15) Weeks, C.A., Sun, C. T., "Modeling Non-Linear Rate-Dependent Behavior in Fiber-Reinforced Composites", Composites Science and Technology **58** (1998) 603-611, Elsevier Science Limited, Great Britain

(16) Todo, M., Takahashi, K., Beguelin, P., Kausch, H. H., "Strain-rate dependence on the tensile fracture behavior of woven-cloth reinforced polyamide composites", Composite Science and Technology **60** (2000) 763-771, Elsevier Science Limited, Great Britain

(17) Johnson, N. L., Houston, D. Q., Coyner, R., Lalik, L., "Automotive Composites Consortium Generic Tube Crush Program: Static Crush Tests of SRIM Tubes", Proceedings of the 13th Annual ESD Advanced Composites Conference and Exposition, September 29, 1998, Detroit, MI

(18) Johnson, N. L., "Automotive Composites Consortium Generic Tube Crush Program: Dynamic Crush Tests of SRIM Tubes", Proceedings of the 13th Annual American Society for Composites Conference, September 21-23, Baltimore, MD

(19) Browne, A. L., Houston, D. Q., Lalik, L., "Automotive Composite Consortium Generic Tube Crush Program: Resin Transfer Molded Tubes", Crashworthiness, Occupant Protection and Biomechanics in Transportation Systems-1998, ASME Publication AMD-Vol. 230 BED-Vol.. 41 pp 75-94

(20) Agaram, V., Bilkhu,S., Fidan, S., Botkin, M., and Johnson, N.,"Simulation of Controlled Failure of Automotive Composite Structures with LS_DYNA3D", ACCE Conference Proceedings, Dearborn, MI April 7-10, 1997

(21) Delsen Test Report T 34773, 01/29/99

(22) ASTM D2584-02 Standard Test Method for Ignition Loss of Cured Reinforced Resins

(23) Delsen Test Report T 37674, 07/23/03

(24) Ford Central Laboratory Test Report #20679, June 3, 2002, Private Communication.

APPENDIX A

Glass Fiber Composite Crush Tube Load Curves

Appendix A1

Glass Fiber Composite Crush Tube
Quasi-Static Rate

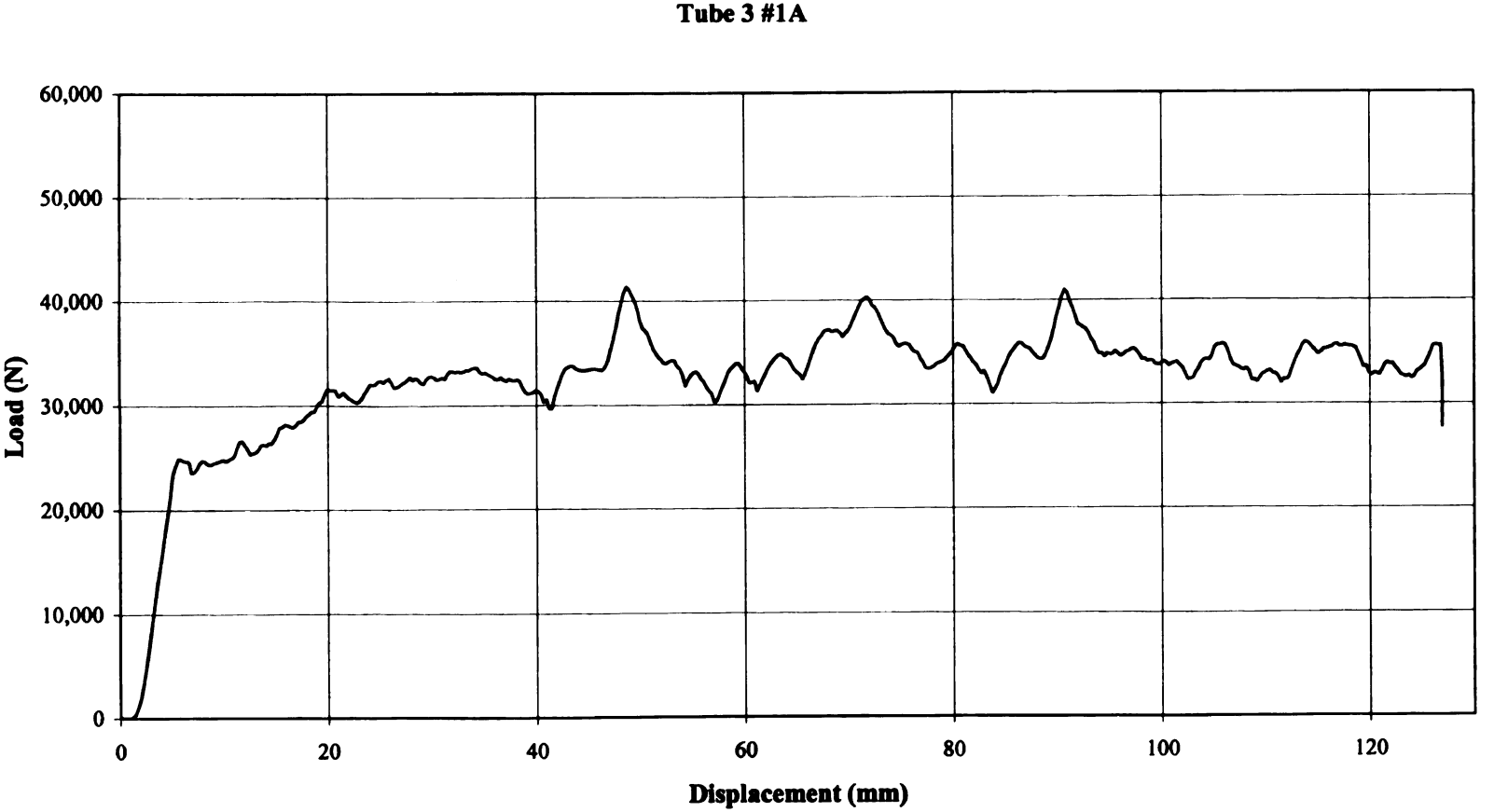

Appendix A2

Glass Fiber Composite Crush Tube
Quasi-Static Rate

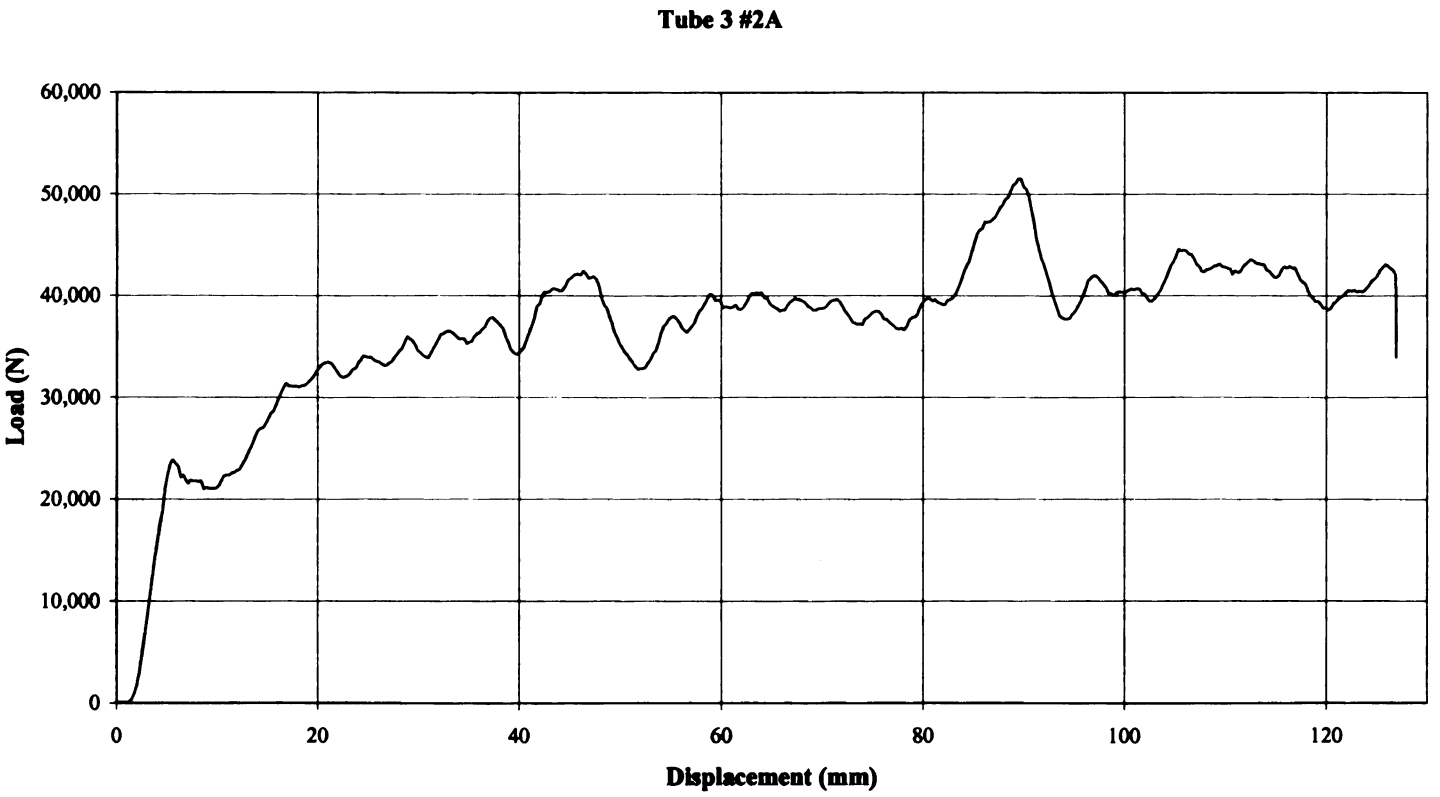

Appendix A3

Glass Fiber Composite Crush Tube
Quasi-Static Rate

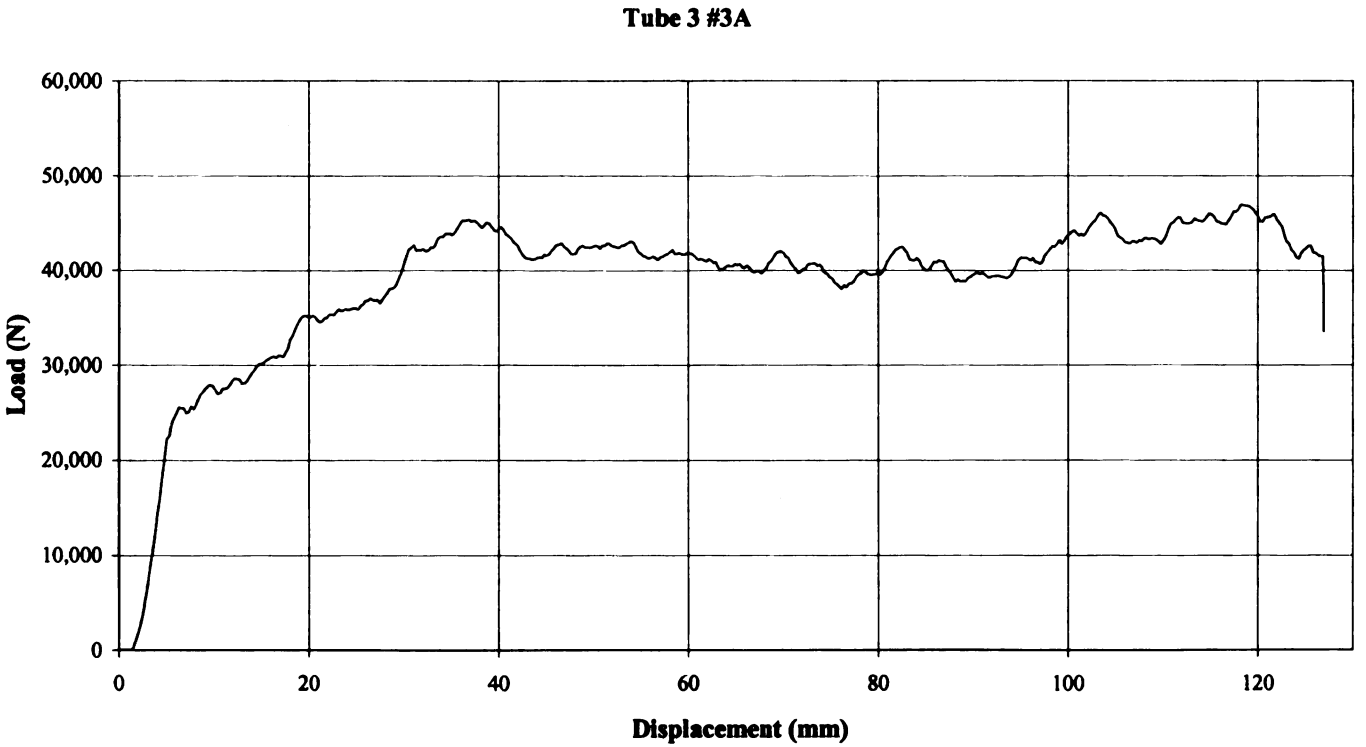

Appendix A4

Glass Fiber Composite Crush Tube
Quasi-Static Rate

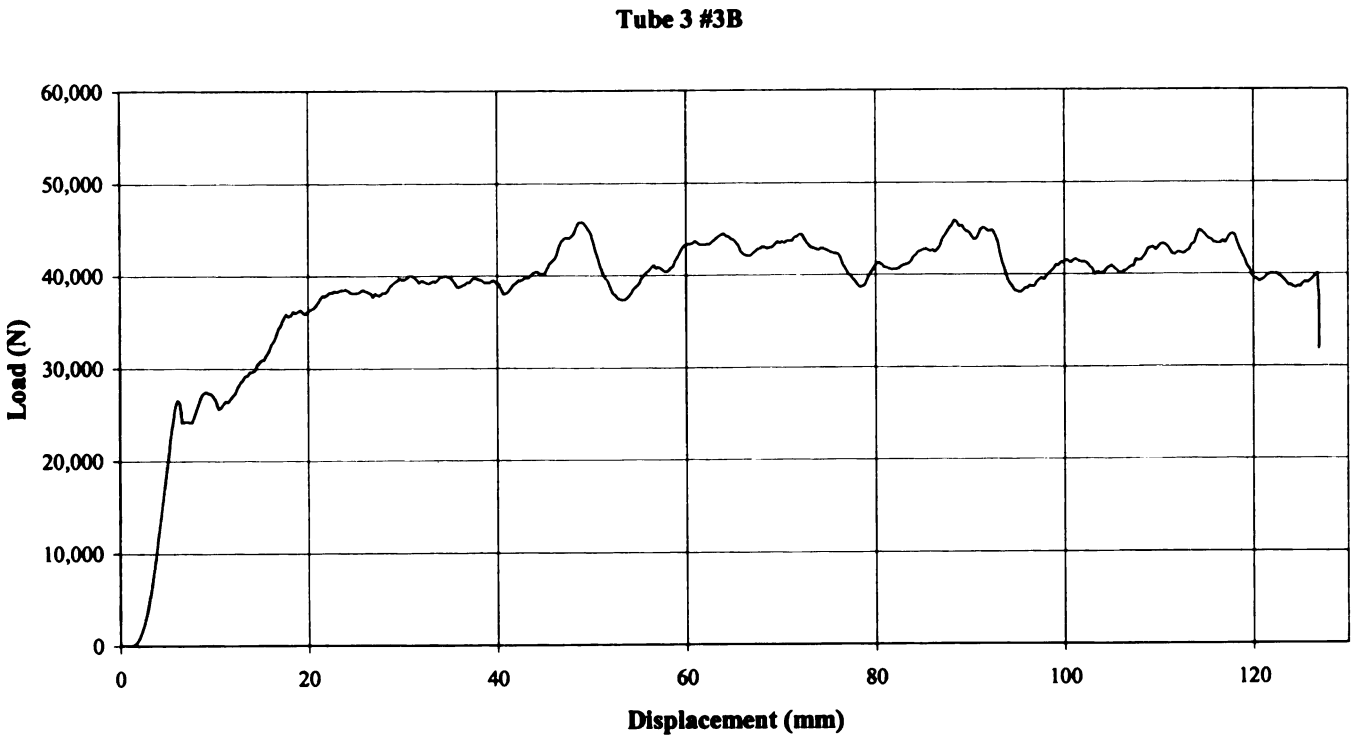

Appendix A5

Glass Fiber Composite Crush Tube
Quasi-Static Rate

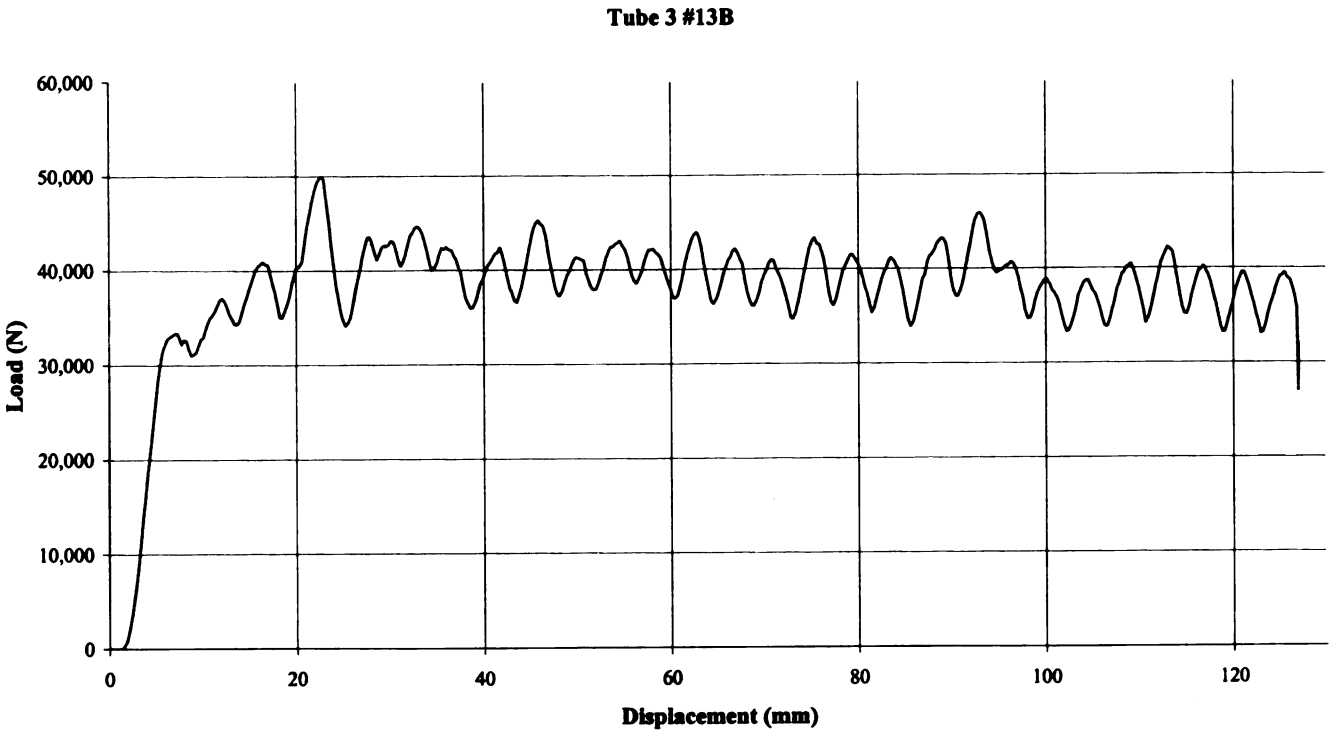

APPENDIX B

Carbon Fiber Composite Crush Tube Load Curves

APPENDIX B1

Carbon Fiber Composite Crush Tube
Quasi-Static Rate

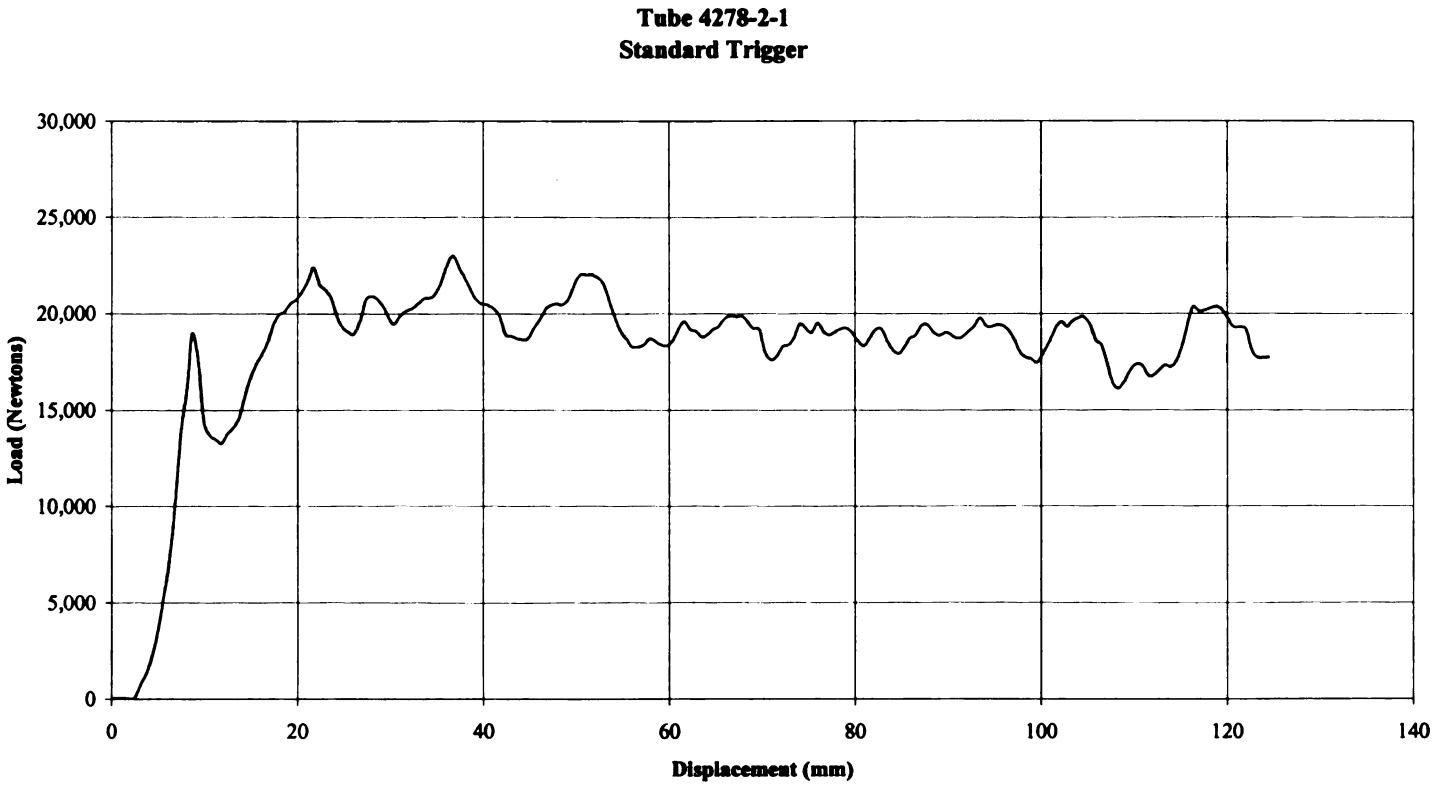

APPENDIX B2

Carbon Fiber Composite Crush Tube
Quasi-Static Rate

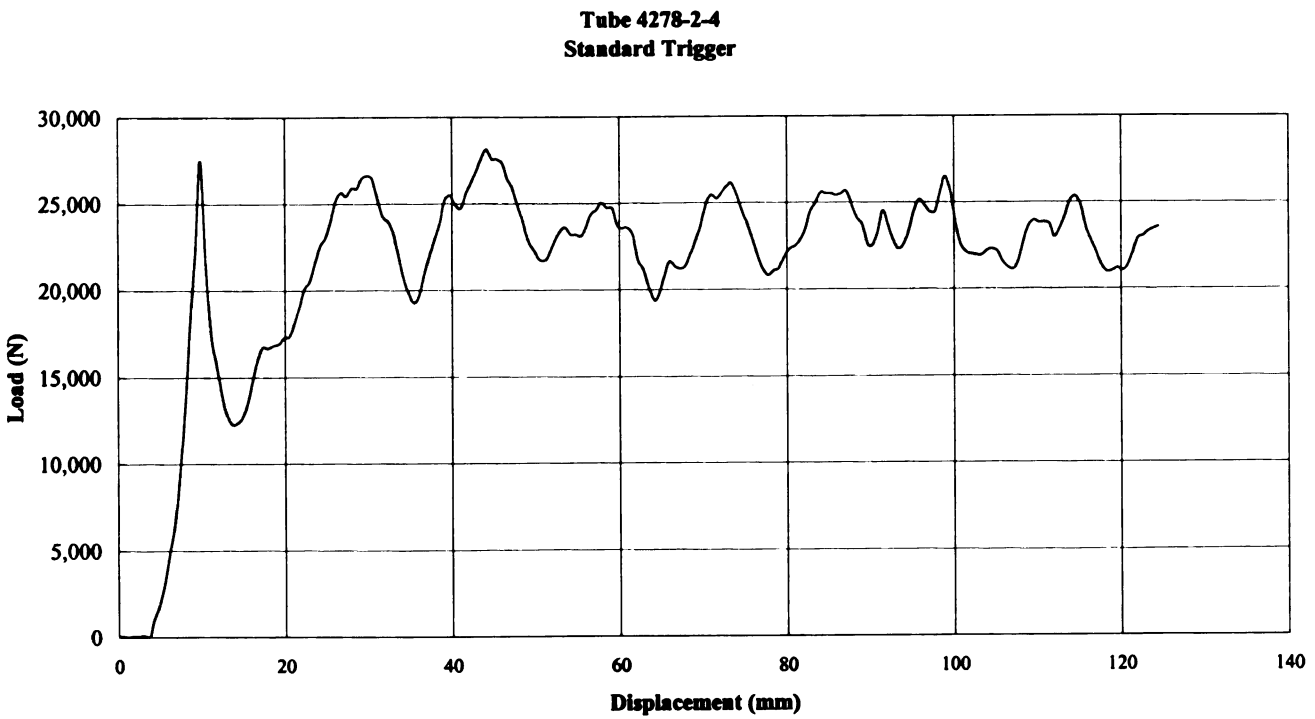

APPENDIX B3

Carbon Fiber Composite Crush Tube
Quasi-Static Rate

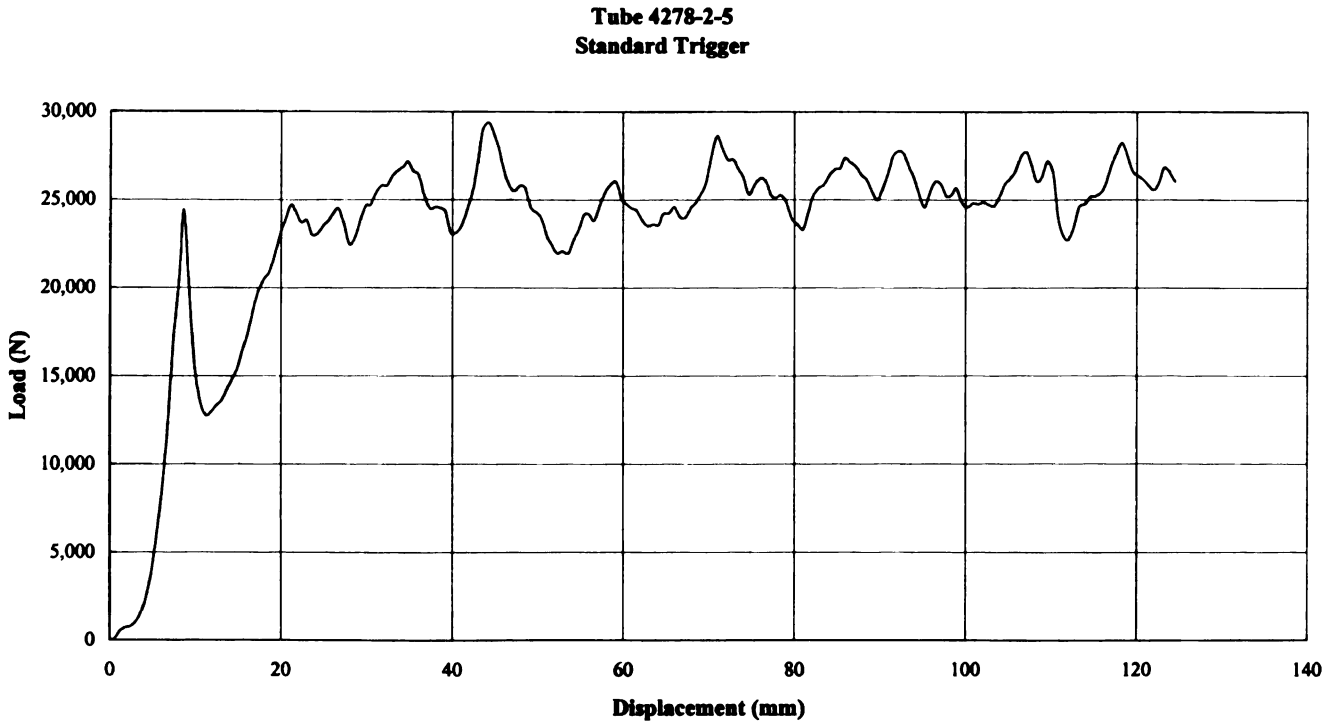

APPENDIX B5

Carbon Fiber Composite Crush Tube
Quasi-Static Rate

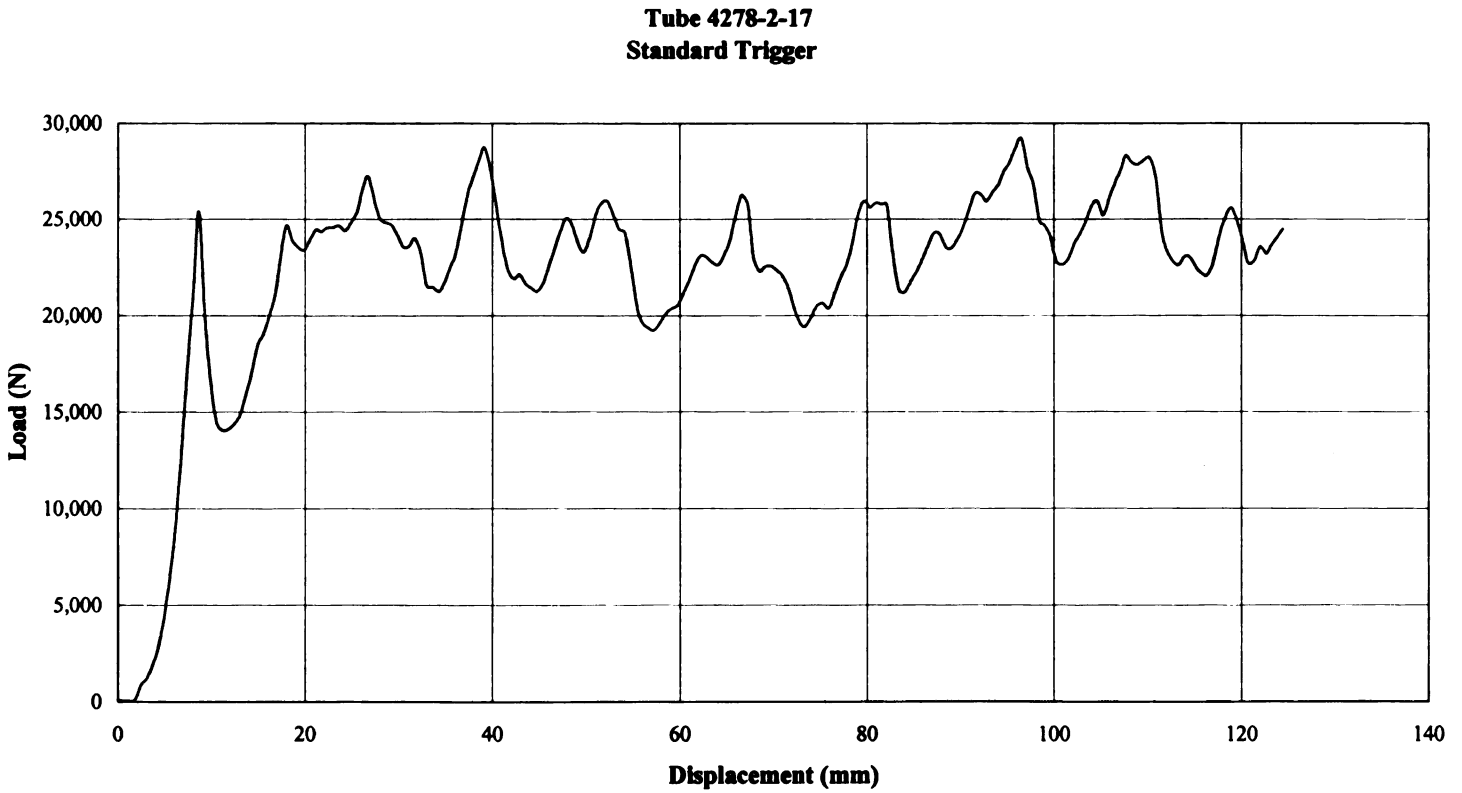

APPENDIX B6

Carbon Fiber Composite Crush Tube
Dynamic Rate (2.0 m/sec)

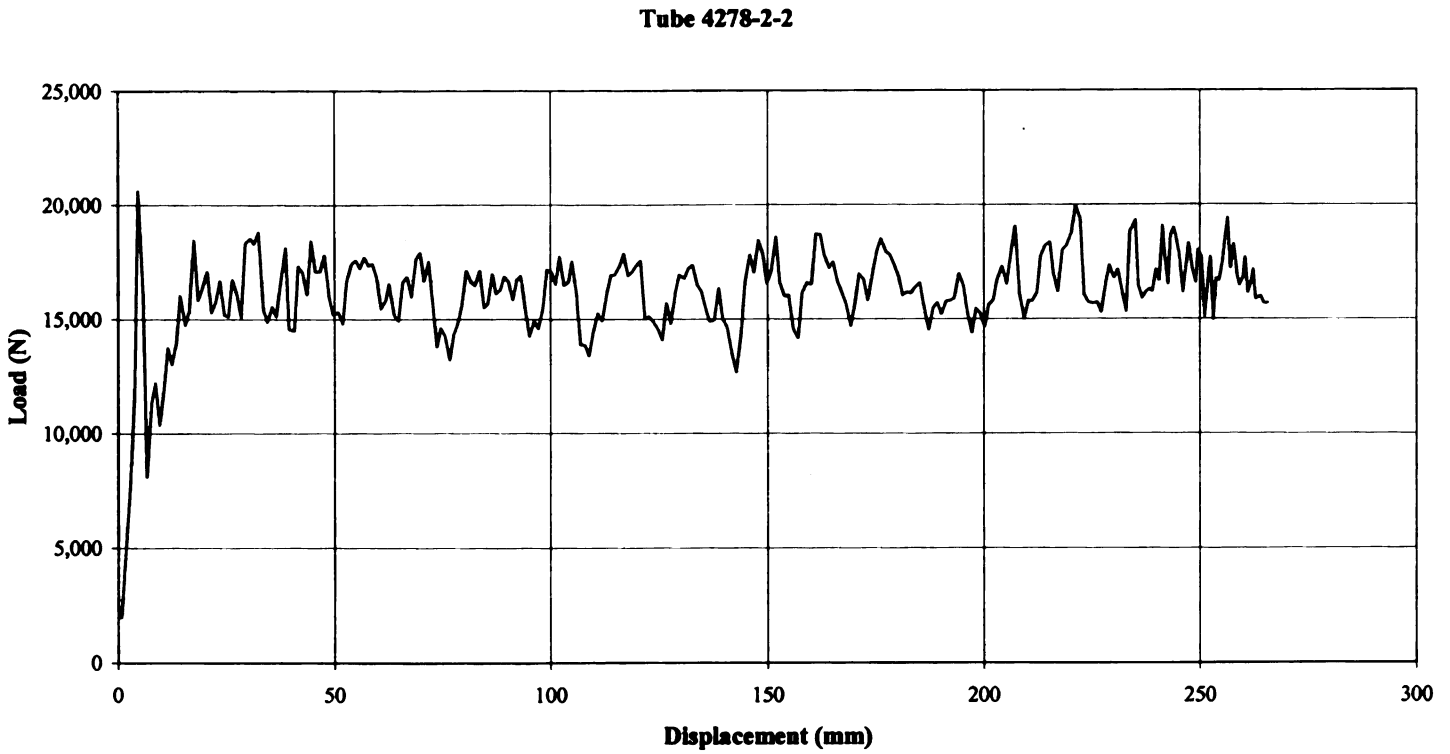

APPENDIX B7

Carbon Fiber Composite Crush Tube
Dynamic Rate (2.0 m/sec)

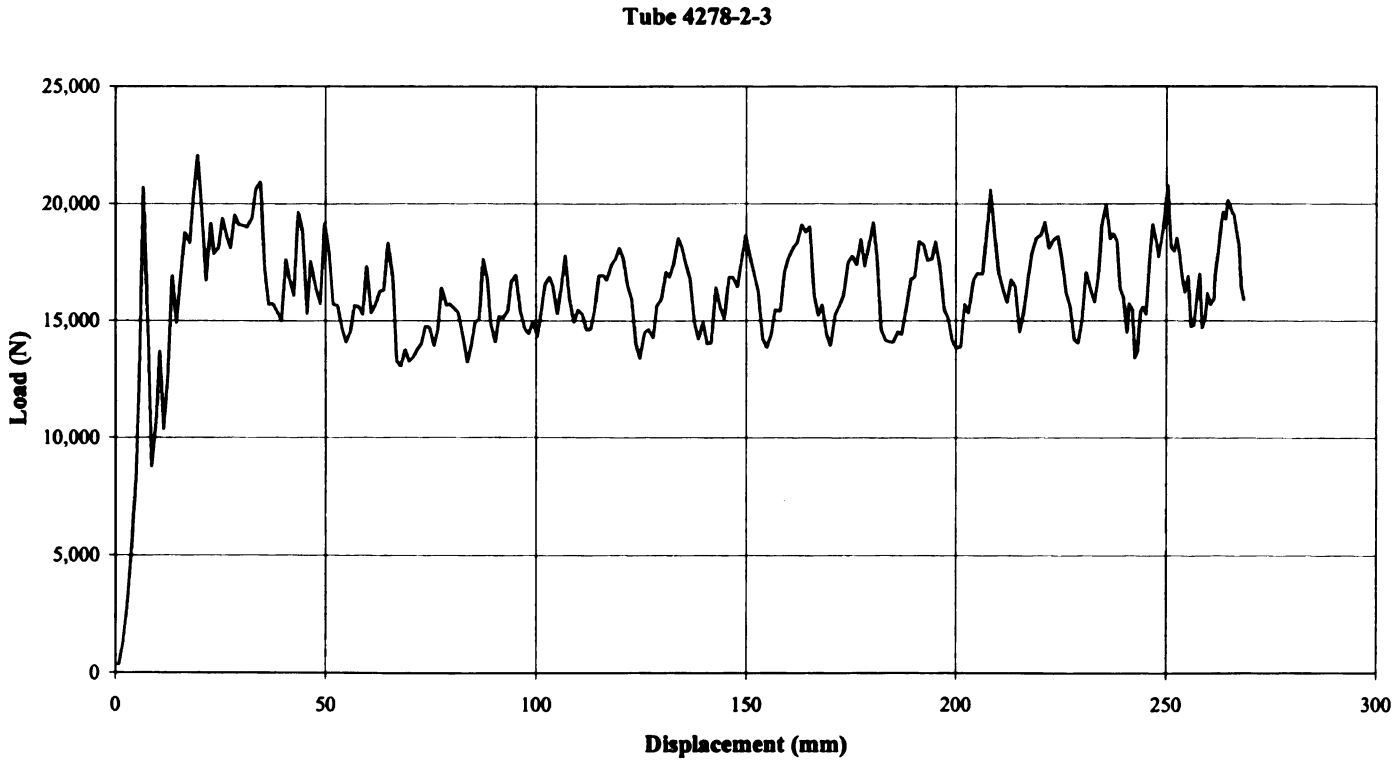

APPENDIX B8

Carbon Fiber Composite Crush Tube
Dynamic Rate (2.0 m/sec)

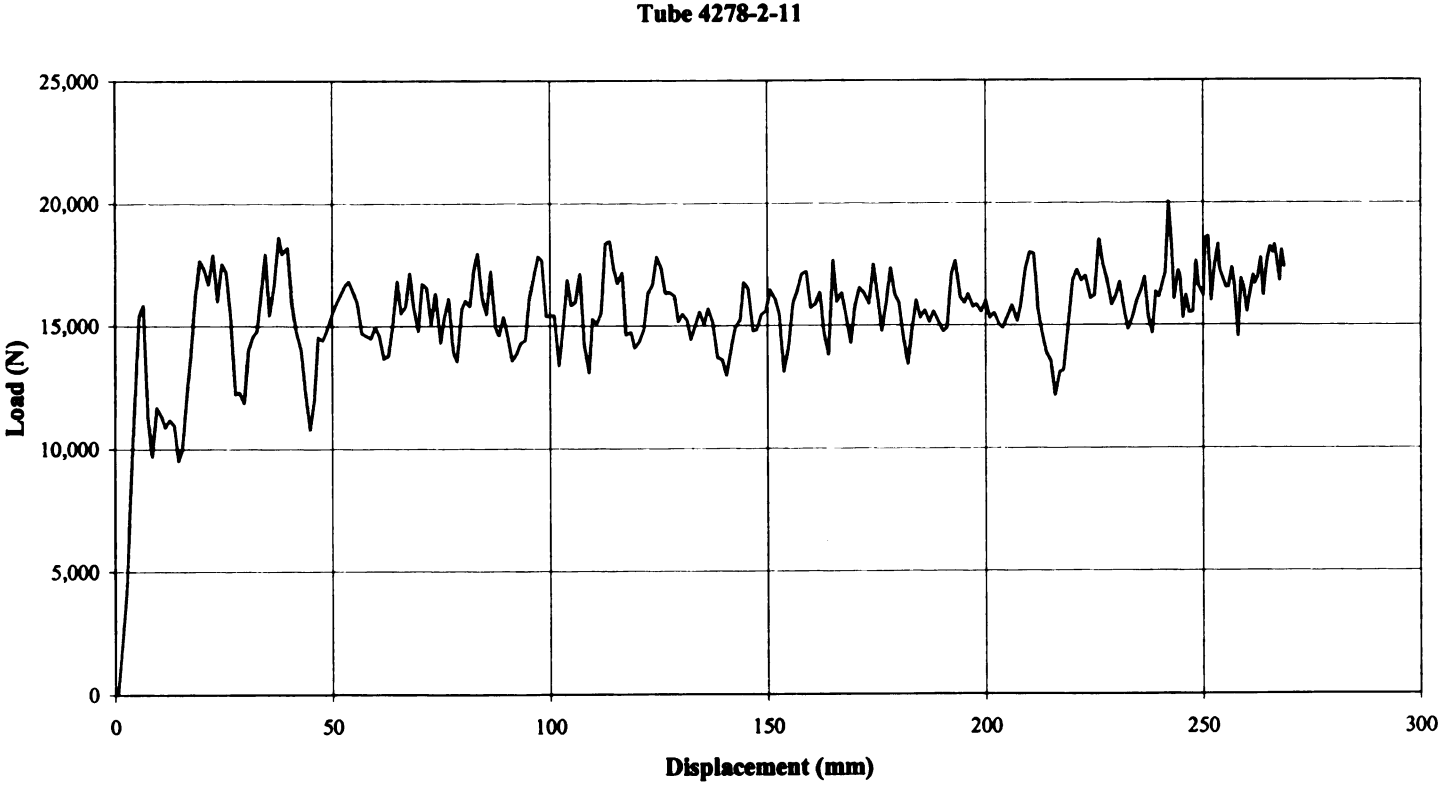

APPENDIX B9

Carbon Fiber Composite Crush Tube
Dynamic Rate (2.0 m/sec)

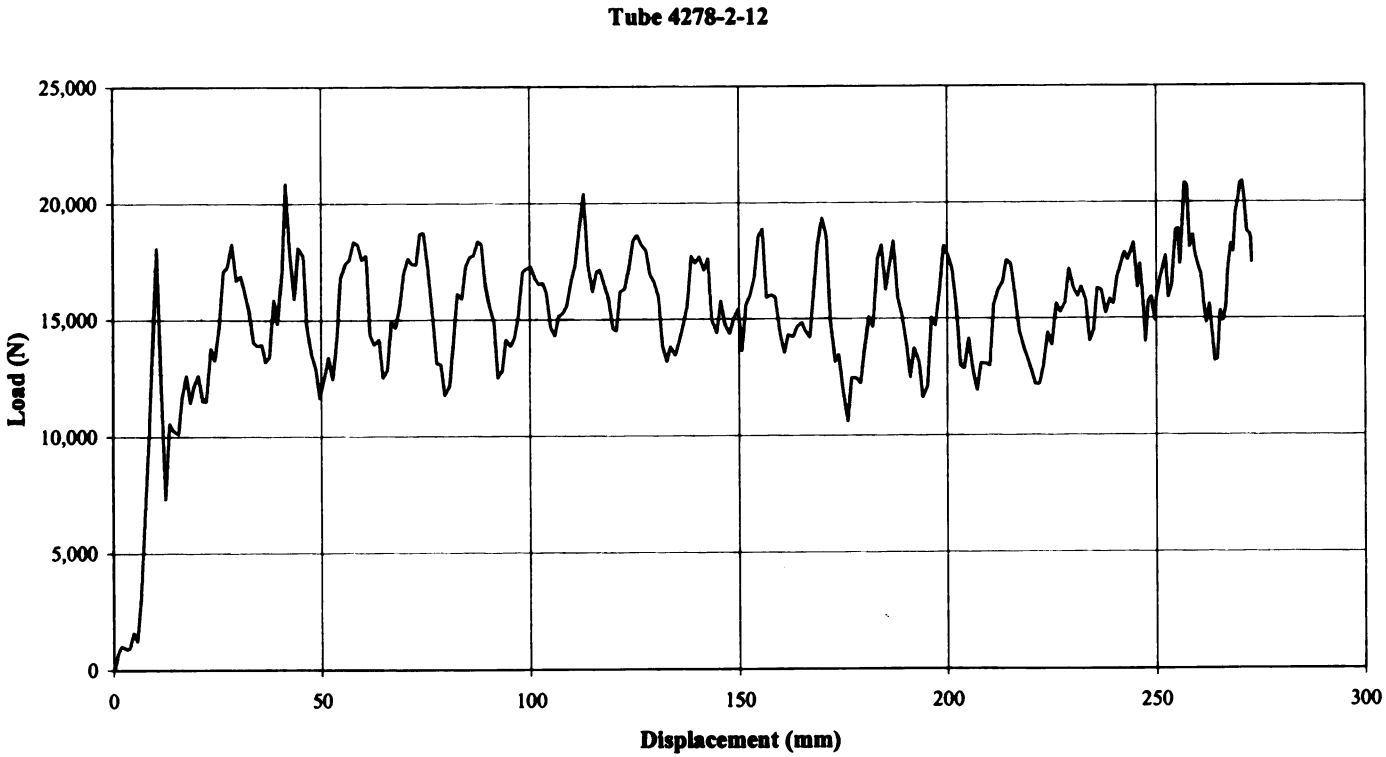

APPENDIX B10

Carbon Fiber Composite Crush Tube
Dynamic Rate (2.0 m/sec)

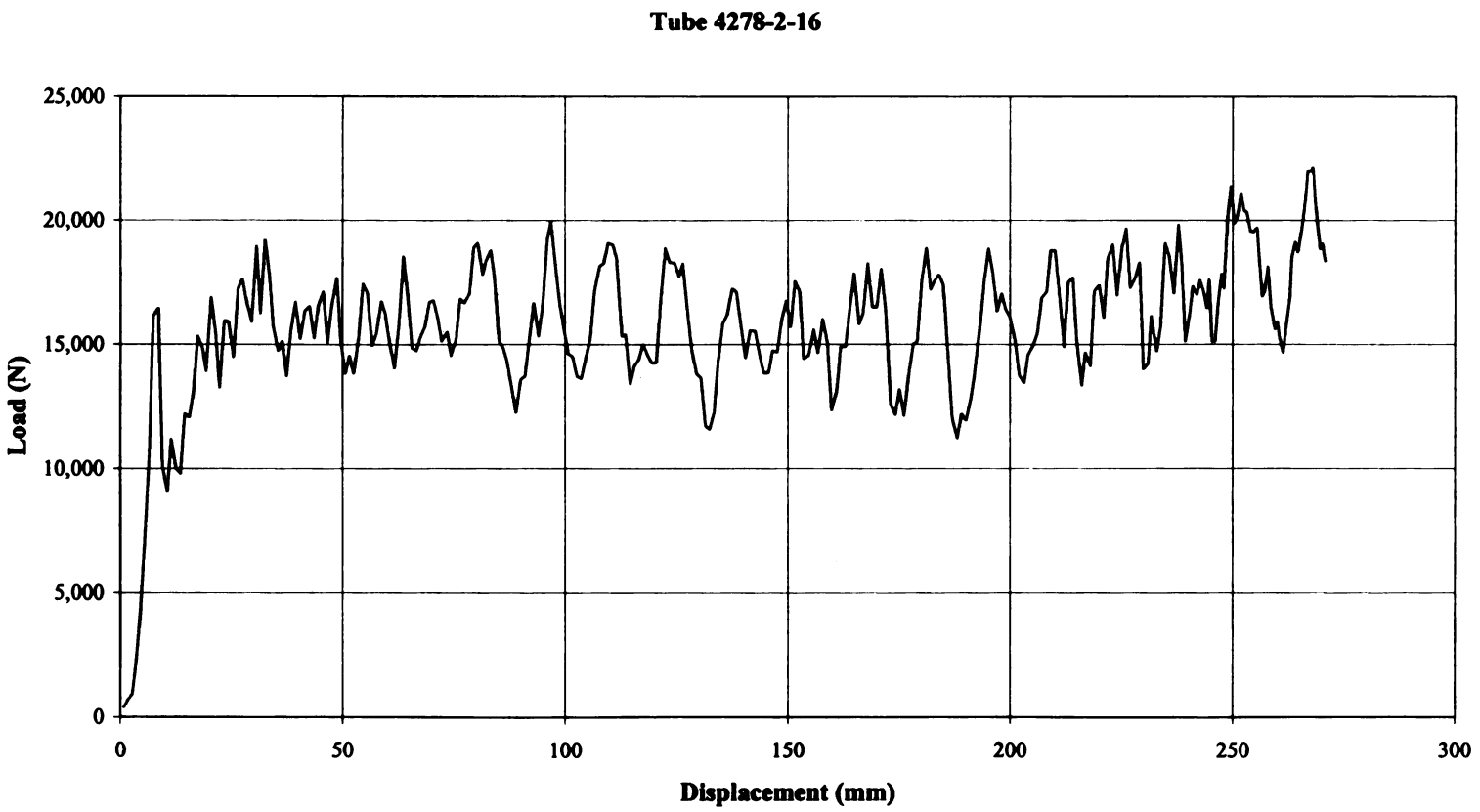

APPENDIX C

Crush Tubes with Tapered Trigger Load Curves

APPENDIX C1

Glass Fiber Composite With Tapered Trigger
Quasi-Static Load Rate

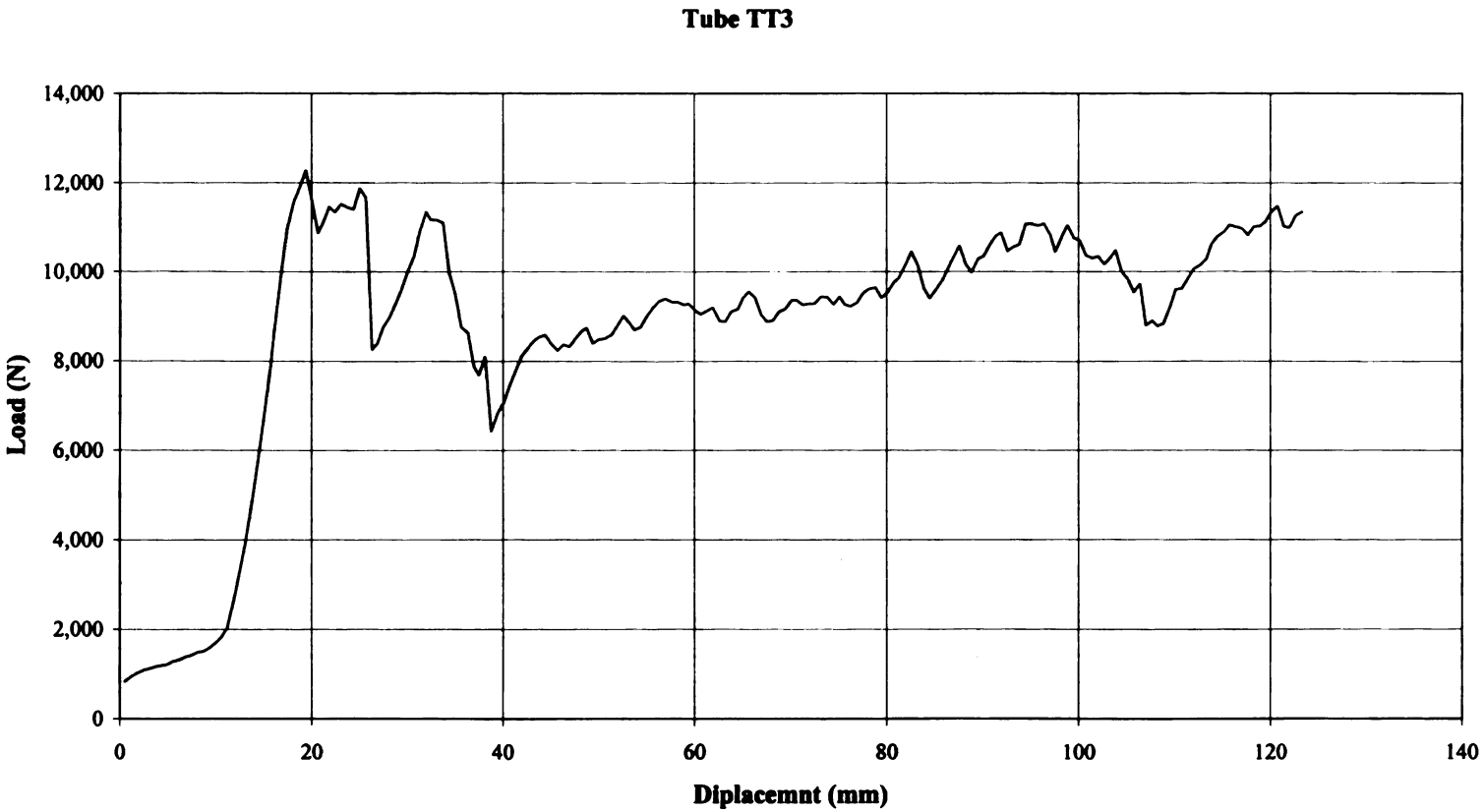

APPENDIX C2

Glass Fiber Composite With Tapered Trigger
Quasi-Static Load Rate

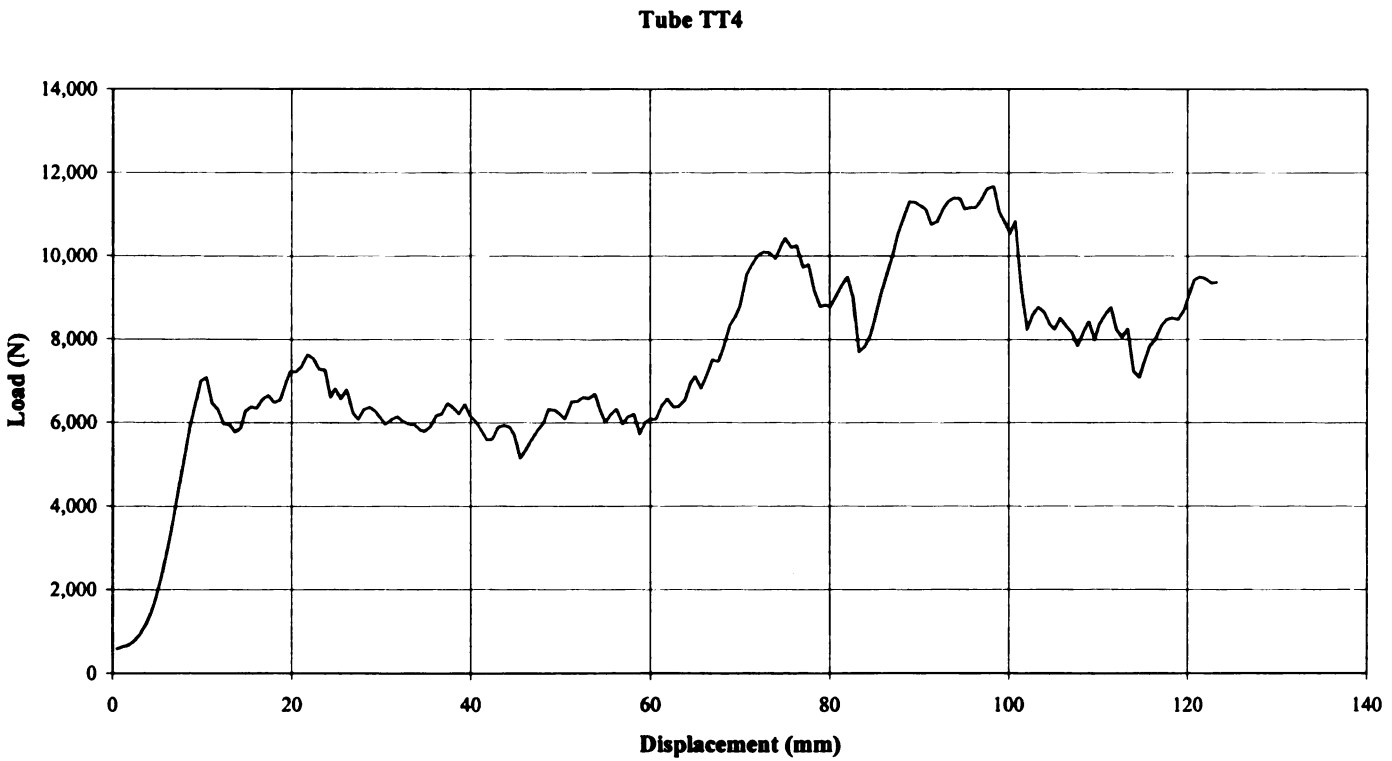

APPENDIX C4

Carbon Fiber Composite With Tapered Trigger
Quasi-Static Load Rate

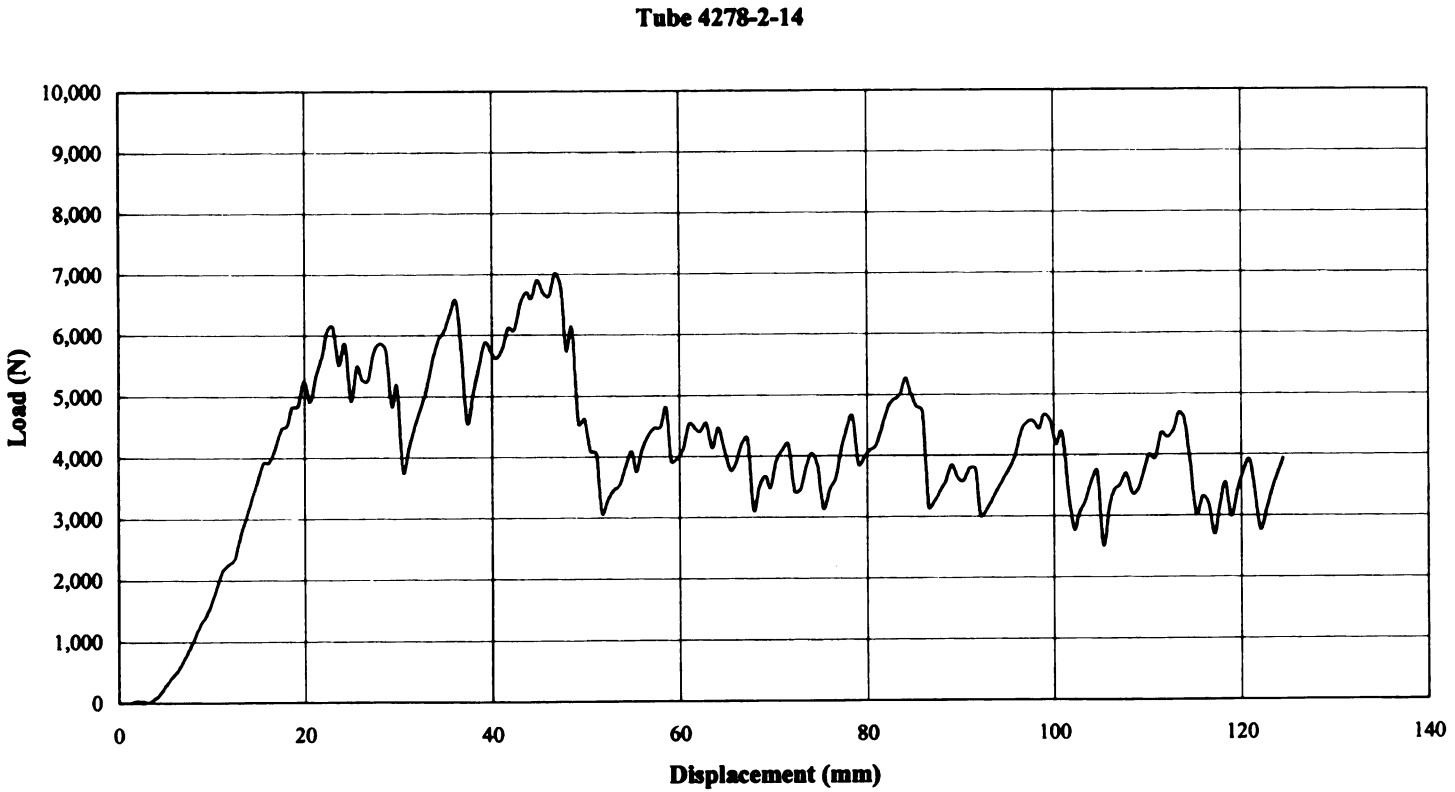

APPENDIX C5

Carbon Fiber Composite With Tapered Trigger
Quasi-Static Load Rate

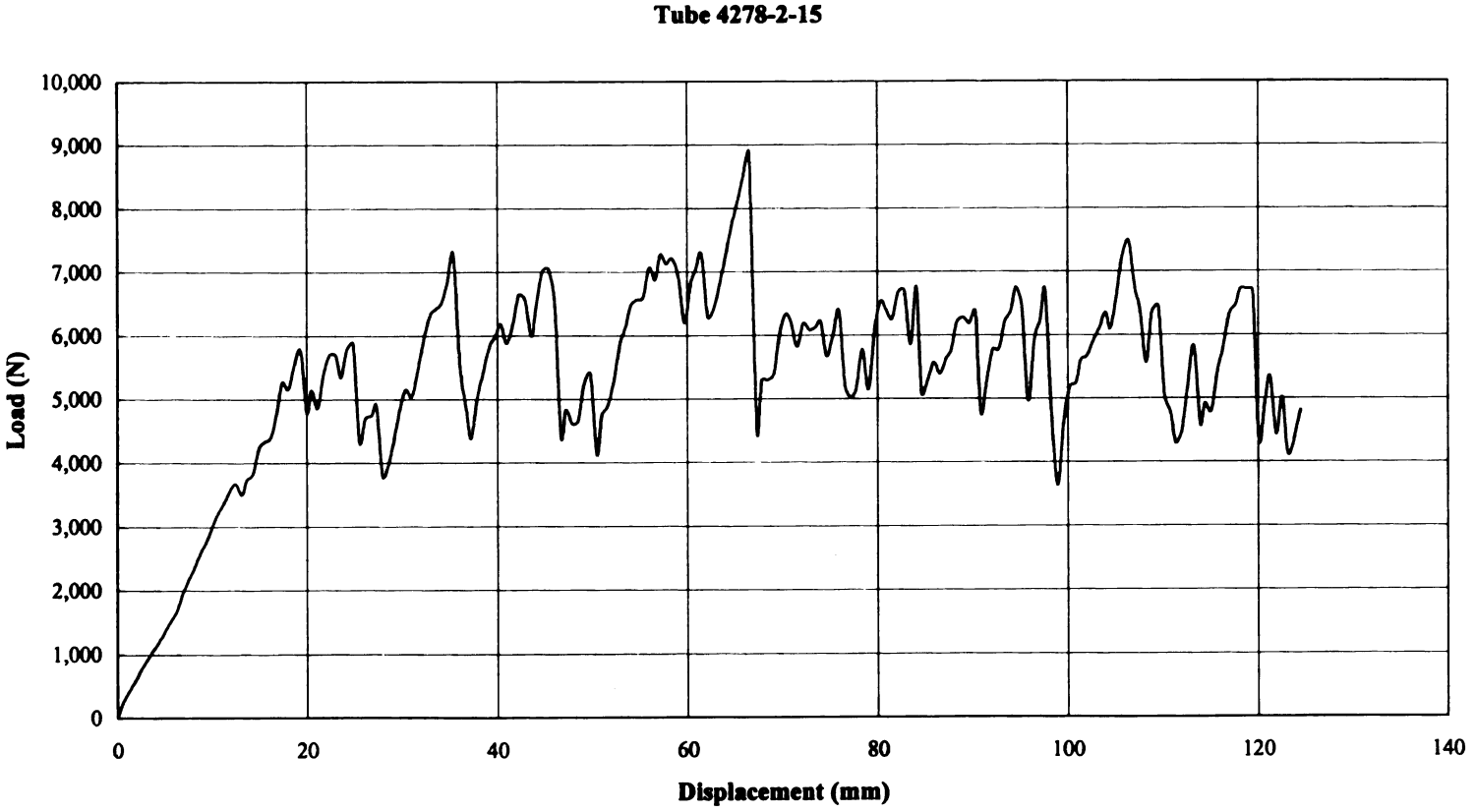

APPENDIX C6

Carbon Fiber Composite With Tapered Trigger
Quasi-Static Load Rate

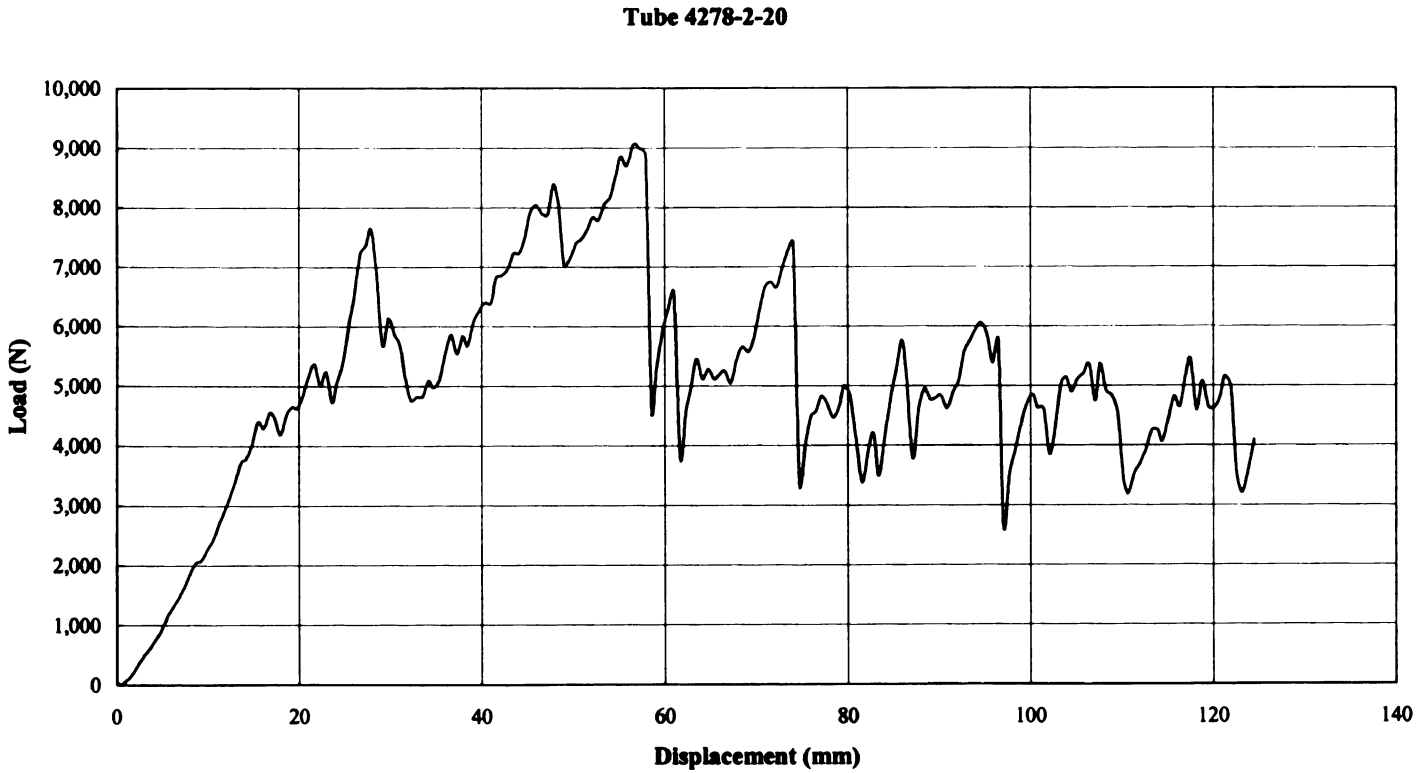

APPENDIX D

Carbon Fiber Composite Strip Test Load Curves

Appendix D1

Carbon Fiber Composite Strip Test
Fixed Roller, Quasi-Static Load Rate

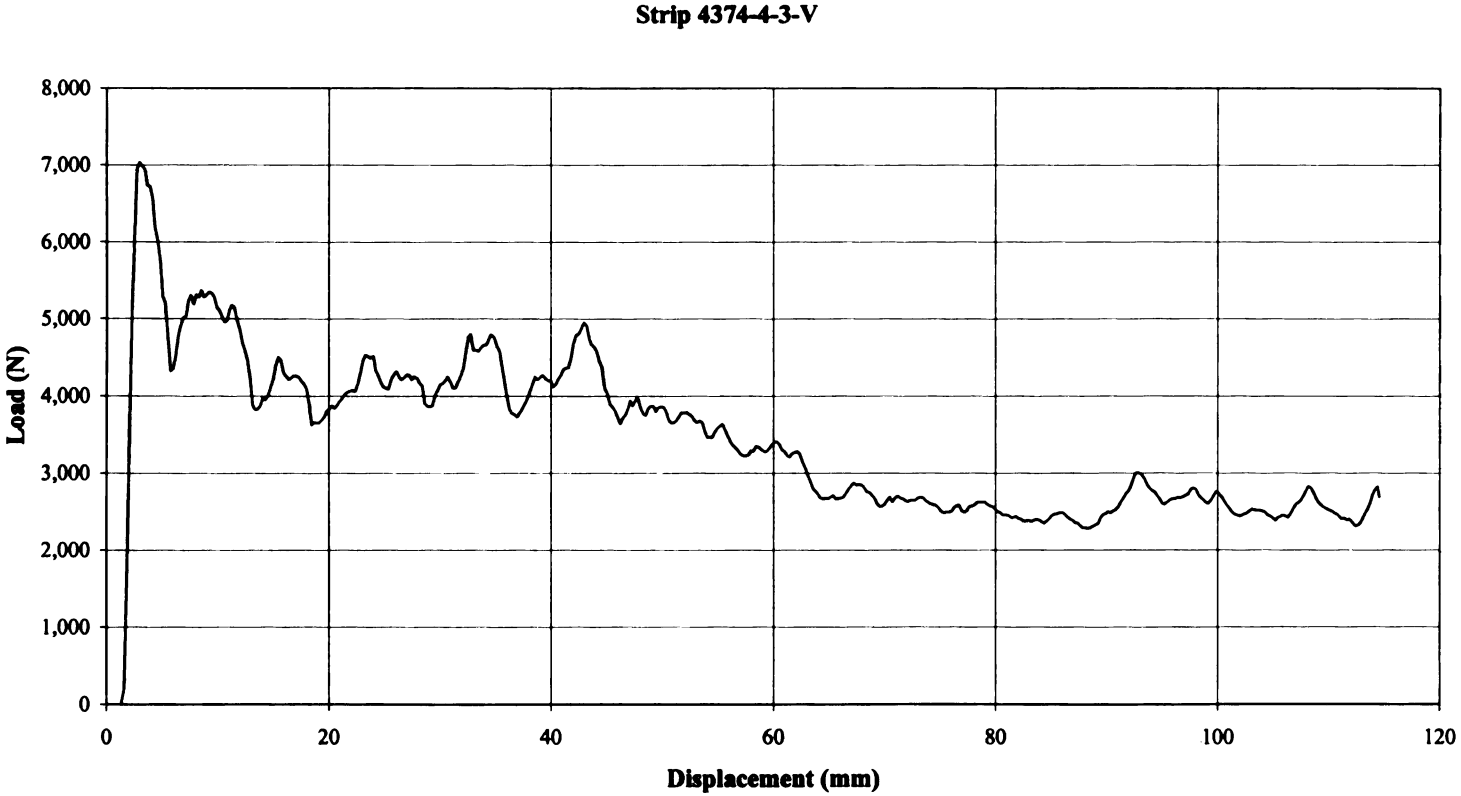

Appendix D2

Carbon Fiber Composite Strip Test
Fixed Roller, Quasi-Static Load Rate

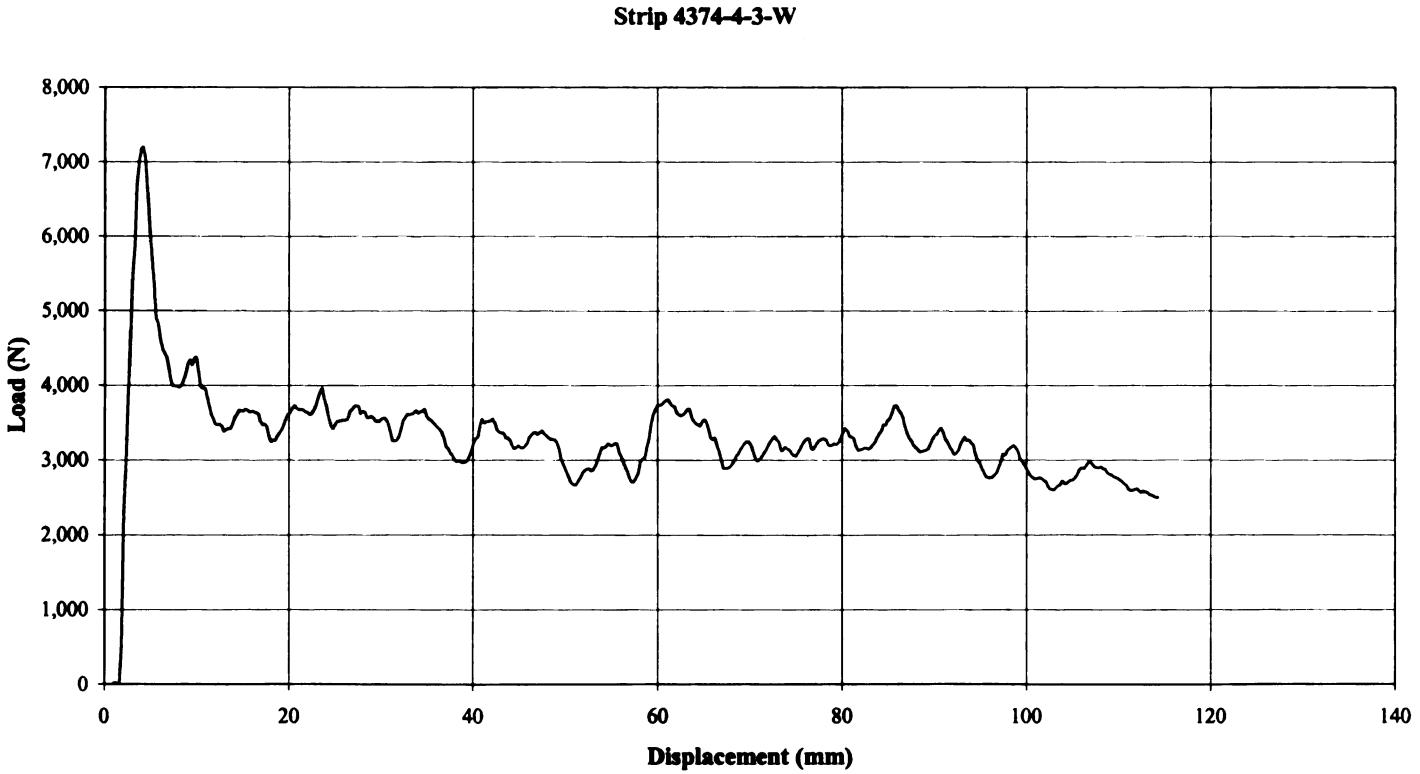

Appendix D3

Carbon Fiber Composite Strip Test
Fixed Roller, Quasi-Static Load Rate

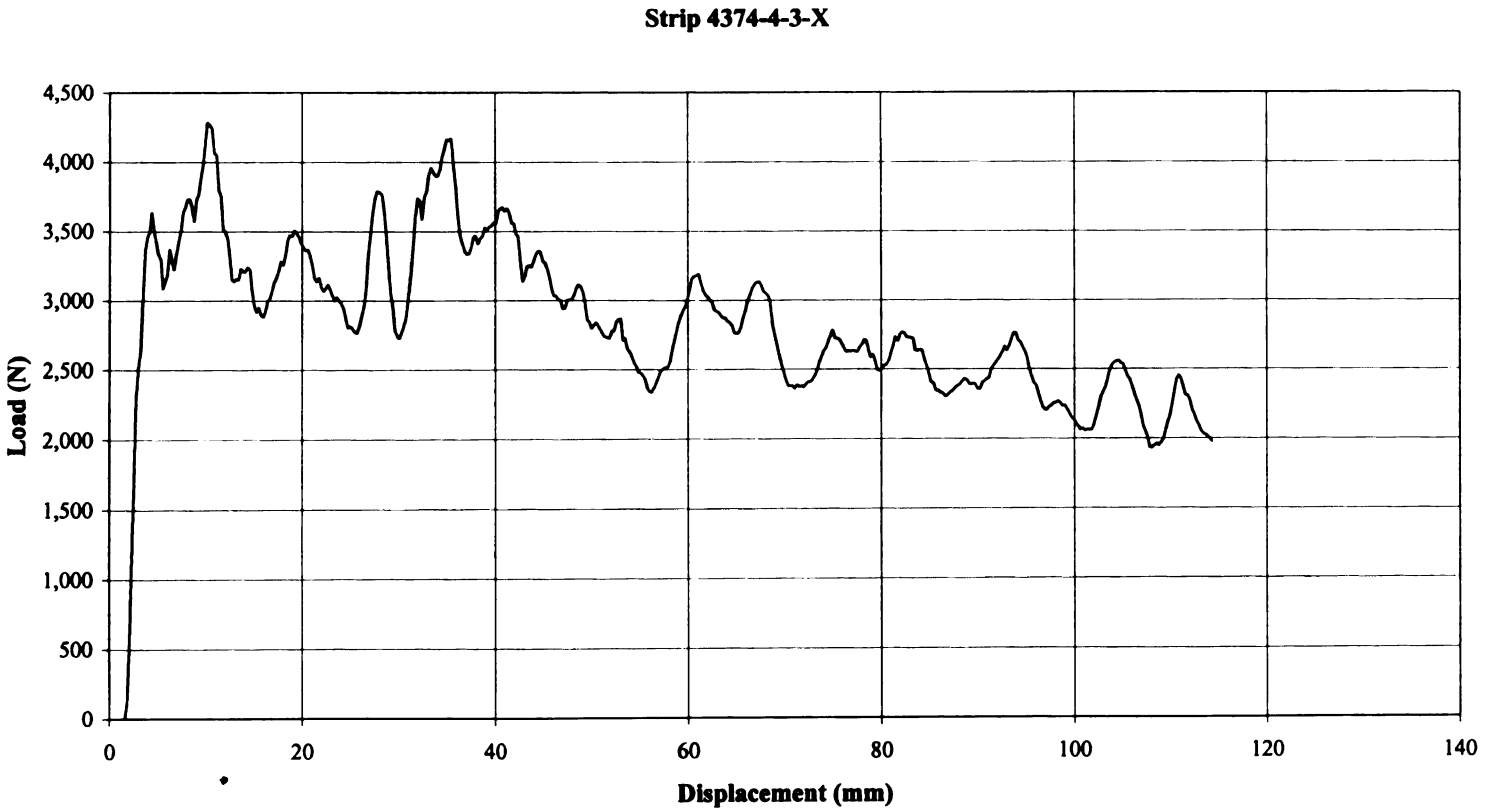

Appendix D4

Carbon Fiber Composite Strip Test
Fixed Roller, Quasi-Static Load Rate

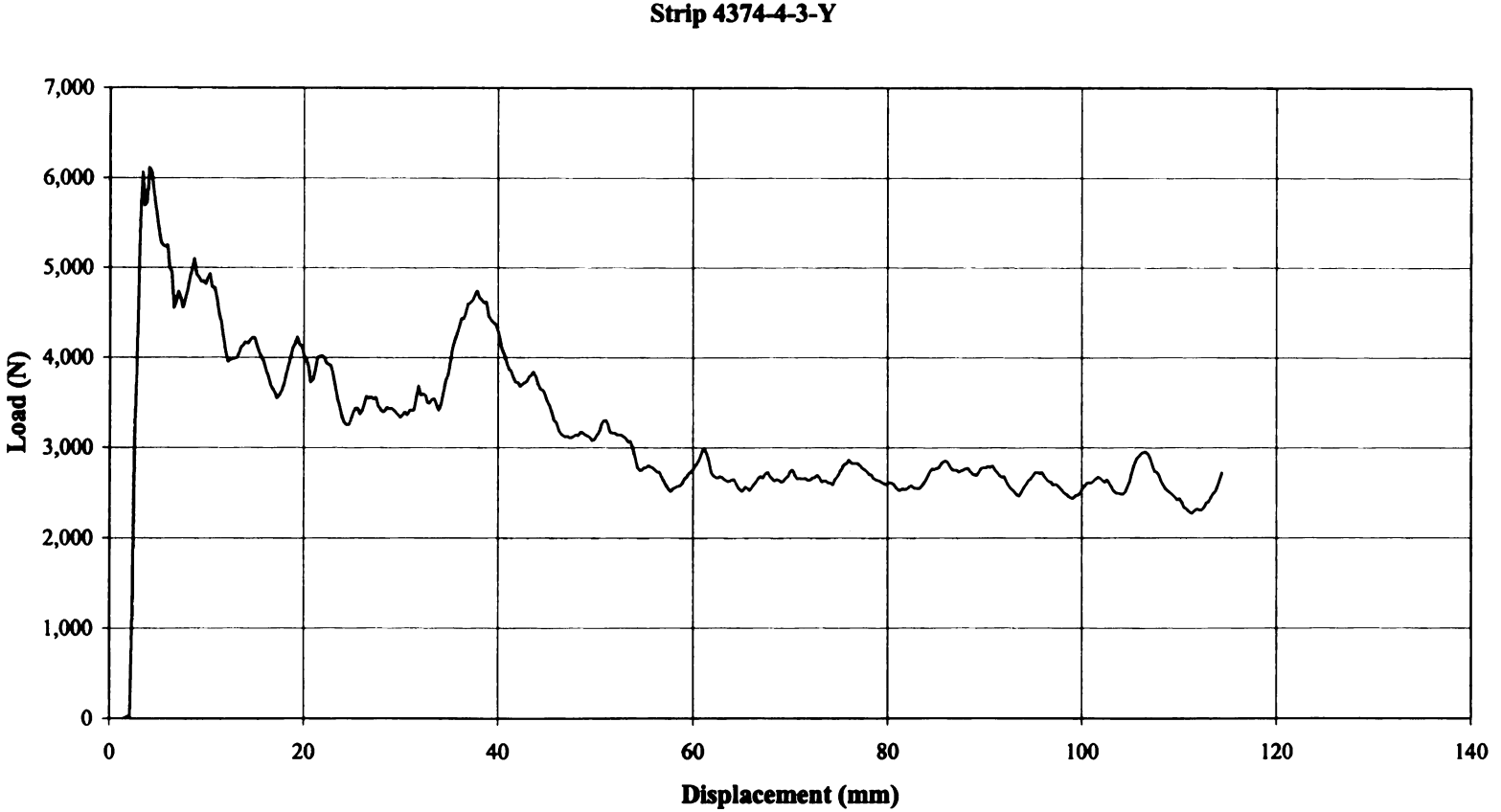

Appendix D5

Carbon Fiber Composite Strip Test
Fixed Roller, Quasi-Static Load Rate

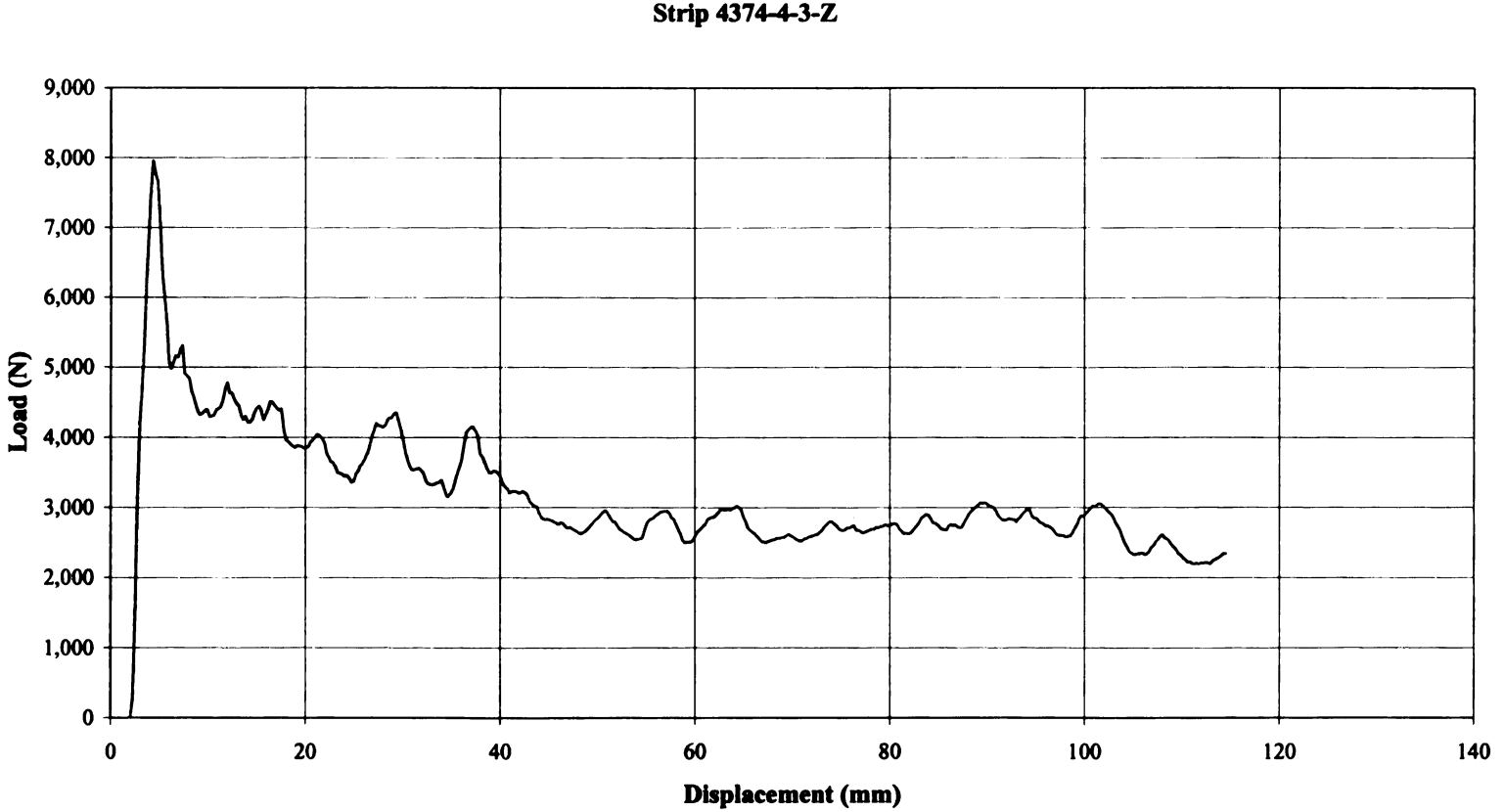

Appendix D6

Carbon Fiber Composite Strip Test
Zinc Stearate Lubrication, Fixed Roller, Quasi-Static Load Rate

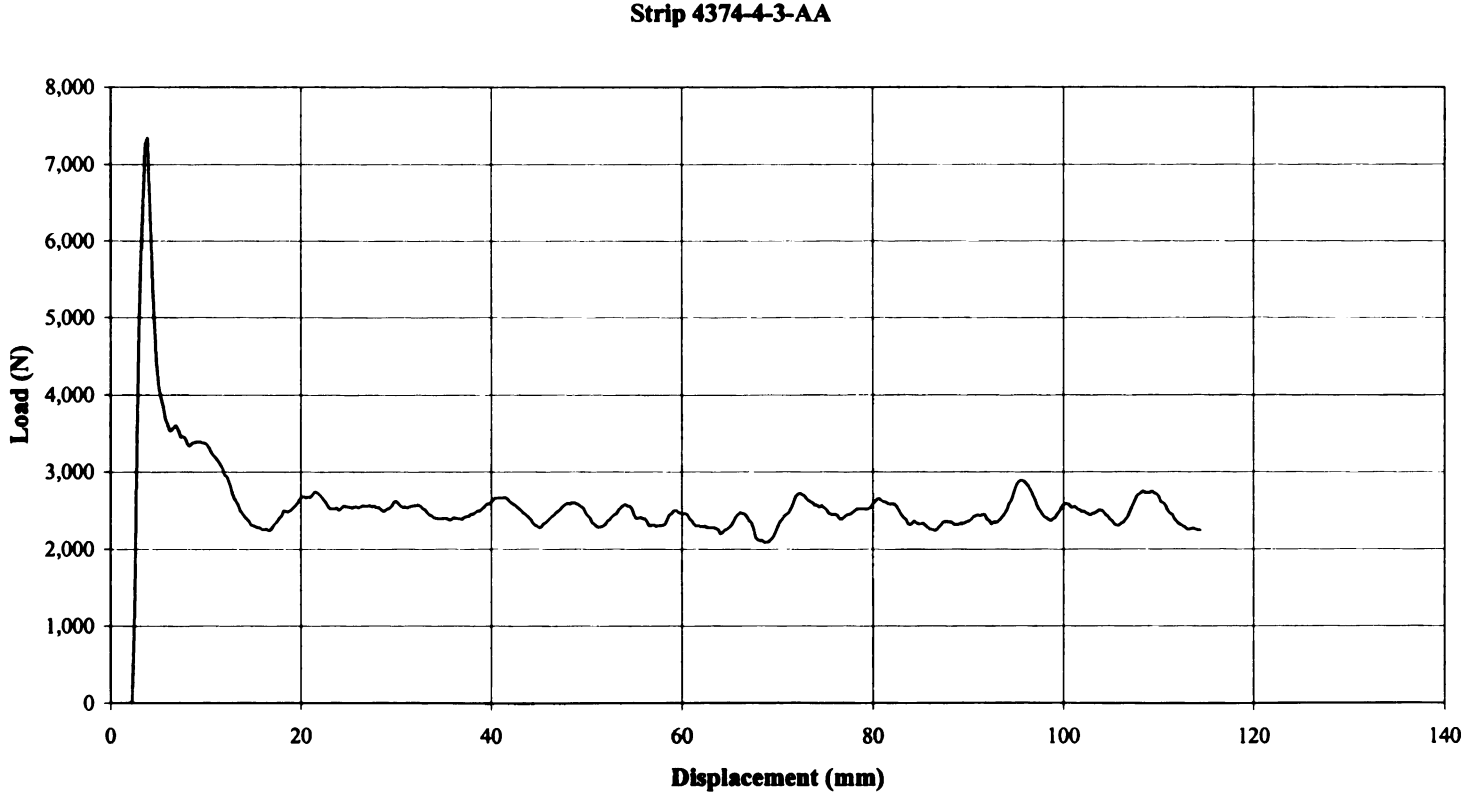

Appendix D8

Carbon Fiber Composite Strip Test
Zinc Stearate Lubrication, Fixed Roller, Quasi-Static Load Rate

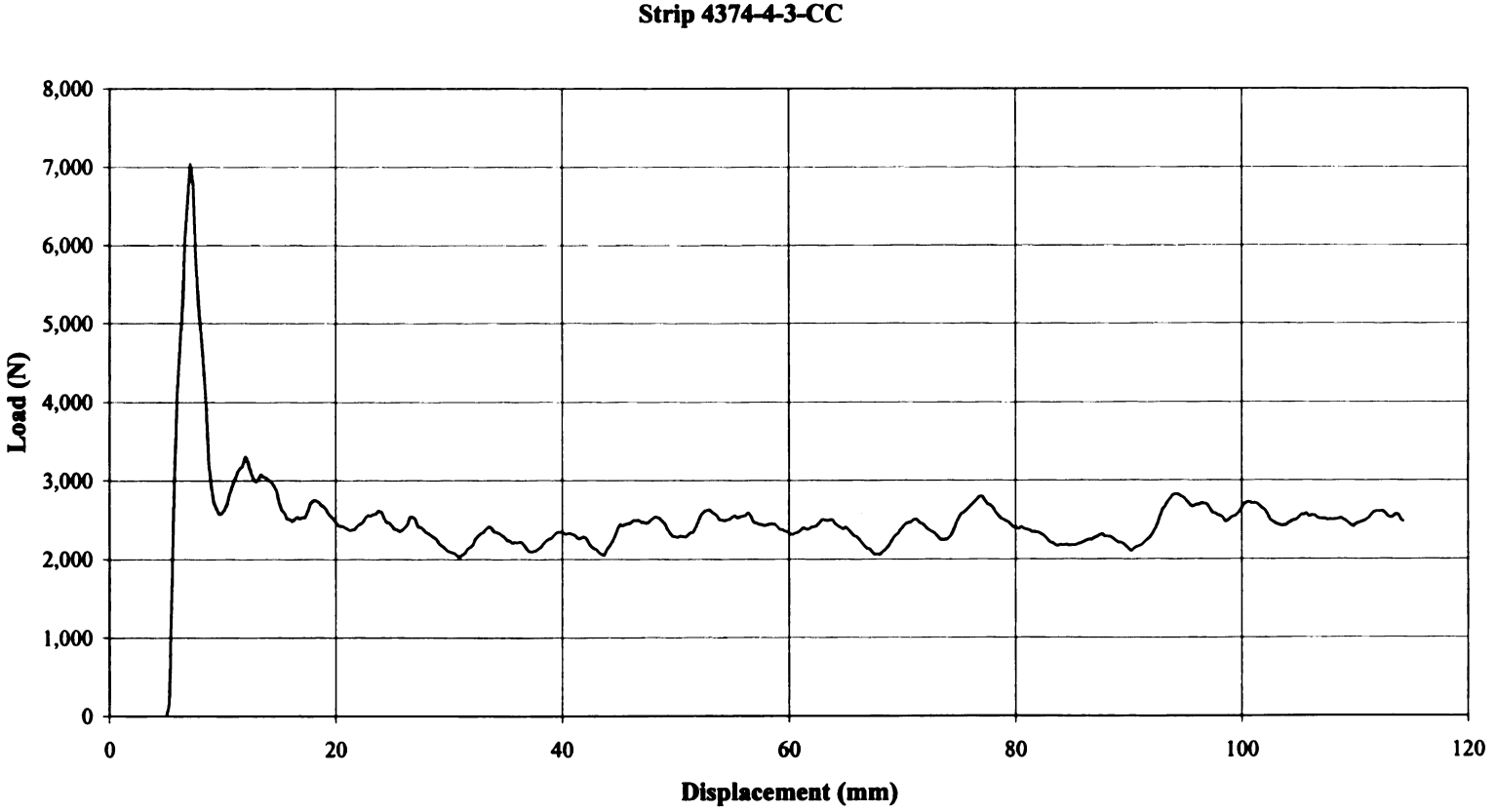

Appendix D9

Carbon Fiber Composite Strip Test
Zinc Stearate Lubrication, Fixed Roller, Quasi-Static Load Rate

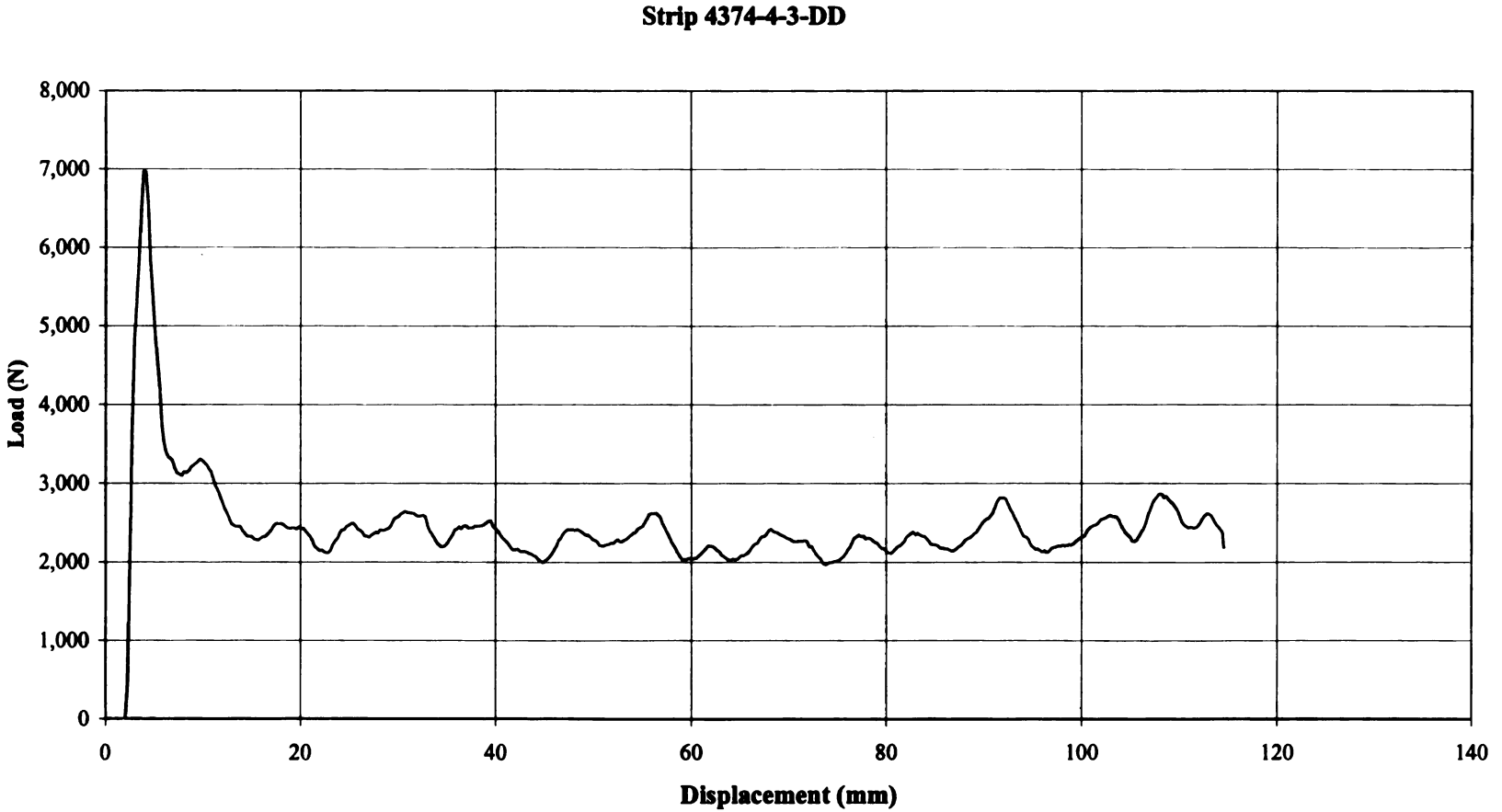

Appendix D10

Carbon Fiber Composite Strip Test
Zinc Stearate Lubrication, Fixed Roller, Quasi-Static Load Rate

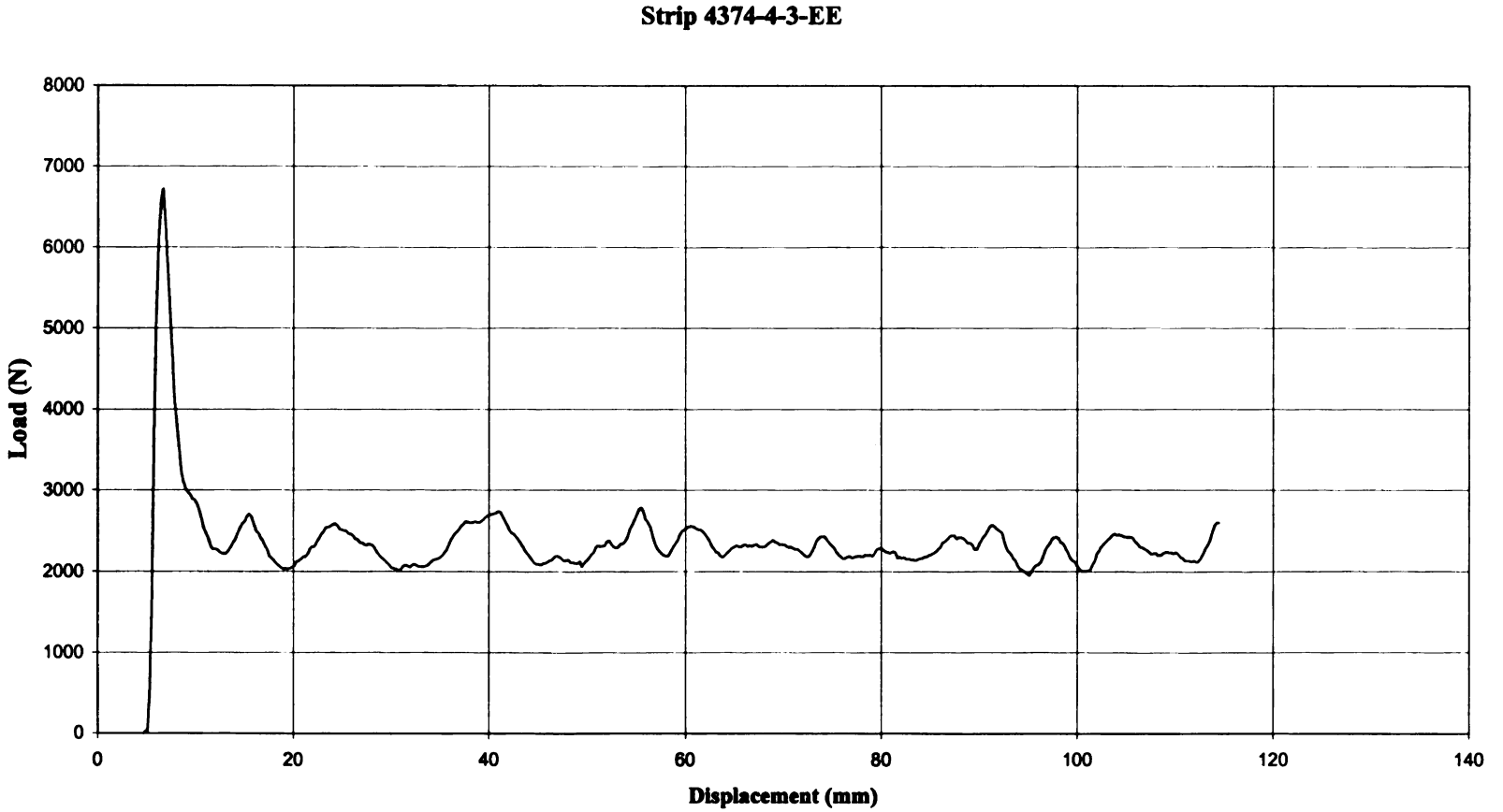

Appendix D11

Carbon Fiber Composite Strip Test
Free Roller, Quasi-Static Load Rate

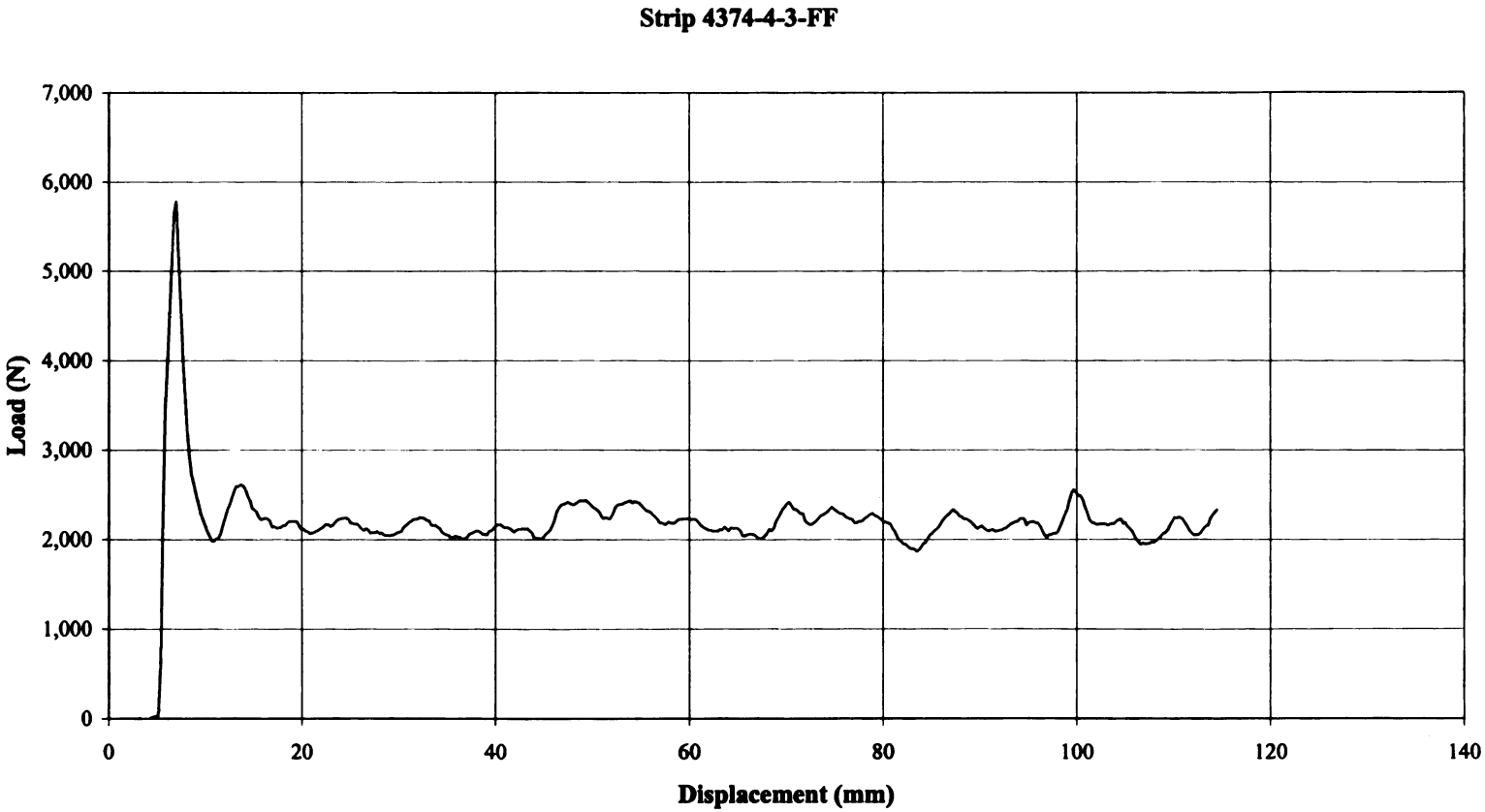

Appendix D13

Carbon Fiber Composite Strip Test
Free Roller, Quasi-Static Load Rate

Appendix D15

Carbon Fiber Composite Strip Test
Free Roller, Quasi-Static Load Rate

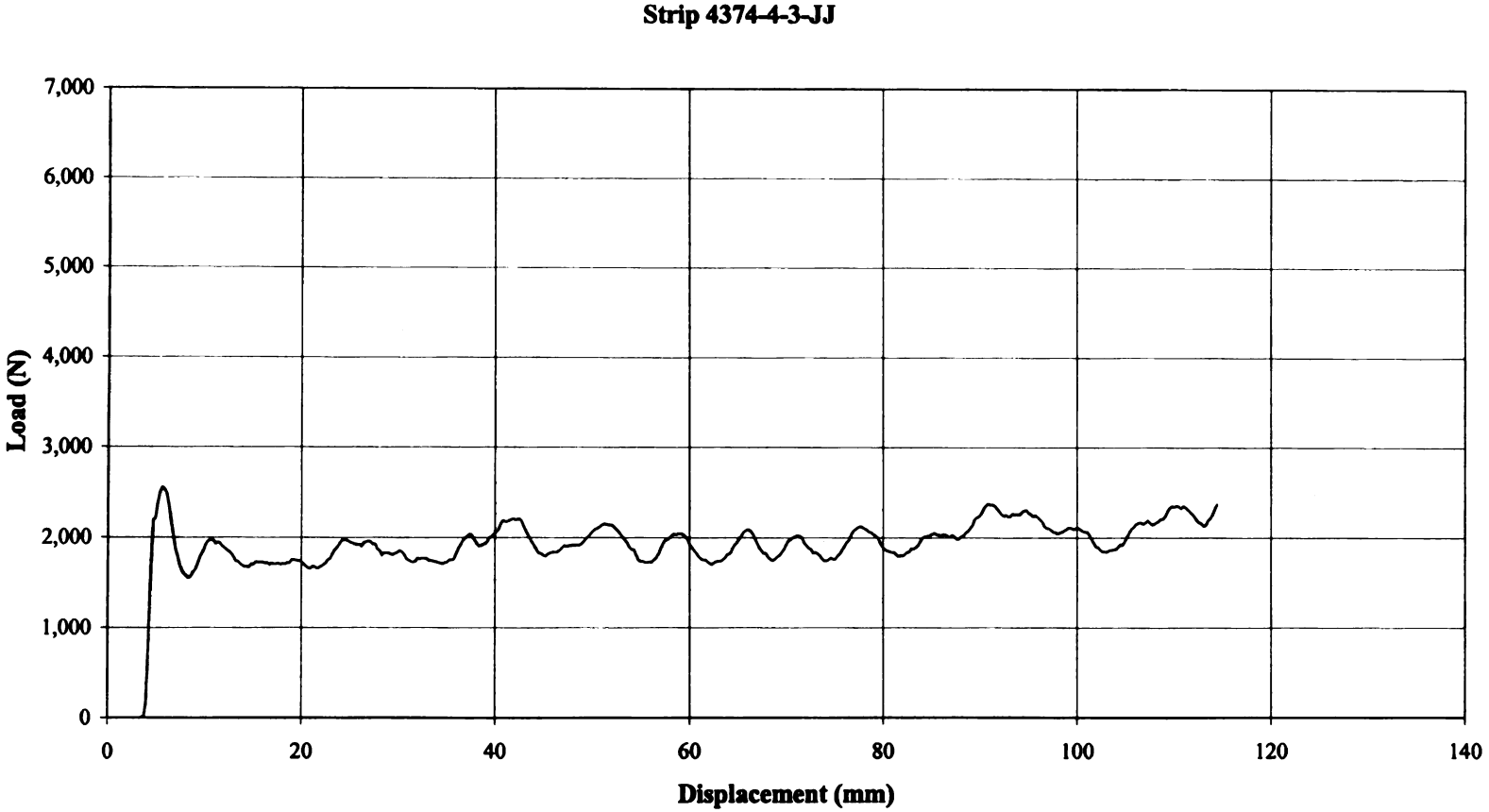

Appendix D16

Carbon Fiber Composite Strip Test
Fixed Roller, Dynamic Load Rate (2.0 m/s)

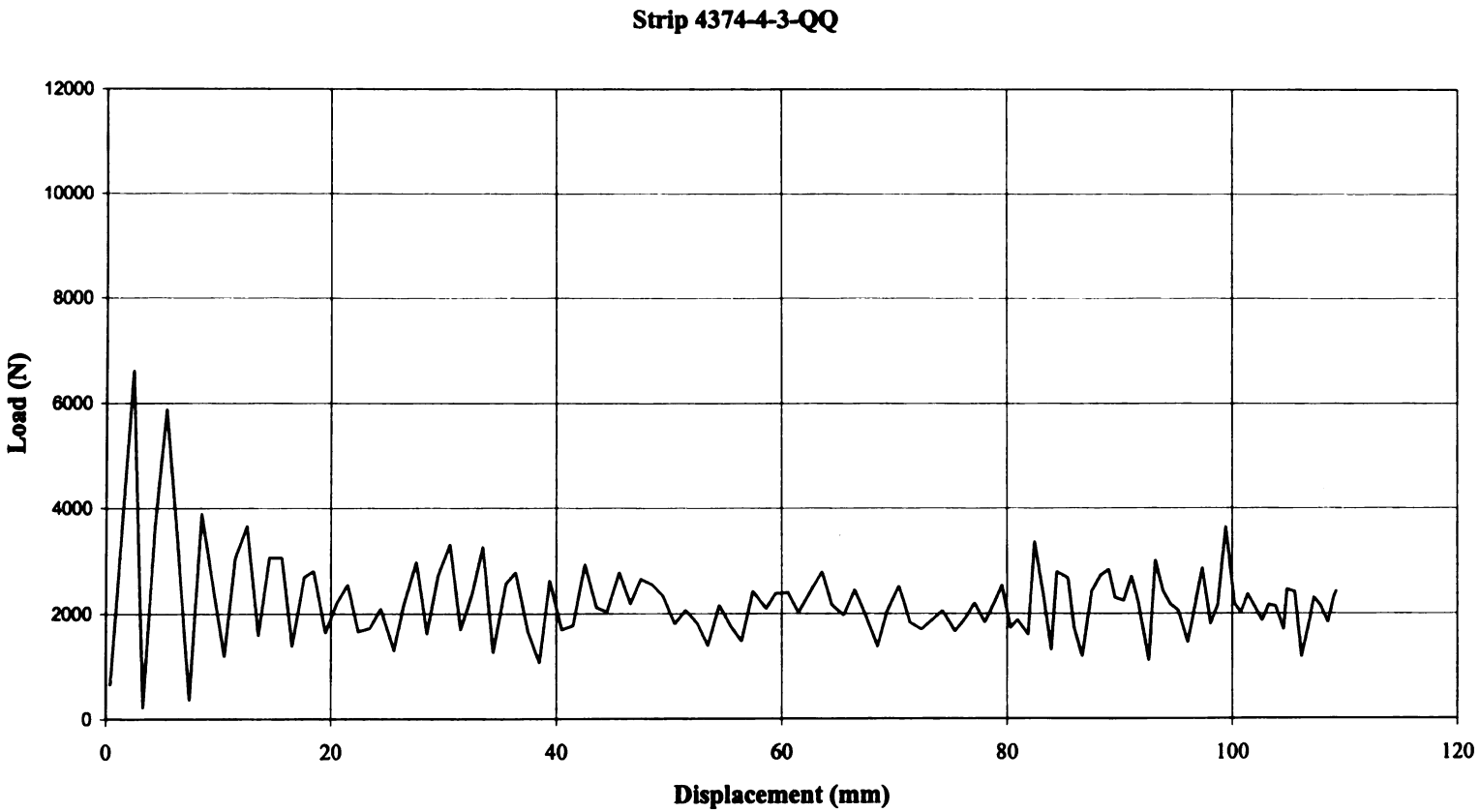

Appendix D17

Carbon Fiber Composite Strip Test
Fixed Roller, Dynamic Load Rate (2.0 m/s)

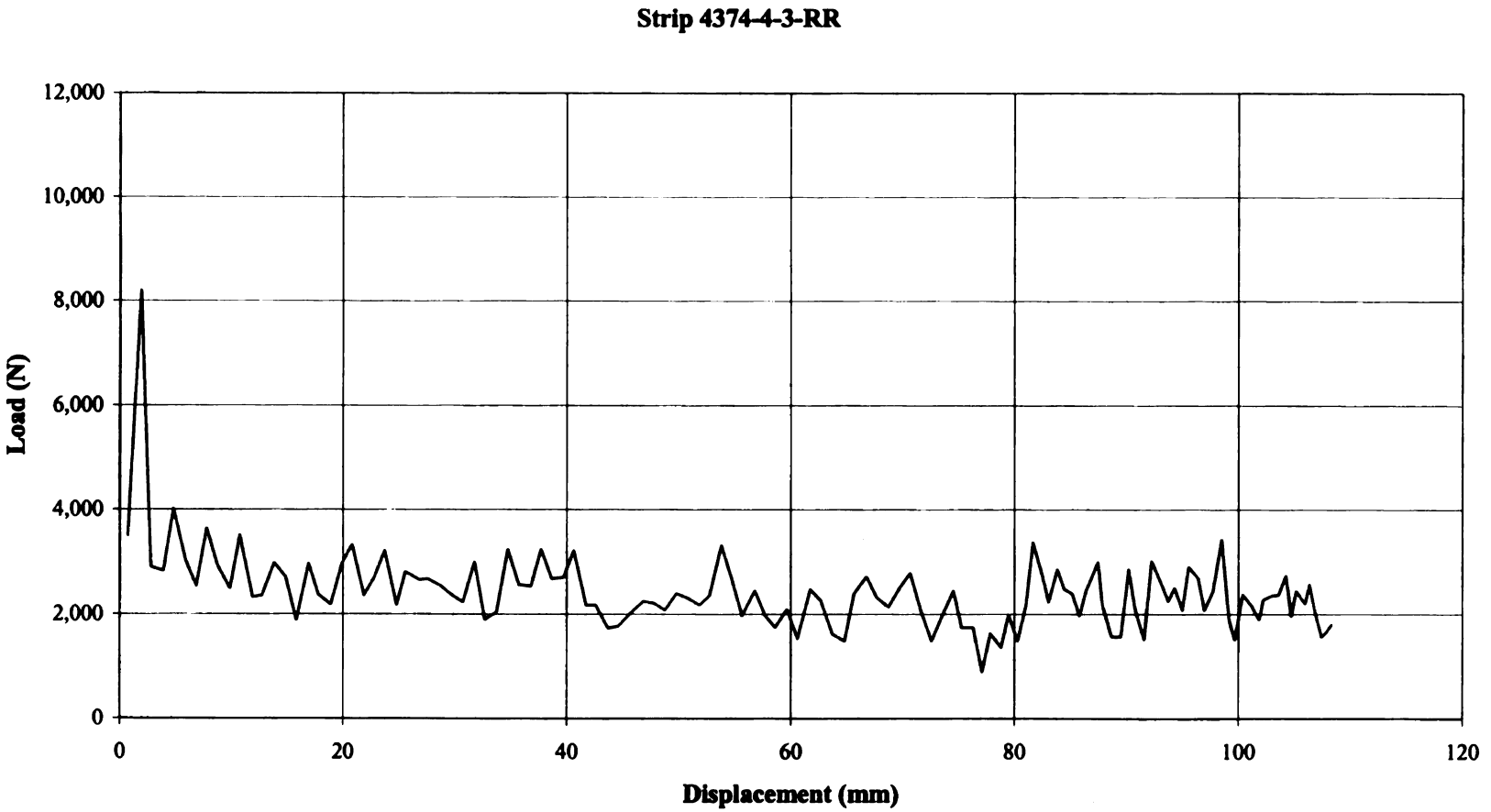

Appendix D18

Carbon Fiber Composite Strip Test
Fixed Roller, Dynamic Load Rate (2.0 m/s)

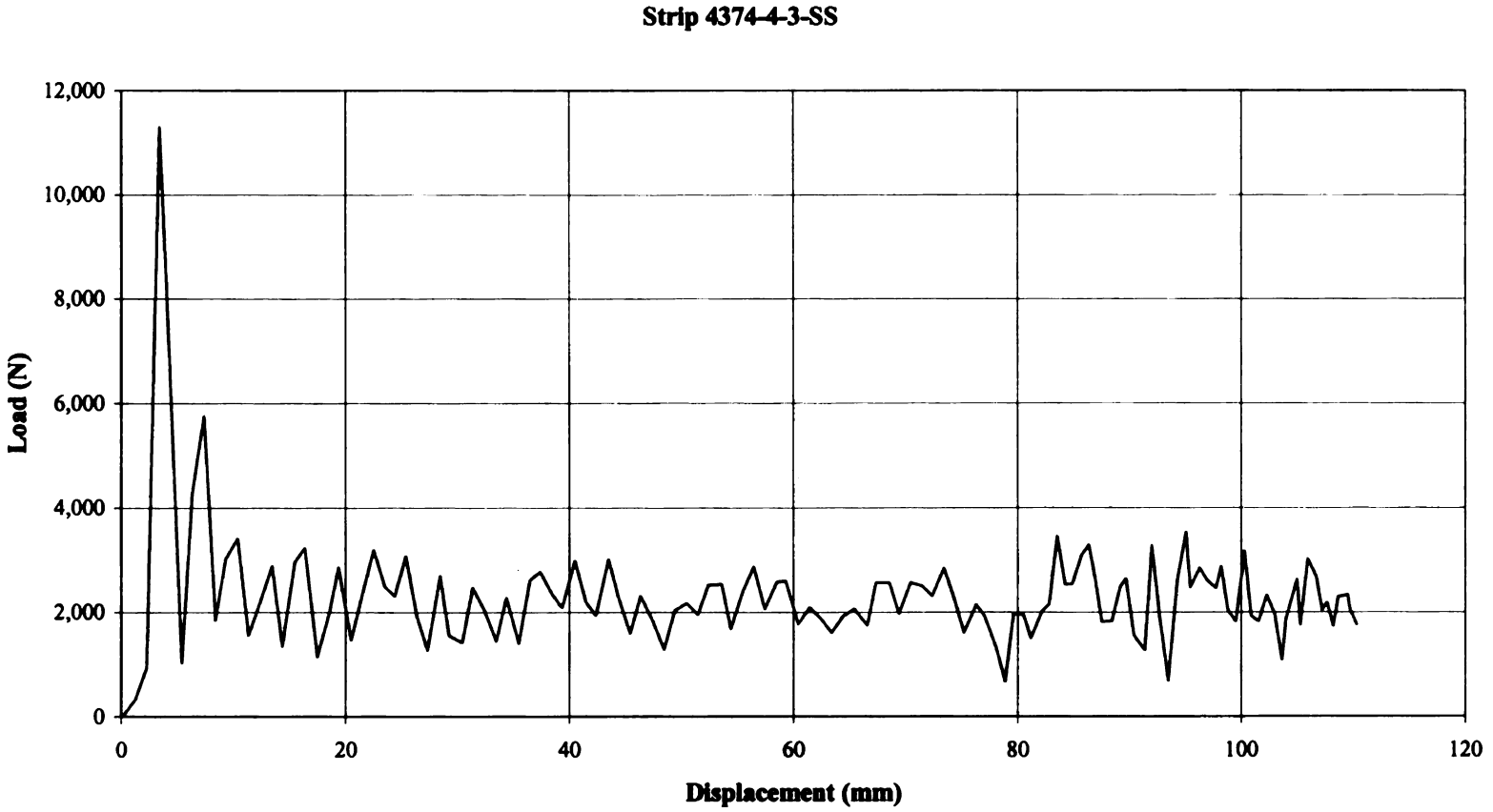

Appendix D19

Carbon Fiber Composite Strip Test
Fixed Roller, Dynamic Load Rate (2.0 m/s)

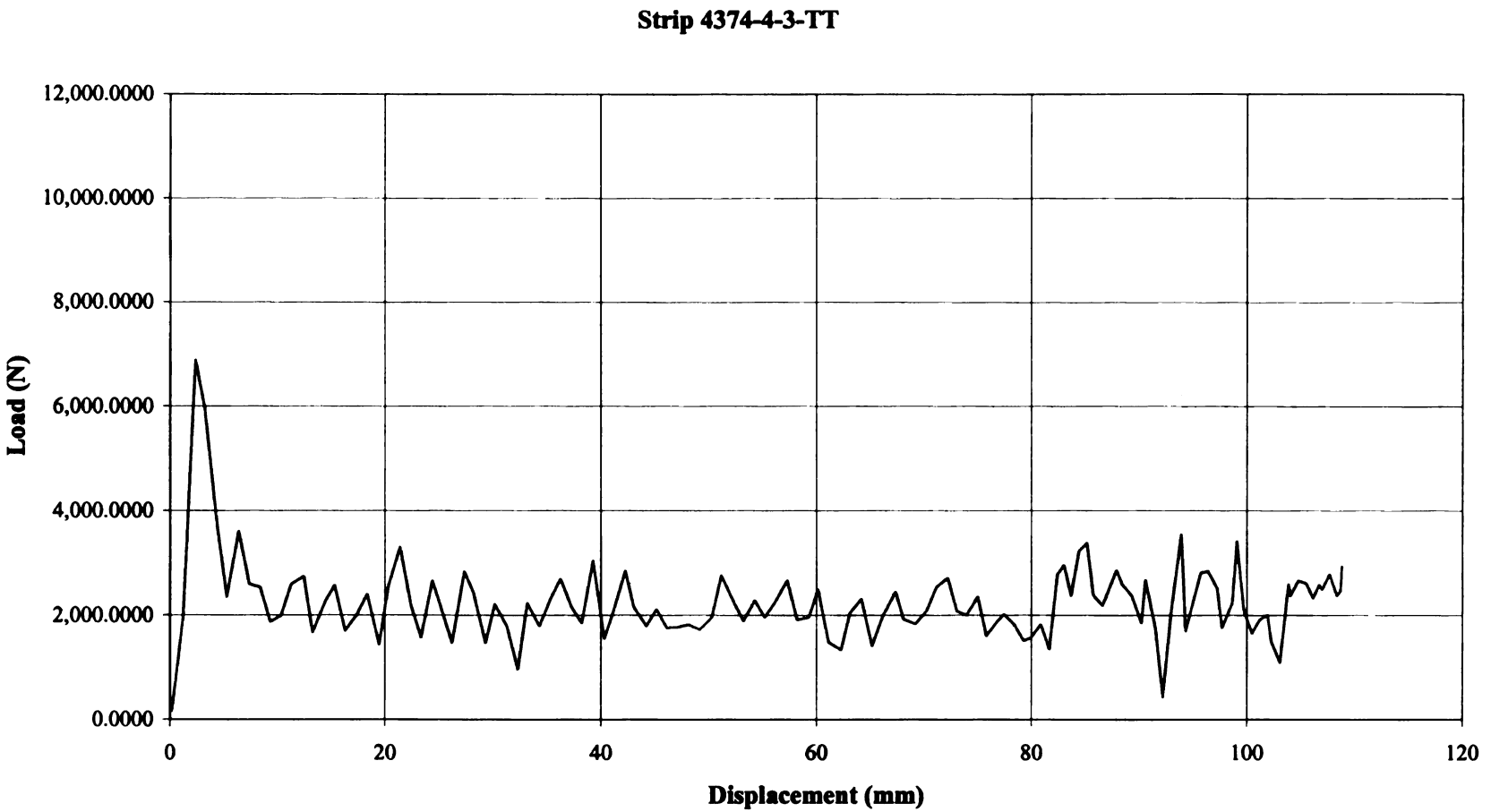

Appendix D20

Carbon Fiber Composite Strip Test
Fixed Roller, Dynamic Load Rate (2.0 m/s)

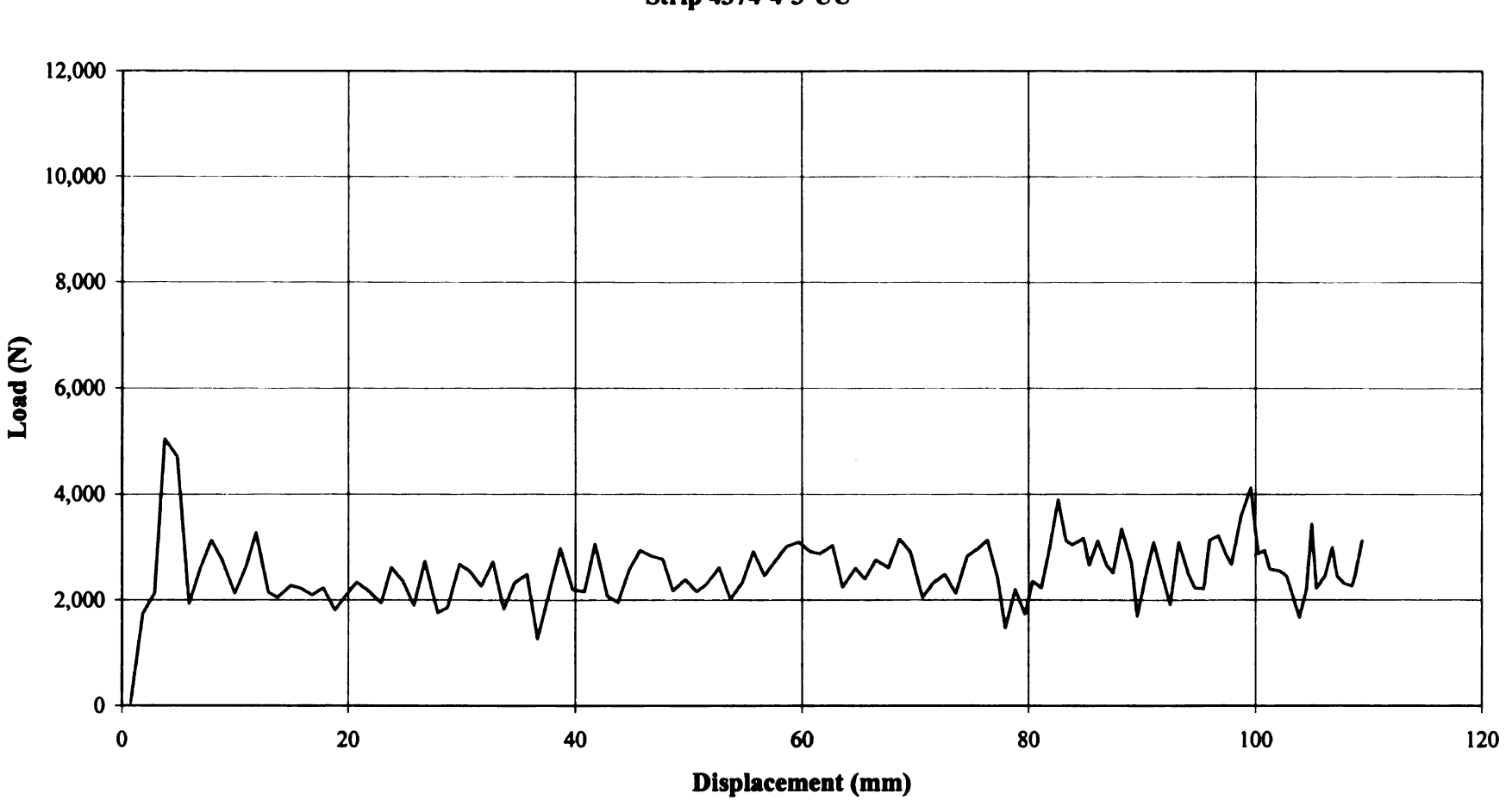

Appendix D22

Carbon Fiber Composite Strip Test
Fixed Roller, Dynamic Load Rate (0.5 m/s)

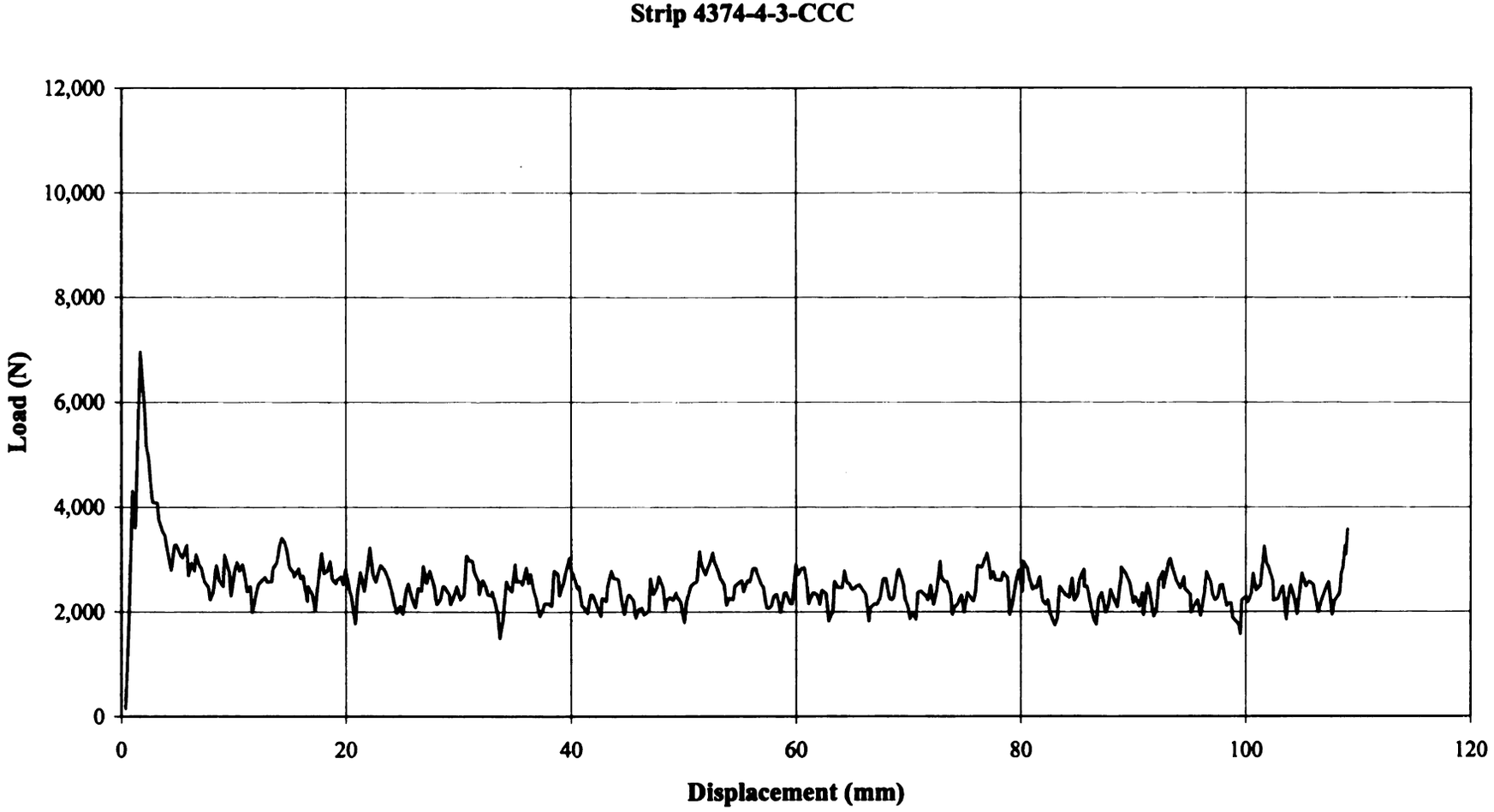

Appendix D23

Carbon Fiber Composite Strip Test
Fixed Roller, Dynamic Load Rate (0.5 m/s)

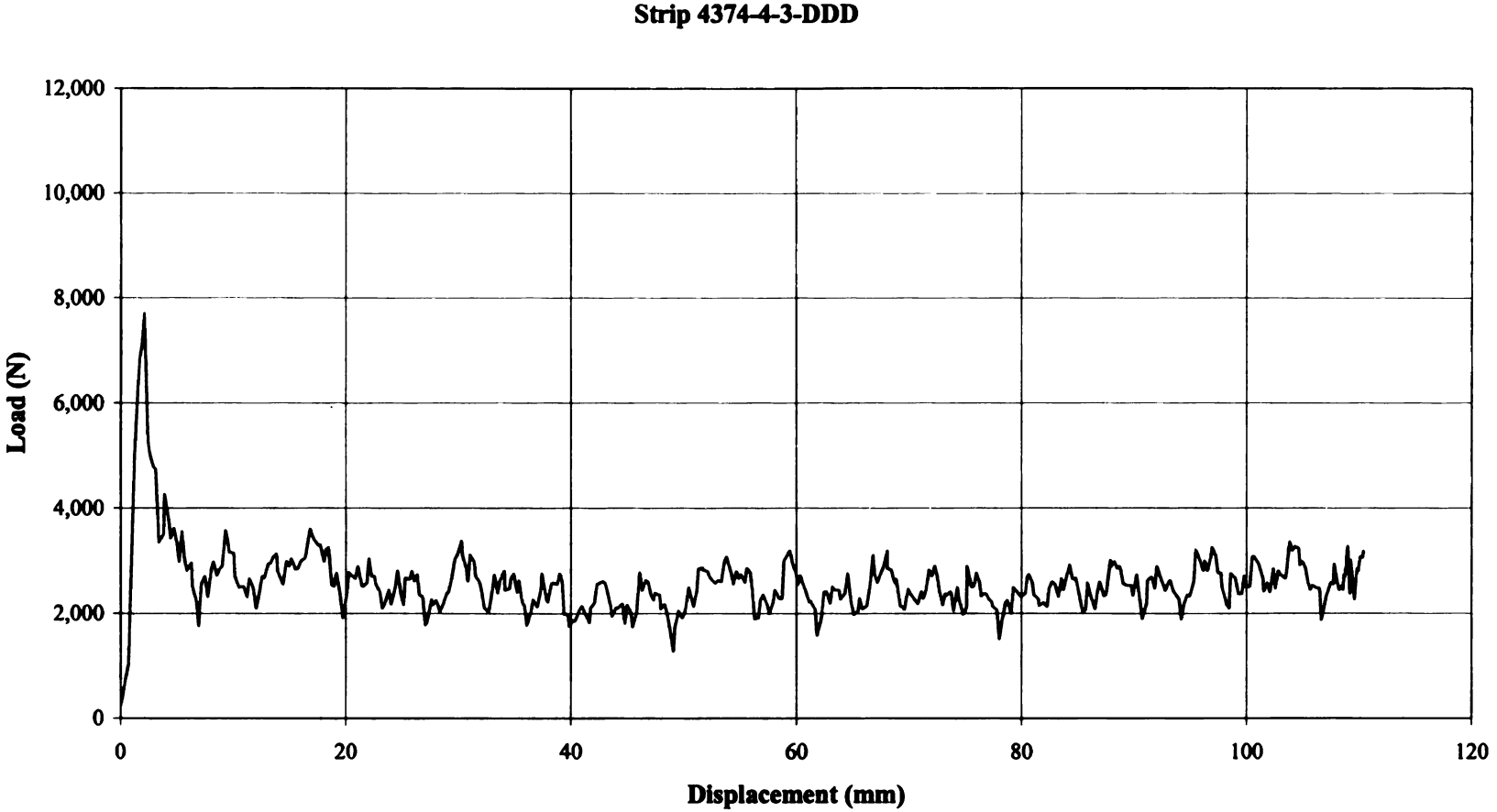

Appendix D24

Carbon Fiber Composite Strip Test
Zinc Stearate Lubrication, Fixed Roller, Dynamic Load Rate (2.0 m/s)

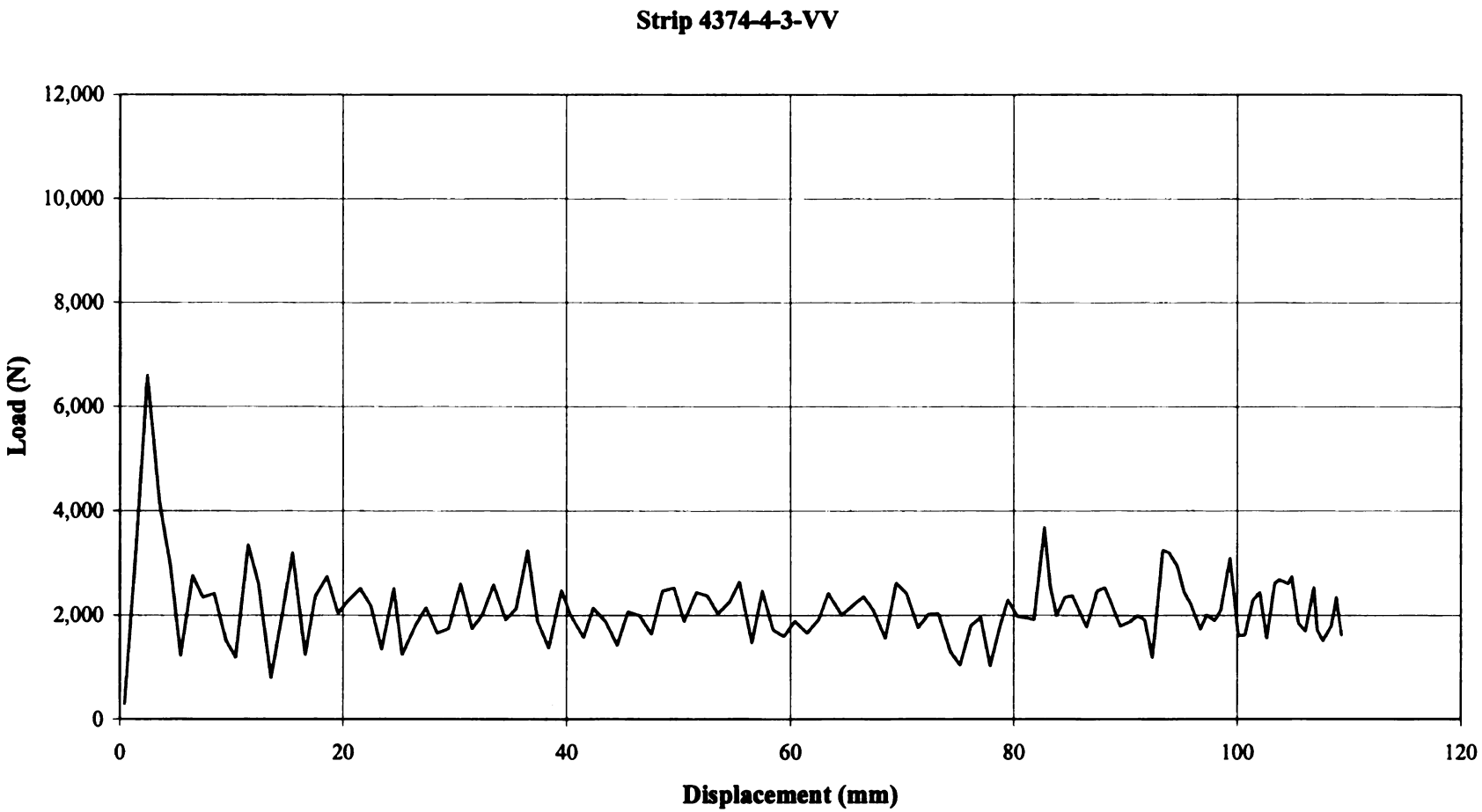

Appendix D26

Carbon Fiber Composite Strip Test
Zinc Stearate Lubrication, Fixed Roller, Dynamic Load Rate (2.0 m/s)

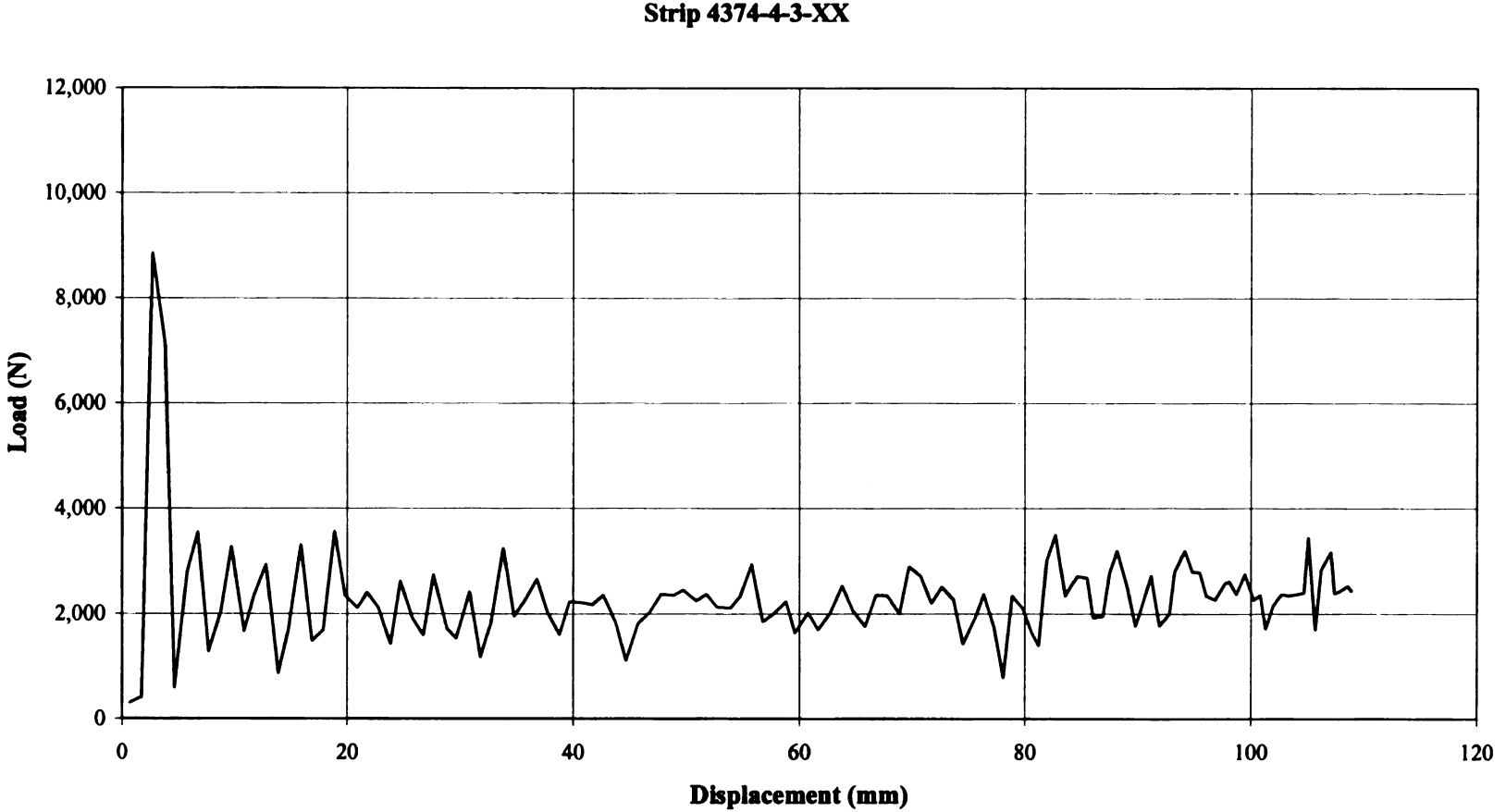

Appendix D27

Carbon Fiber Composite Strip Test
Zinc Stearate Lubrication, Fixed Roller, Dynamic Load Rate (2.0 m/s)

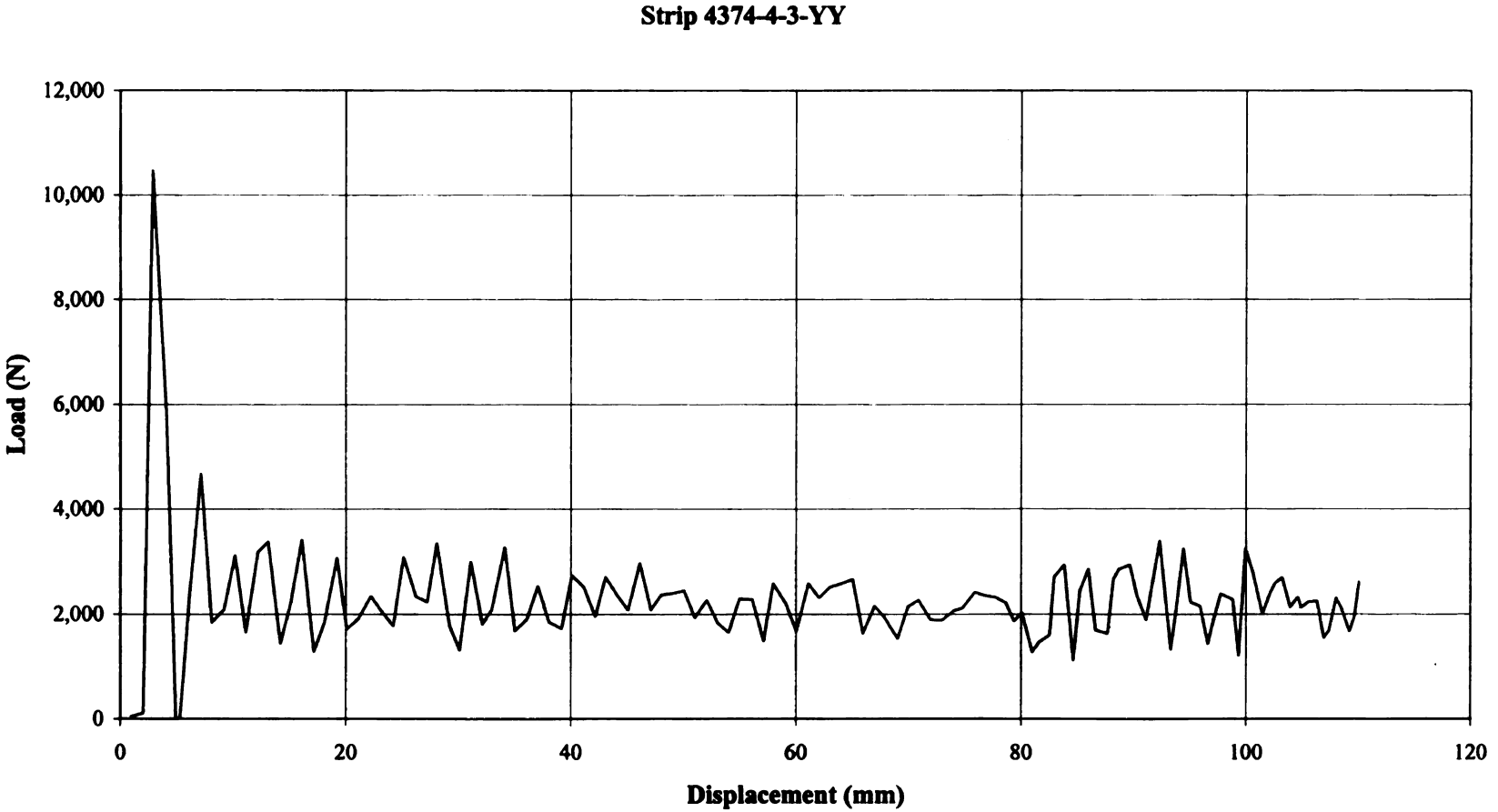

Appendix D28

Carbon Fiber Composite Strip Test
Zinc Stearate Lubrication, Fixed Roller, Dynamic Load Rate (2.0 m/s)

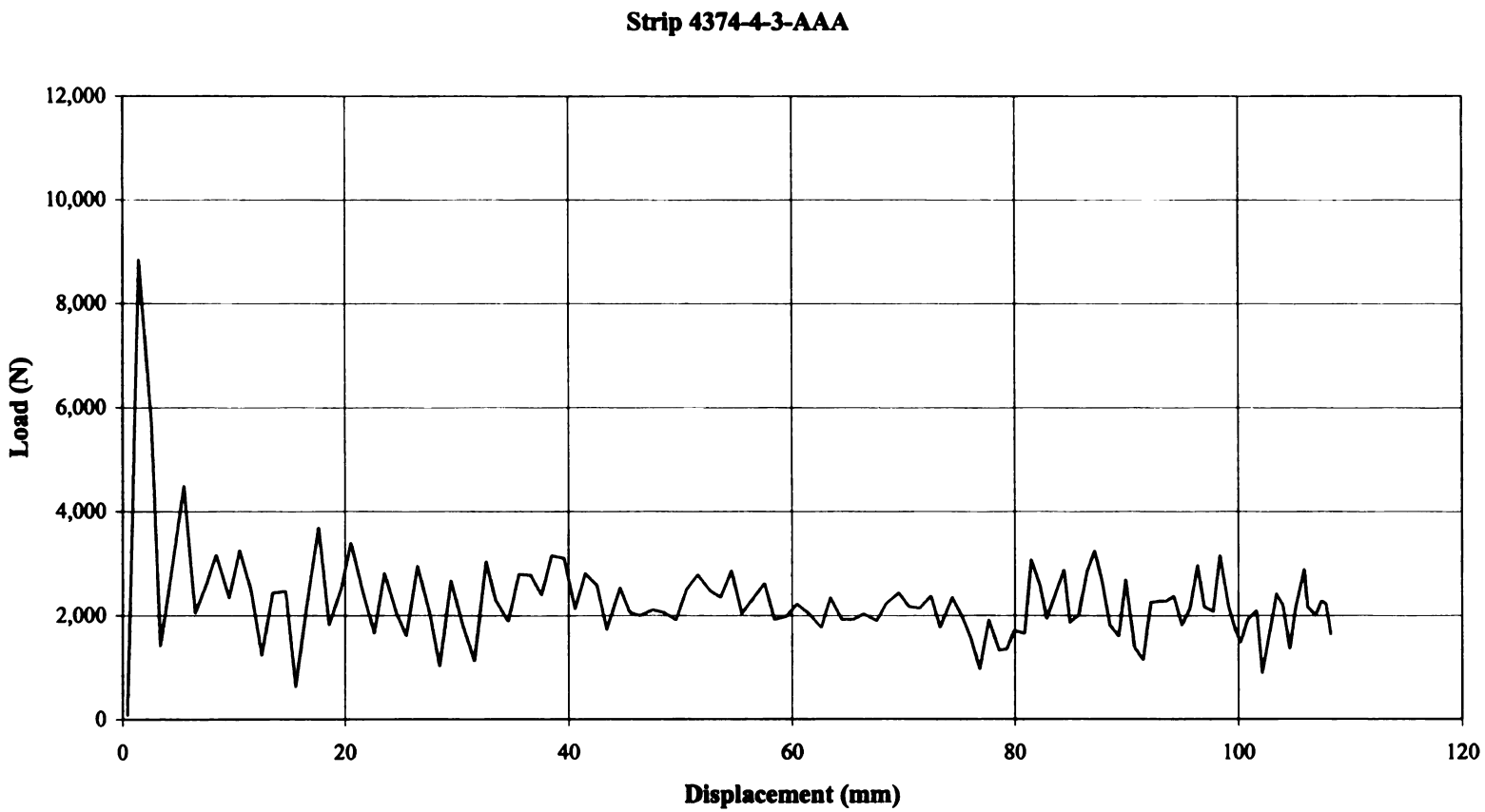

Appendix D29

Carbon Fiber Composite Strip Test
Free Roller, Dynamic Load Rate (2.0 m/s)

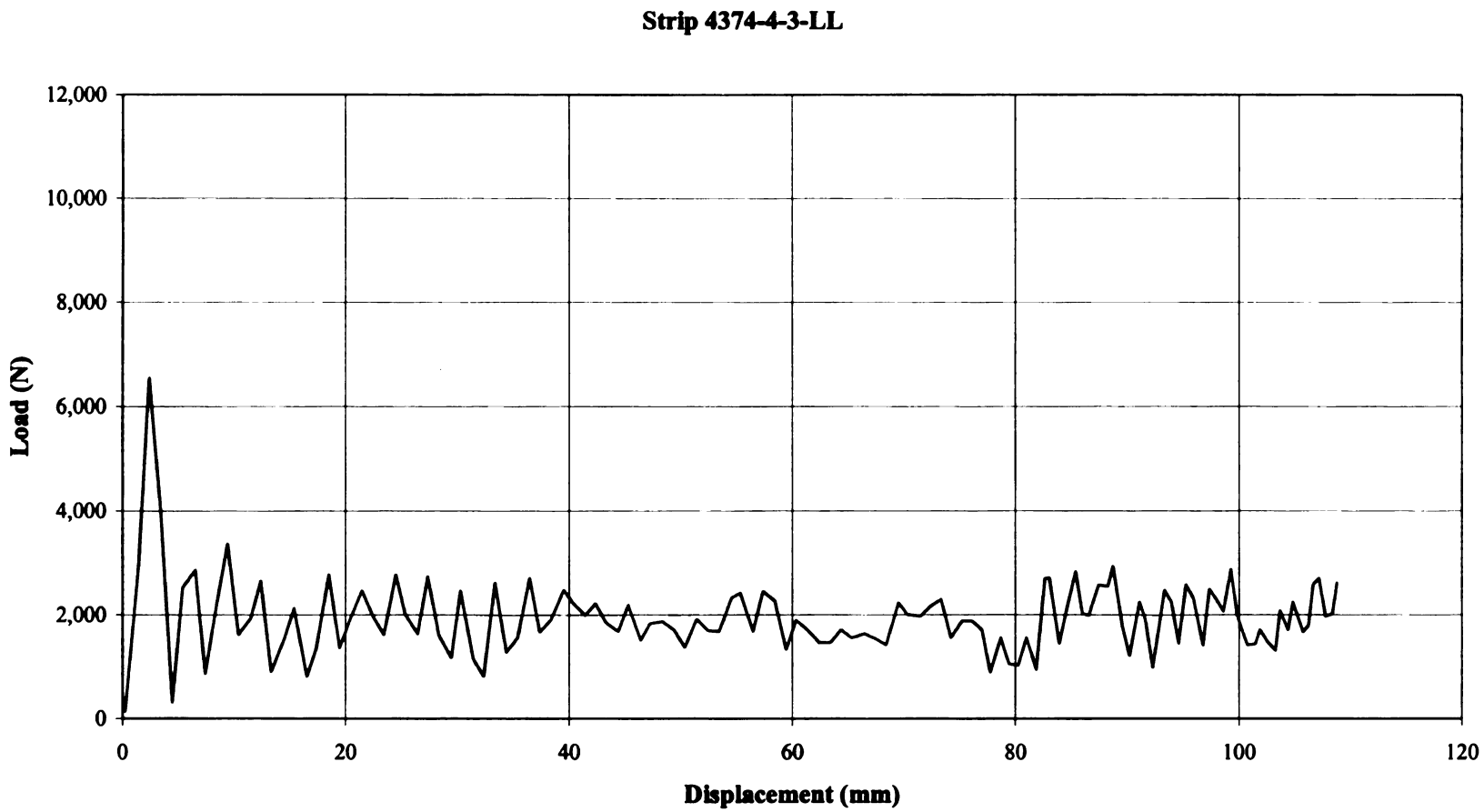

Appendix D30

Carbon Fiber Composite Strip Test
Free Roller, Dynamic Load Rate (2.0 m/s)

Strip 4374-4-3-MM

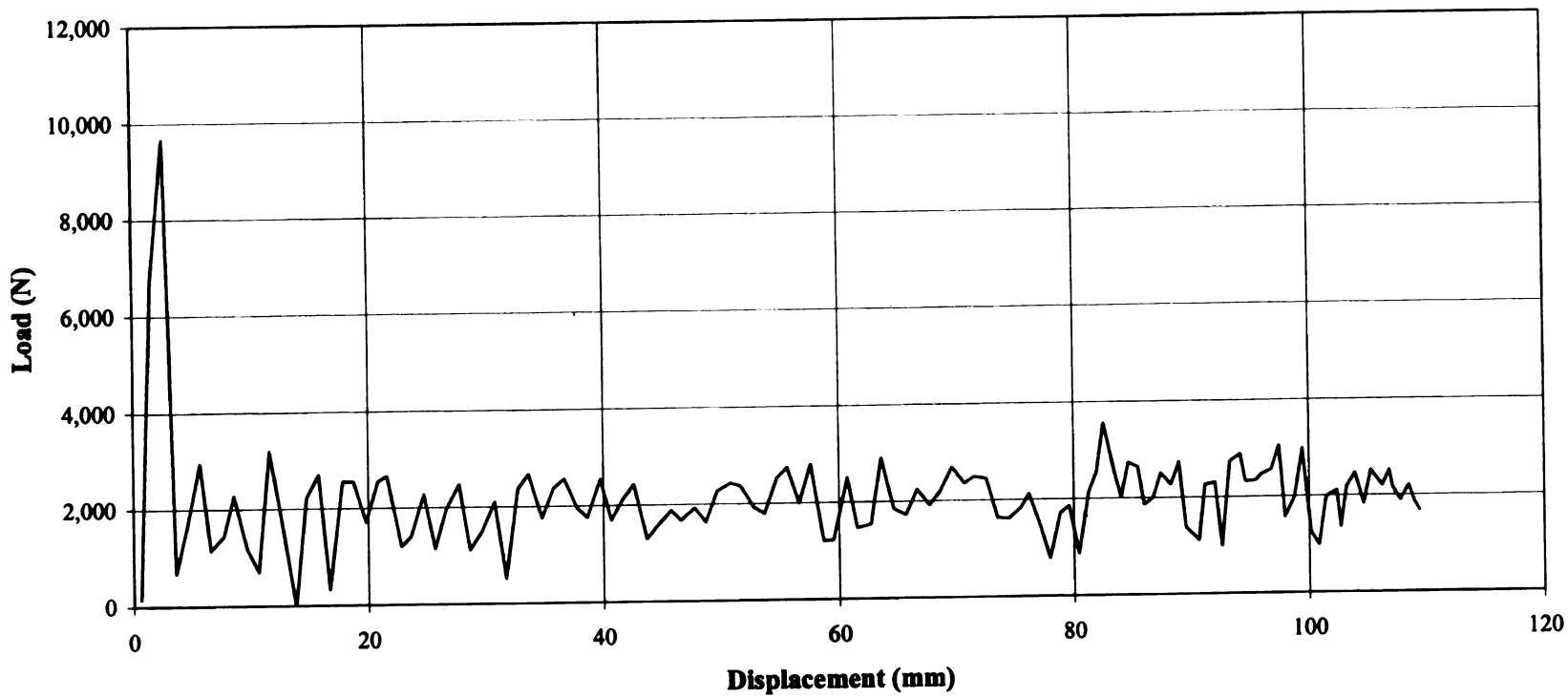

Appendix D31

Carbon Fiber Composite Strip Test
Free Roller, Dynamic Load Rate (2.0 m/s)

Strip 4374-4-3-NN

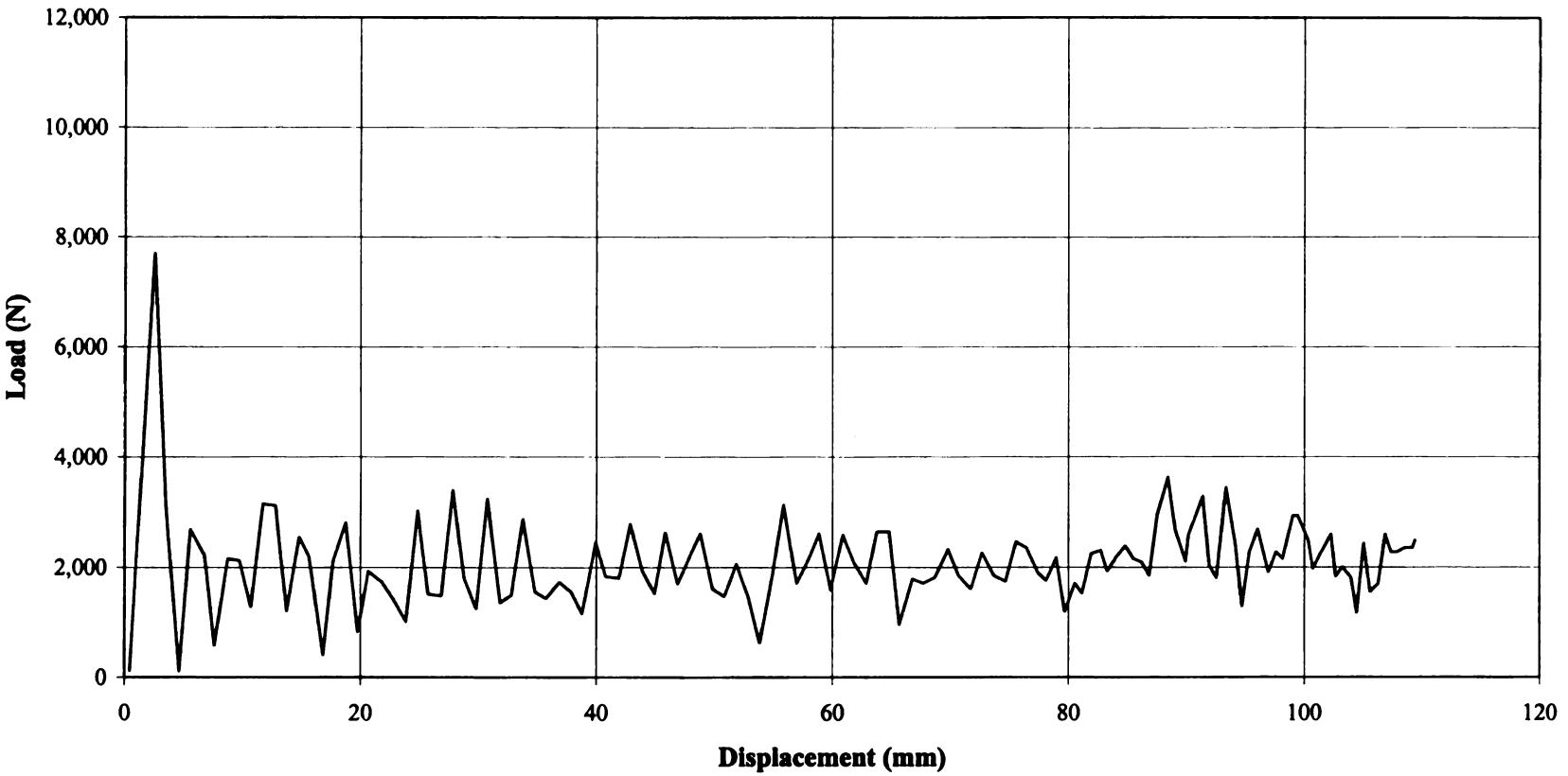

Appendix D32

Carbon Fiber Composite Strip Test
Free Roller, Dynamic Load Rate (2.0 m/s)

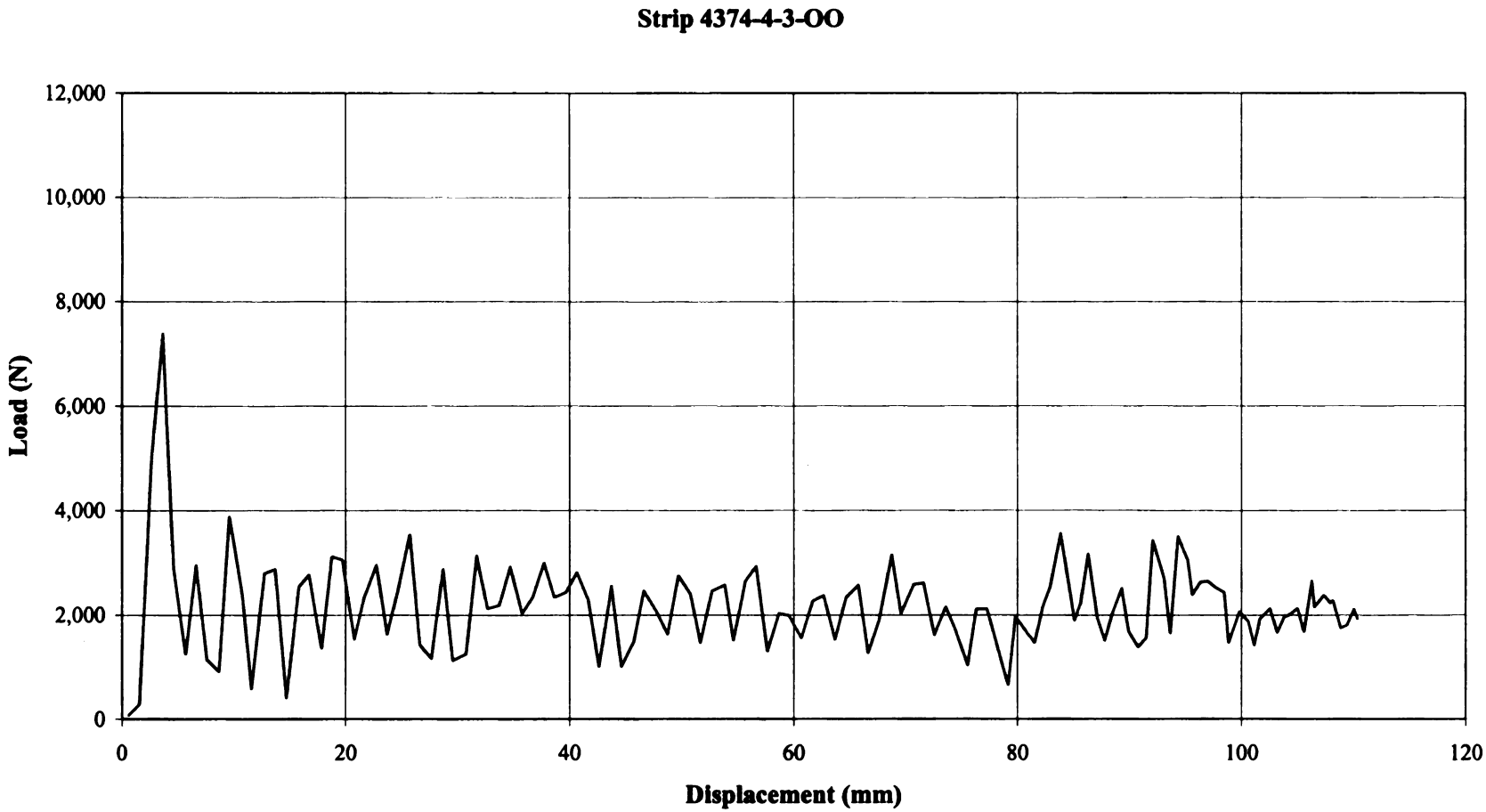

Appendix D33

Carbon Fiber Composite Strip Test
Free Roller, Dynamic Load Rate (2.0 m/s)

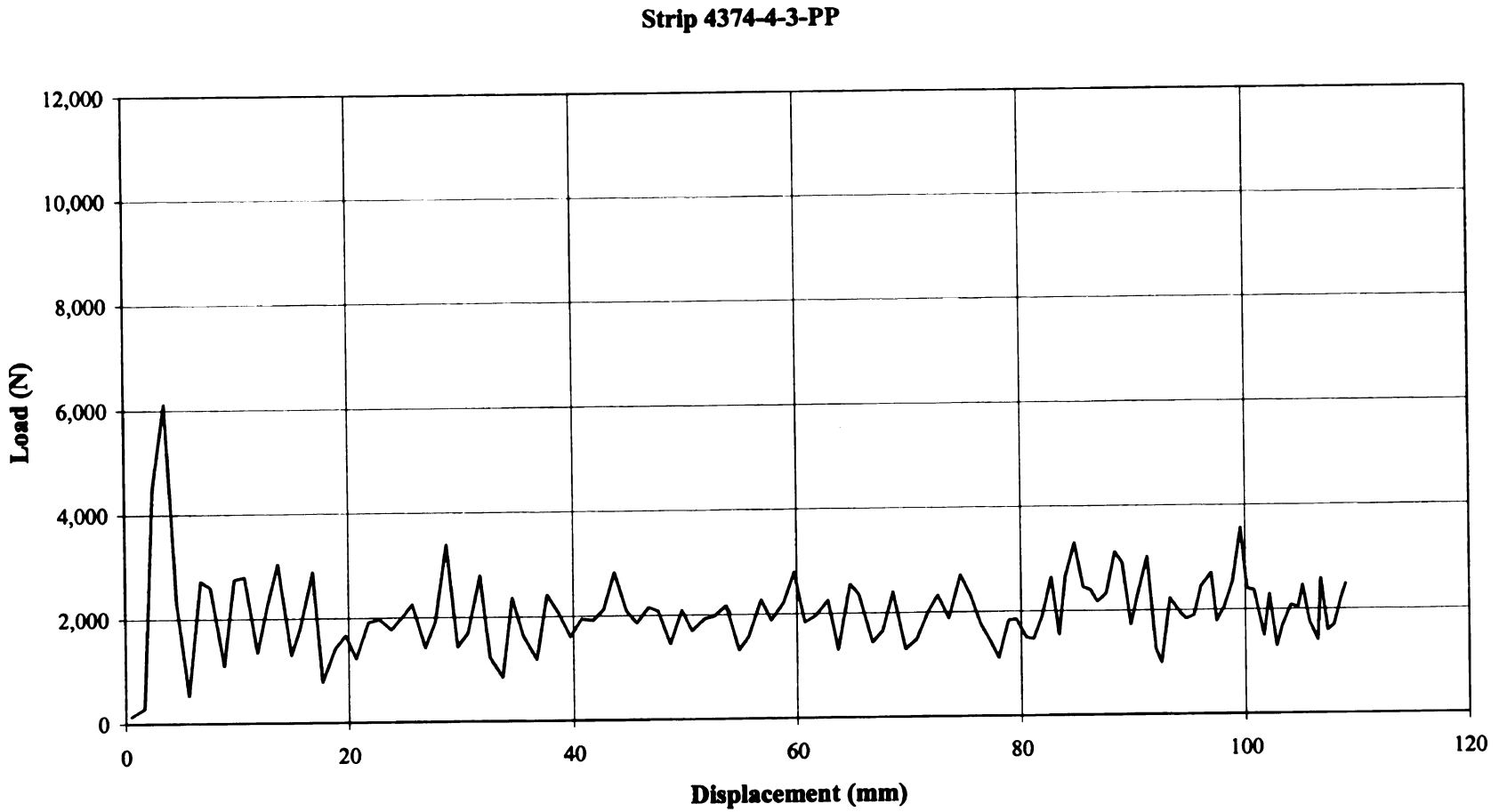

Appendix D34

Carbon Fiber Composite Strip Test
Free Roller, Dynamic Load Rate (0.5 m/s)

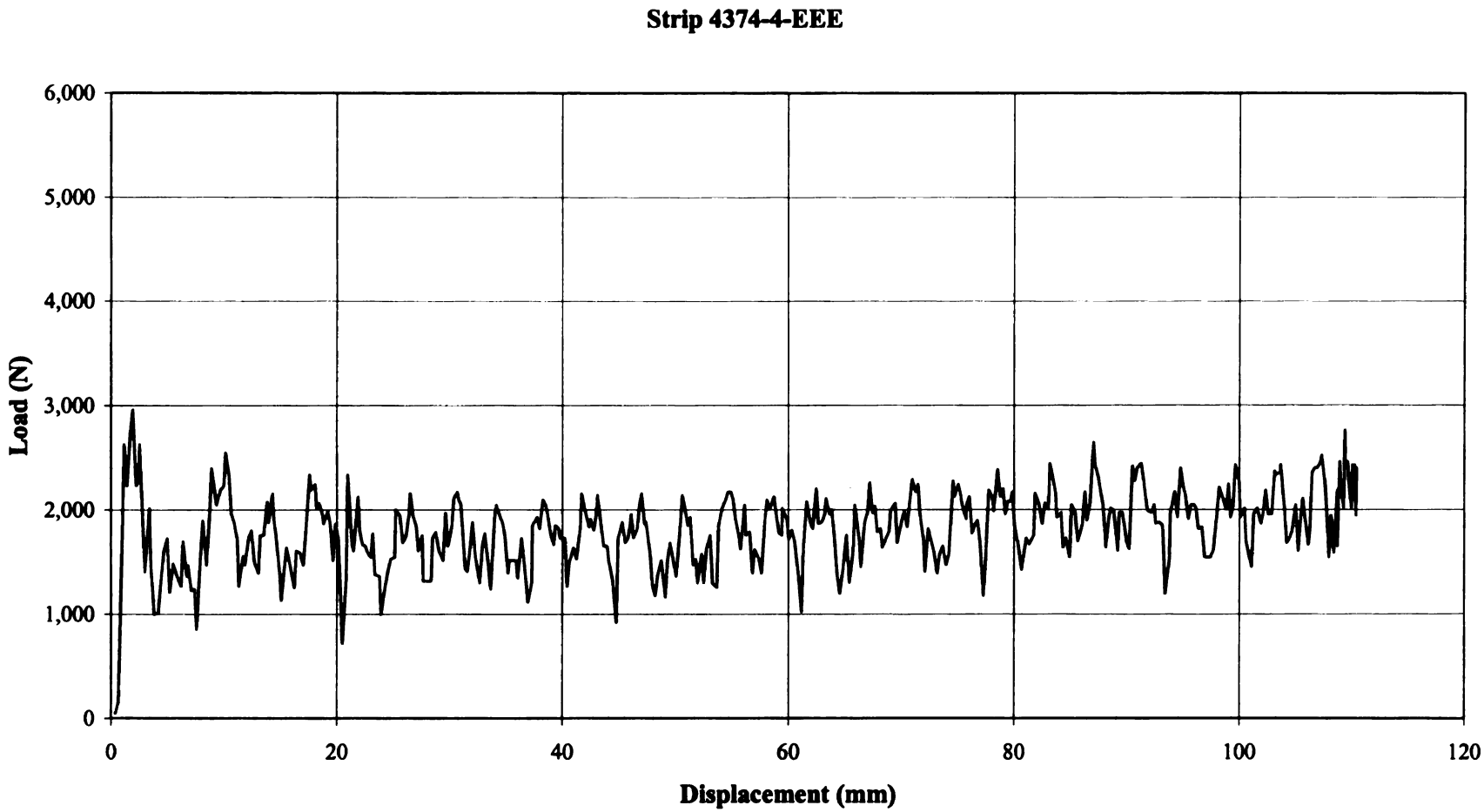

Appendix D35

Carbon Fiber Composite Strip Test
Free Roller, Dynamic Load Rate (0.5 m/s)

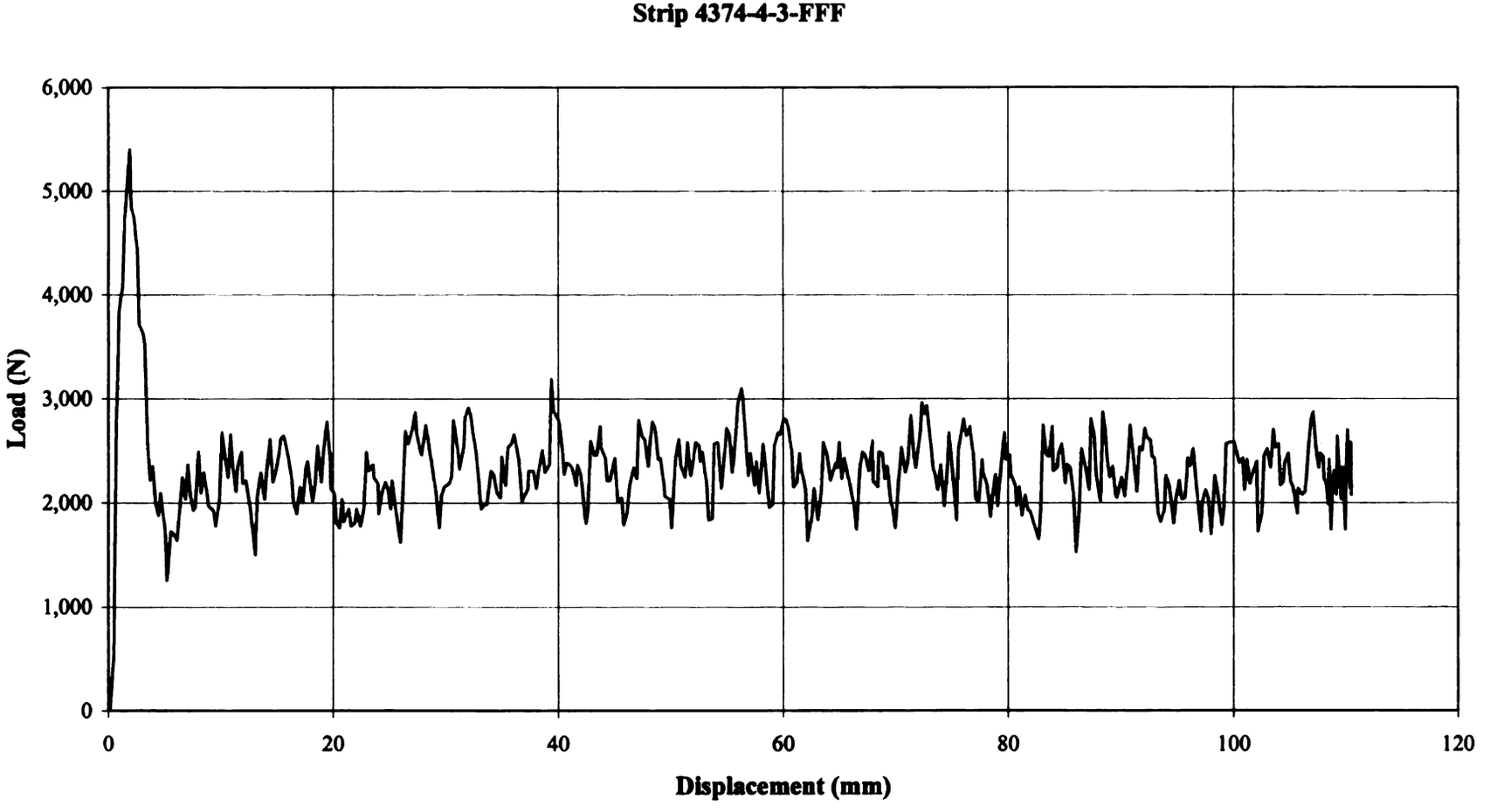

Appendix D36

Carbon Fiber Composite Strip Test
Free Roller, Dynamic Load Rate (0.5 m/s)